

# 12

## Matrix Isolation in Heterocyclic Chemistry

José P. L. Roque, Cláudio M. Nunes, Rui Fausto

University of Coimbra, Coimbra Chemistry Centre (CQC) and Department of Chemistry, Rua Larga 3004-535, Coimbra, Portugal

### Contents

- 12.1 Introduction
- 12.2 Structural characterization
- 12.3 UV-Induced photochemical reactivity
- 12.4 Thermal reactivity
- 12.5 IR-Induced processes
- 12.6 Tunneling in heterocyclic chemistry
- 12.7 Conclusion and Perspectives
- 12.8 References

### 12.1 Introduction

The matrix isolation method has been used as a research tool in organic chemistry since the beginning of the 70ies of the last century. It was proposed first in 1954, almost simultaneously by George Pimentel (Berkeley, CA) and George Porter (Cambridge, UK) [1,2], but it only became popular among the organic chemistry community after publication of the papers by Lin and Krantz [3], Chapman, McIntosh and Pacansky [4], and Pong and Shirk [5], all of them describing the photochemistry of  $\alpha$ -pyrone as a precursor of cyclobutadiene, whose existence was, at the time, still under discussion. Upon ultraviolet (UV) irradiation, matrix-isolated  $\alpha$ -pyrone **1** was found to undergo fast photoequilibration with its isomeric open-ring aldehyde-ketene **2**, as well as a slower ring closure isomerization to a bicyclo  $\beta$ -lactone **3** followed by CO<sub>2</sub> elimination to generate cyclobutadiene **4** (Figure 12.1).

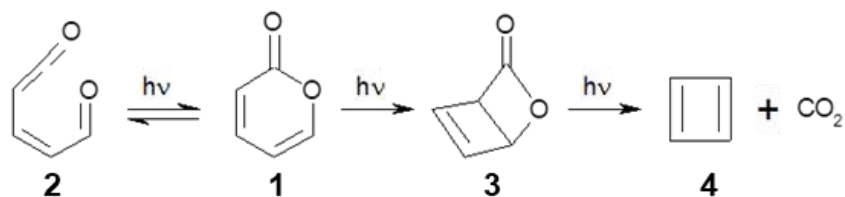


**Figure 12.1**  $\alpha$ -Pyrone photochemical reaction pathways: fast photoequilibration with the isomeric aldehyde-ketene and slow ring-closure to its Dewar isomer (bicyclo  $\beta$ -lactone). The aldehyde-ketene is produced as a mixture of several conformers. The bicyclo  $\beta$ -lactone isomer releases  $\text{CO}_2$ , giving rise to cyclobutadiene [3-6].

Isolation of molecules in a cryogenic matrix provides ideal conditions for structural studies when conjugated with a structure-sensitive probing technique, like infrared spectroscopy. But the technique has also an enormous potential for studies of chemical reactivity, which has been explored since its debut as a privileged experimental tool in organic chemistry, in particular to study light-induced processes.

In a matrix isolation experiment, molecules are trapped from the gas phase into an environment of a solidified inert gas (in general a frozen noble gas) at temperatures close to absolute zero. Under these conditions, chemical processes with an activation barrier larger than a few  $\text{kJ mol}^{-1}$  are virtually quenched, except if they occur *via* the quantum mechanical tunneling (QMT) mechanism [7]. This opens the gate to the direct study of unstable intermediates, otherwise inaccessible to experimentation, thus allowing for detailed mechanistic investigations.

In addition, the matrix being a solid, rigidity prevents diffusion of the sample, and, as a consequence, molecular fragments resulting from different precursor molecules in general do not recombine. Such feature is commonly known as “cage effect” and simplifies extraordinarily the mechanistic studies. On the other hand, recombination of species produced from the same molecule is a highly probable event. This, however, can be controlled appropriately in most cases by judicious choice of the experimental conditions (e.g., matrix host, temperature).

*In situ* irradiation and/or matrix annealing at a given temperature allow for introduction of energy in a molecule in a controlled way, defining the range of possible chemical transformations of the isolated species. Ultraviolet (UV) and visible irradiation may lead either to bond-breaking/bond-forming processes or conformational isomerizations (or to the two types of processes in simultaneous), while irradiation at the longer infrared (IR) wavelengths most of times can only give rise to conformational changes, though we have recently reported an example of a bond-breaking/bond-forming reaction induced by infrared light (the bidirectional hydroxyl-thiol tautomerization of thiotropolone [8], which will be described in details latter in this chapter; Section 12.6). On the other hand, thermal processes are limited to processes with very low energy barriers (of only a few  $\text{kJ mol}^{-1}$ ), since the matrices start to lose their properties at still considerably low temperatures (the maximum work-temperatures for argon and xenon matrices, for example, are ca. 40 and 70 K, respectively, above which the matrices start to sublime extensively).

In general, heterocycles are prone to react photochemically, frequently exhibiting competitive reaction pathways. The use of narrowband selective irradiation allows to select a given species formed along the reaction and make it generate a specific product, while keeping other species present in the matrix unreactive. Such possibility has been used successfully to shed light on mechanistic details of reactions undergone by heterocyclic compounds to an unprecedented level, with the detection and characterization of the reactivity of a large number and types of intermediates that are highly reactive under other experimental conditions.

Another relevant area of application of matrix isolation in heterocyclic chemistry is the study of tunneling-driven reactions. Since at the very low temperature conditions of a matrix isolation experiment most of the thermal processes are suppressed, the direct observation of tunneling becomes accessible to experimentation. The use of matrix isolation to address QMT has been recently revitalized by observation of several fascinating examples of the very rare heavy-atom tunneling phenomenon in heterocyclic compounds [7,9,10]. Indeed, the QMT of atoms (both of hydrogen atom and of heavy atoms) has newly been recognized to be more important to chemical reactivity than it was previously assumed, with recent studies demonstrating that the impact of QMT on chemical reactivity can be so relevant that it can even control how reactions proceed, i.e., a chemical process can take place exclusively by tunneling, leading to a product whose reaction path faces a barrier higher than those related with other *a priori* possible products, thus superseding kinetic control and breaking the Transition State Theory rules [11].

In the next sections, several illustrative cases of application of the matrix isolation method for the investigation of the structure and reactivity of a variety of heterocyclic compounds will be presented. We will concentrate on our own recent investigations, and focus on selected examples of different types of reactivity: thermal, photochemical and tunneling-driven. In the case of the photochemical reactions, examples of both IR and UV-visible triggered processes will be provided.

We shall here mention a previous publication dedicated to the use of matrix isolation in heterocyclic chemistry, which can be considered complementary to the present Chapter regarding some aspects. In that publication [12], written upon invitation from one of the editors of this book (T. M. V. Pinho e Melo), one of the authors of the present chapter (R. Fausto), together with his coworkers I. Reva and A. Gómez-Zavaglia, described the use of the technique in the investigation of some of the most important families of heterocyclic compounds (which were grouped according to their ring size, from 3- to 6-membered ring compounds), by providing examples of relevant studies that had then been recently published in the specialized literature. To the best of our knowledge, no other publication addressing this subject in a comprehensive way has been reported since then. We also invite the readers that may be interested to look in deeper details to the relevance of the QMT in organic chemistry reactivity to look to our recent publication on the subject appearing in the book “*Tunnelling in Molecules: Nuclear Quantum Effects from Bio to Physical Chemistry*”, edited by J. Kästner and S. Kozuch and published by the Royal Society of Chemistry [7]. For those that may want to further explore

the capabilities and technical details of the matrix isolation method, we shall recommend the books on the subject authored or edited by Meyer [13], Andrews and Moskovits [14], Barnes *et al.* [15], Dunkin [16], Fausto [17], and Khriachtchev [18], as well as the review by Frija *et al.* [19], where strategies for *in situ* preparation of rare organic molecules resulting from UV-visible irradiation of matrix-isolated tetrazole precursors are addressed in great detail, and the special issue of the Journal of Molecular Structure (Elsevier) edited by Nunes, Gudmundsdottir and Fausto, on the structure, spectroscopy and chemistry of organic reactive species [20].

## 12.2 Structural Characterization

Matrix isolation infrared spectroscopy is an extremely powerful research tool to structurally characterize heterocyclic compounds. An interesting example has been reported by Breda *et al.* [21], where the isomeric diazines, pyrazine, pyrimidine and pyridazine (Figure 12.2) were investigated. The compounds were isolated in argon matrices and their infrared spectra assigned with the help of vibrational calculations performed based on electronic structure calculations undertaken at the DFT(B3LYP)/6-311++G(d,p) level of theory.

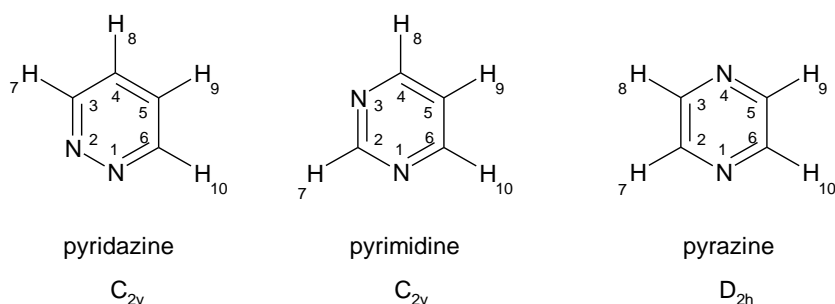


**Figure 12.2** Pyridazine, pyrimidine and pyrazine. The symmetry point groups of the molecules are indicated in the figure. Reprinted from Ref. 21, Copyright 2006, with permission from Elsevier.

The first interesting fact to note is that, in spite of being isomers, the studied diazines have infrared spectra under matrix isolation conditions that differ very much from each other (Figure 12.3). This is particularly notorious for pyrazine, since the symmetry of the molecule is different ( $D_{2h}$  vs.  $C_{2v}$  for the other two compounds) leading to a smaller number of active infrared modes in this molecule (12 vs. 22 in pyrimidine and 20 in pyridazine), but the spectra of pyrimidine and pyridazine are also significantly distinct.

Spectra/structure correlations can be extracted from the vibrational data, in particular regarding the degree of aromaticity exhibited by the three molecules. The relative values of the CC stretching frequencies are a good indicator of the degree of aromaticity, since they correlate with the bond lengths. The  $\nu(C4C5)$  stretching vibration in pyridazine has the highest frequency ( $1572.9\text{ cm}^{-1}$ ) amongst all CC stretching vibrations in the studied diazines, while the average frequency of the stretching modes associated with the C3C4 and C5C6 bonds in the same

molecule is the smallest one ( $1243.4\text{ cm}^{-1}$ ). Both in pyrazine and pyrimidine the average  $\nu(\text{CC})$  frequency values ( $\approx 1320\text{ cm}^{-1}$ ) are in between the two extreme values observed for the CC vibrations in pyridazine. The observed  $\nu(\text{C4C5})$  frequency ( $1572.9\text{ cm}^{-1}$ ) is typical of a CC bond with a large double bond character, indicating a high degree of  $\pi$ -electron localization in the pyridazine ring, and allowing to conclude that in this molecule the contribution of the canonic form where the C4C5 bond corresponds to a double bond is considerably more important than the alternative canonic form where this bond corresponds to a single bond. This conclusion is reinforced also by the small vibrational frequency of the  $\nu(\text{N1N2})$  mode in pyridazine ( $967.3\text{ cm}^{-1}$ ), which is typical of a single bond. Contrarily to what happens in pyridazine, the  $\pi$ -electron systems in both pyrazine and pyrimidine rings are strongly delocalized over all heavy-atoms.

In the described investigation [21], the authors were also able to observe the UV-induced photoisomerization of pyrazine into pyrimidine (Figure 12.4), suggesting that the mechanism for the phototransformation most probably involves intermediacy of a benzvalene-like transient species generated from the prefulvene diradical, which is believed to be a primary photoproduct in the photochemistry of pyrazine (and also of benzene) [22-25].

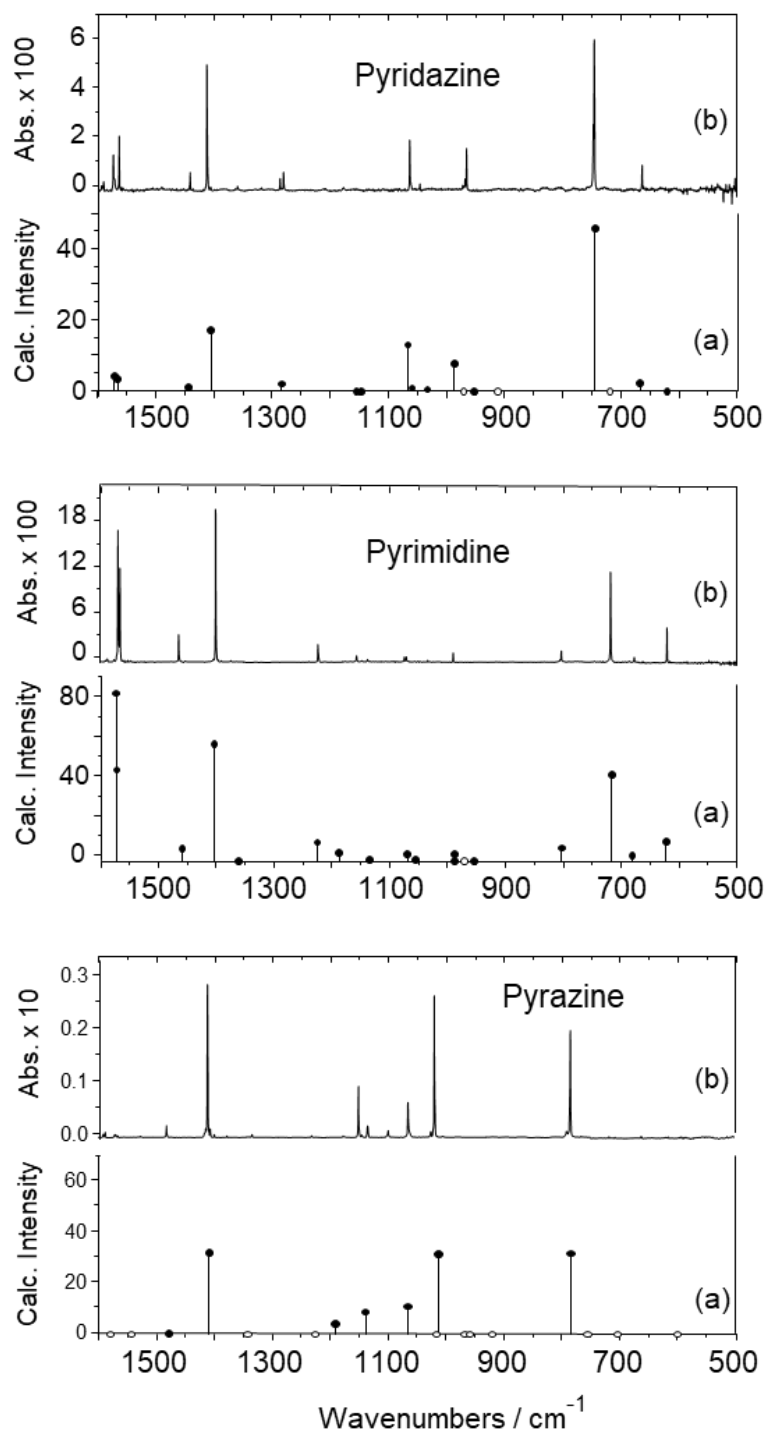


**Figure 12.3** B3LYP/6-311++G(d,p) calculated infrared spectrum of pyridazine, pyrimidine and pyrazine (a) and the observed infrared spectra of the compounds isolated in solid argon at 10 K (b). In the calculated spectra, open circles indicate the positions of the IR inactive modes. Calculated frequencies are scaled by a single factor 0.978; calculated intensities are in  $\text{km mol}^{-1}$ . Adapted from Ref. 21, with permission from Elsevier. Adapted from Ref. 21, Copyright 2006, with permission from Elsevier.

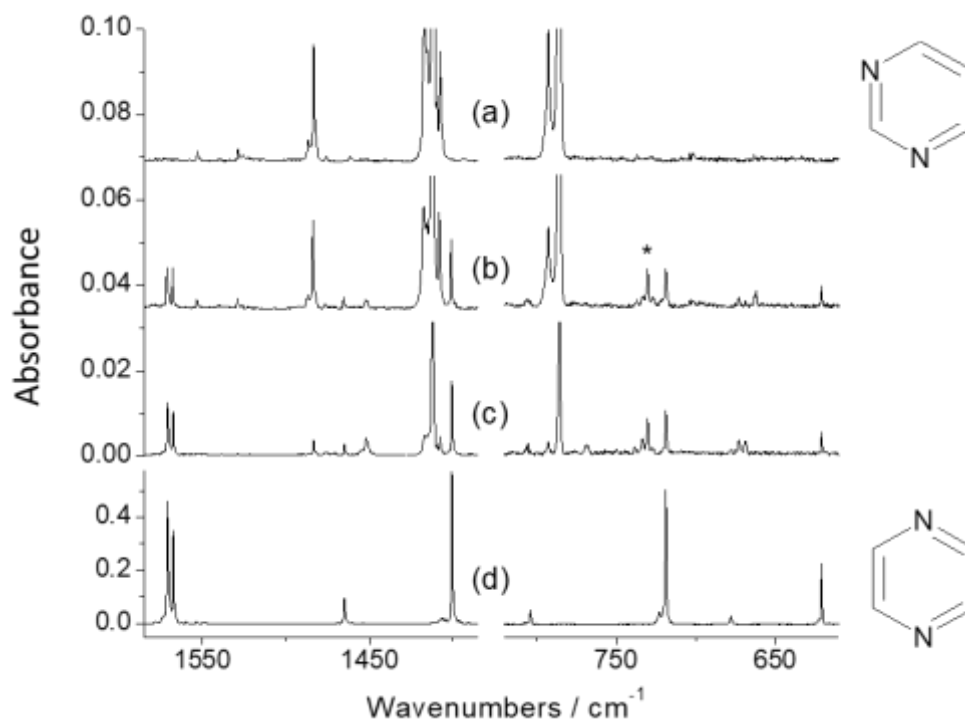


**Figure 12.4** Fragments of the infrared spectra of pyrazine isolated in an Ar matrix: (a) – recorded after deposition of the matrix; (b) – recorded after 3 hours of irradiation with high pressure mercury lamp fitted with a cut-off filter transmitting light with  $\lambda > 270$  nm; (c) – recorded (in a separate experiment) after 20 minutes of irradiation with a pulsed excimer laser  $\lambda = 308$  nm; (d) – corresponding fragments of the spectrum of pyrimidine isolated in an Ar matrix. The asterisk indicates the band (at  $730\text{ cm}^{-1}$ ) that should be assigned to the bending vibration of the HCN photoproduct. Adapted from Ref. 21, Copyright 2006, with permission from Elsevier.

Another interesting example of a structural characterization by matrix isolation infrared spectroscopy that was used to confirm the chemical identity of the reaction product has been reported by Lopes *et al.* [26]. This is an interesting case where the technique was shown to surpass the most commonly used NMR and mass spectrometry analyses.

The investigation appeared following a series of studies on the thermolysis of 2-benzoyl-2-halo-2*H*-azirine-3-carboxylates **5** (Figure 12.5) [27]. These compounds were found to undergo ring expansion giving products in high yield, which were first identified as being 4-haloisoxazoles **6**. Both  $^1\text{H}$  NMR and mass spectrometry measurements gave results compatible with formation of isoxazoles [27]. In addition, it is known that thermolysis of 2*H*-azirines usually takes place by cleavage of the N–C single bond, resulting in a transient vinyl nitrene that can subsequently evolve to the corresponding isoxazole. This reaction is essentially the reverse of the cyclization of vinyl nitrenes commonly used to prepare 2*H*-azirines [28]. Nevertheless, the reactivity pattern of 2*H*-azirine derivatives is in fact difficult to establish *a priori*, since it is significantly dependent on the nature of the substituents. For example, methyl

2-chloro-3-methyl-2*H*-azirine-2-carboxylate and methyl 3-methyl-2*H*-azirine-2-carboxylate isolated in argon matrices were found to undergo both C–C and N–C bond cleavages, leading to production of nitrile ylides or methylated ketene imines, respectively [29-31]. 2*H*-Azirines bearing an aromatic substituent at C2 [32,33] were also found to undergo competitive C–C and N–C bond cleavages, with the tendency towards the N–C bond cleavage increasing with the electron-withdrawing ability of the ring substituents.

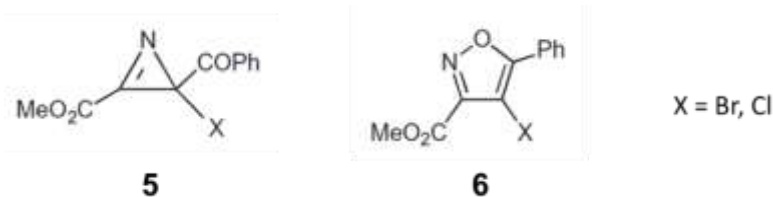


**Figure 12.5** 2-Benzoyl-2-halo-2*H*-azirine-3-carboxylates and suggested products of thermolysis, 4-haloisoxazoles.

In their study, Lopes *et al.* [26] demonstrated that the matrix isolation IR spectrum of the product of thermolysis of methyl 2-benzoyl-2-chloro-2*H*-azirine-3-carboxylate **7** corresponds to that of oxazole **8** (methyl 4-chloro-5-phenyl-1,3-oxazole-2-carboxylate) and not to that of the initially postulated product, its isomeric isoxazole **9** (methyl 4-chloro-5-phenylisoxazole-3-carboxylate) (Figure 12.6). The two isomers (**8** and **9**) give rise to similar <sup>1</sup>H and <sup>13</sup>C NMR spectra and similar patterns of fragmentation in mass spectrometry experiments, while their matrix isolation IR spectra are very much distinct, thus allowing for their easy differentiation (Figure 12.7).

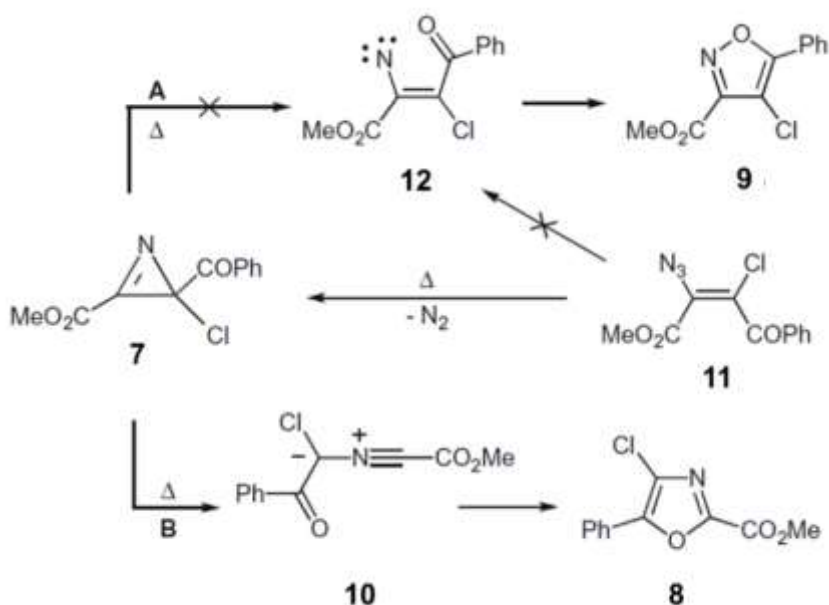




**Figure 12.6** General mechanism for thermolysis of 2-benzoyl-2-chloro-2*H*-azirine-3-carboxylate **7**, prepared from the corresponding chloroazidoalkene **11**. **A** and **B** correspond to the two *a priori* possible reaction pathways, associated respectively to the C–N and C–C bond cleavages of the azirine ring. Adapted from Ref. 26, Copyright 2009, with permission from Elsevier.

The formation of oxazole **8** from the 2*H*-azirine **7** can be explained considering the thermal cleavage of the C–C bond of the azirine to give nitrile ylide **10** followed by recyclization. Interestingly, since the oxazole is obtained in high yield (98%) [27], this means that, for the type of molecules investigated, the C–C bond cleavage strongly dominates over the N–C one. Furthermore, the unequivocal identification by matrix isolation IR spectroscopy of oxazole **8** as the single reaction product of thermolysis of **7** leads also to the conclusion that the formation of the 2*H*-azirine ring from its precursor haloazidoalkene **11** must take place *via* a concerted process. Otherwise the formation of the putative vinyl nitrene intermediate **12** should lead to formation of the isoxazole **9**.

In conclusion, the matrix isolation IR spectroscopy studies doubtlessly established that the thermolysis of 2-benzoyl-2-halo-2*H*-azirine-3-carboxylates leads to oxazoles and not, as initially suggested [27], to isoxazoles.

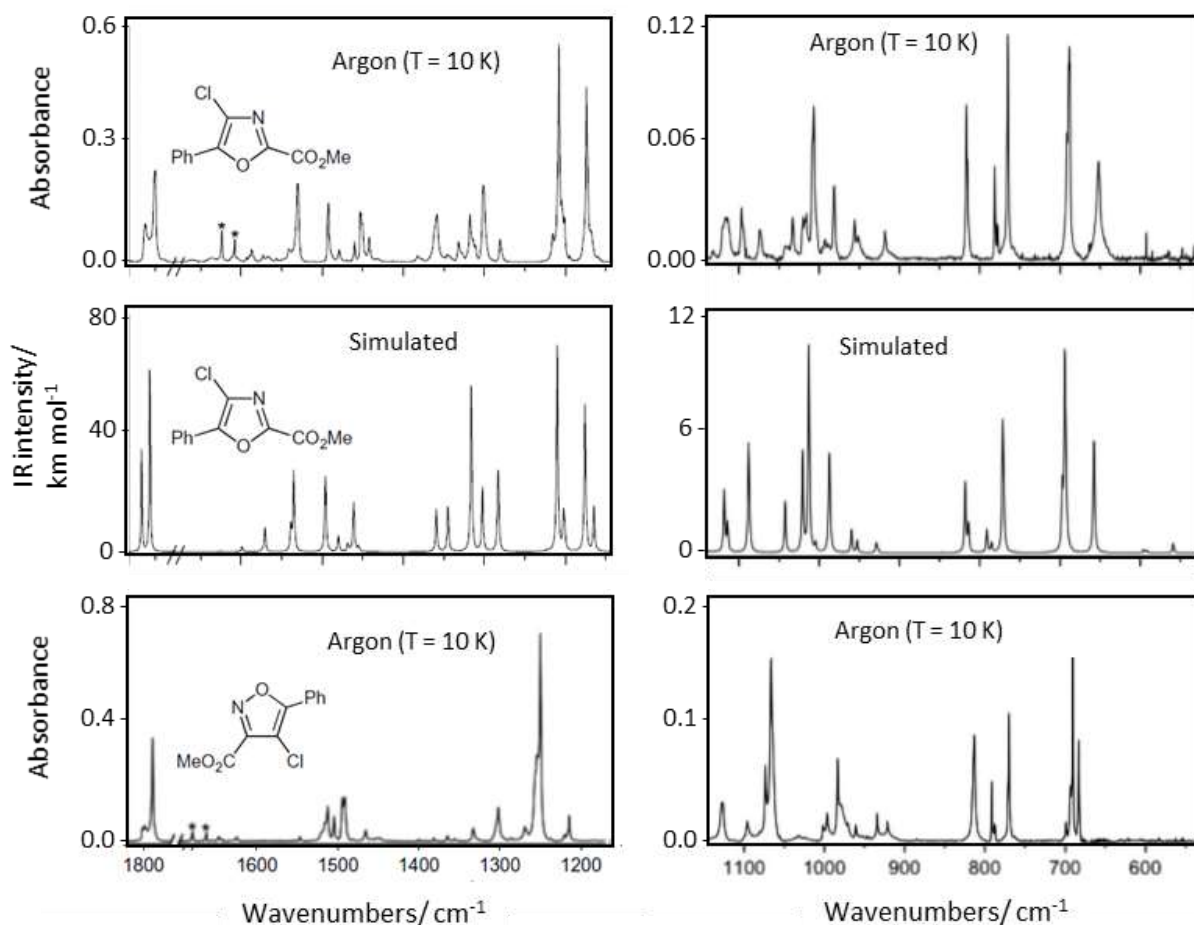


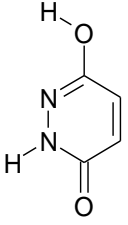
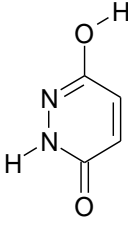
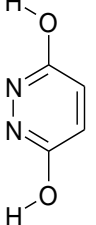
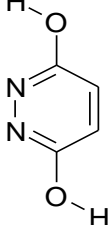
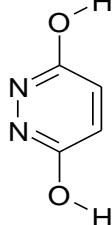
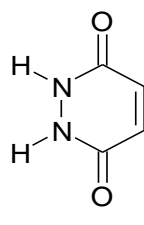
**Figure 12.7** *Top panels:* infrared spectrum of the product of thermolysis of the azirine **7** in an argon matrix, in the 1800–1145 and 1100–550  $\text{cm}^{-1}$  regions. *Middle panels:* simulated IR spectrum of isoxazole **8** (in the same spectral regions) based on the DFT(B3LYP)6-311++G(d,p) calculated wavenumbers – scaled by 0.9817 – and intensities for the two lowest energy conformers of isoxazole **8** weighted by their expected populations in the gas phase at 323 K (temperature of deposition of the matrix of the product of thermolysis of the azirine **7**). *Bottom panels:* spectrum of matrix isolated isoxazole **9**. Bands marked with an asterisk are due to monomeric water impurity. Adapted from Ref. 26, Copyright 2009, with permission from Elsevier.

Another interesting study where matrix isolation infrared spectroscopy was shown to be instrumental to identify the structural nature of the compound under investigation was reported by Reva *et al.* [34], and deals with the identification of the most stable tautomer of maleic hydrazide and its preferred conformer in the gas phase. The matrix isolation experimental studies were complemented by a series of quantum chemical calculations.

The electronic energies for the different tautomers of maleic hydrazide (and their conformational states) were obtained at the QCISD level of theory (Table 12.1), which predicted the oxo-hydroxy conformer **13a** as the most stable form of the compound. The oxo-hydroxy conformer **13b** as well as the dihydroxy forms **14a**, **14b** and **14c** were predicted to be

higher in energy by 23.1, 20.3, 47.7 and 76.3 kJ mol<sup>-1</sup>, respectively, while the dioxo tautomer **15** was predicted to have a relative energy of 21.0 kJ mol<sup>-1</sup>.

**Table 12.1** Relative energies ( $\Delta E$ , kJ mol<sup>-1</sup>) of the isomeric forms of maleic hydrazide obtained using the electronic energies calculated at the QCISD/6-31++G(d,p) level and zero-point corrections obtained at the DFT(B3LYP)/6-31++G(d,p) level. Adapted from Ref. 34, Copyright 2012, with permission from Elsevier.

						
	<b>13a</b>	<b>13b</b>	<b>14a</b>	<b>14b</b>	<b>14c</b>	<b>15</b>
	oxo-hydroxy		dihydroxy			Dioxo
Symmetry	C <sub>s</sub>	C <sub>s</sub>	C <sub>2v</sub>	C <sub>s</sub>	C <sub>2v</sub>	C <sub>2</sub>
	0.0	23.1	20.3	47.7	76.3	21.0

The infrared spectrum of maleic hydrazide isolated in an Ar matrix was found to exhibit characteristic bands due to the stretching vibrations of the OH, NH and C=O groups, respectively at 3588, 3441 and 1708/1707/1699 cm<sup>-1</sup>. The presence of these characteristic bands indicates that the molecules of the compound exist in the matrix (and in the gas phase from where they were trapped in the cryogenic medium) as the oxo-hydroxy conformer **13a**. This conclusion is strongly supported by the good general agreement between the experimental IR spectrum and the spectrum theoretically predicted for **13a** (Figure 12.8), which demonstrates that **13a** is in fact the only species present in the matrix.

Why it is so that the oxo-hydroxy form **13a** is by far the most stable form of maleic hydrazide, while uracil, that is an isomer of maleic hydrazide with switched positions of one pair of NH and C=O groups, is known [35] to exist exclusively in the dioxo tautomeric form? The key structural feature to understand the high stability of structure **13a** is the presence of two vicinal nitrogen atoms in the pyridazine ring of the maleic hydrazide molecule. The same hybridization at these two nitrogen atoms is strongly destabilizing to the system [36]: in the dihydroxy tautomer **14**, energy rises due to repulsion of lone electron pairs at the nitrogen atoms, while in the dioxo tautomer **15**, repulsion of the positively loaded hydrogen atoms of the two NH groups strongly destabilizes the system. Only in the oxo-hydroxy **13**, the destabilizing repulsive effects (described above) are replaced by an energy-lowering, attractive interaction between the hydrogen atom of the NH group and the lone electron pair of the other nitrogen atom.

Conformer **13a** is more stable than **13b** because in the first case two stabilizing interactions, of O–H···N and N–H···O types, exist, while in **13b** the stabilizing O–H···N interaction is replaced by the destabilizing H–O···N repulsion.

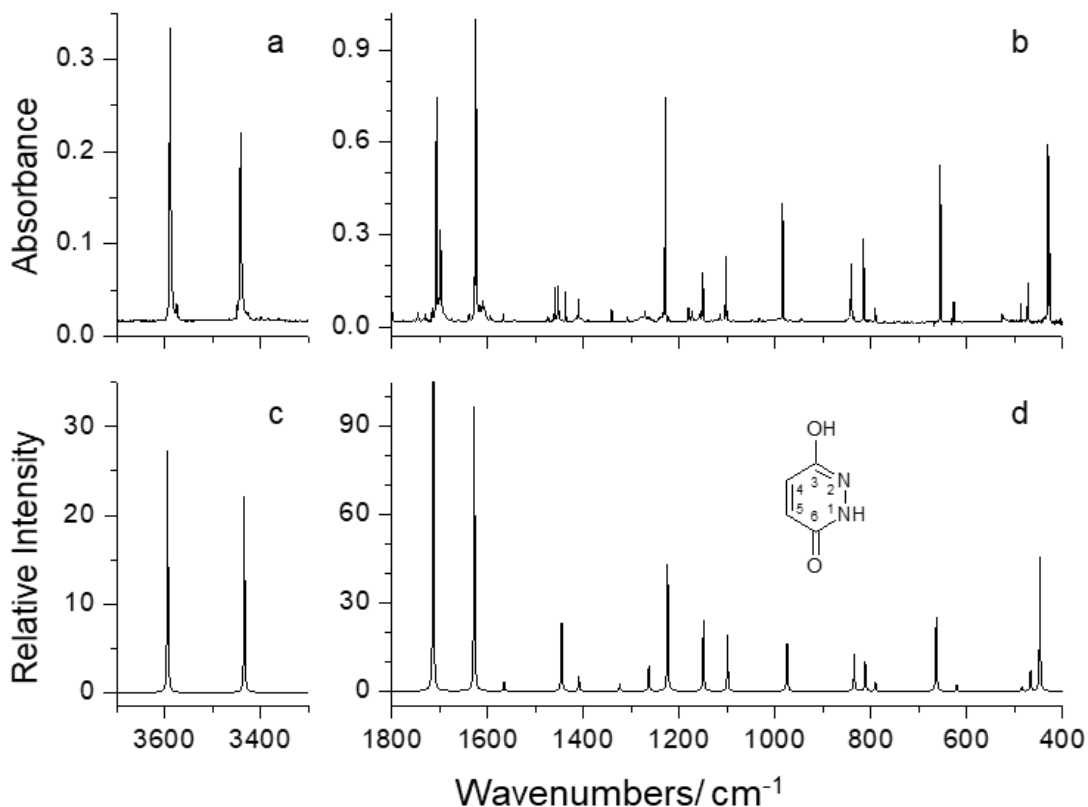


**Figure 12.8** Top panels (a,b): Experimental IR spectrum of maleic hydrazide isolated in an argon matrix at 15 K. Bottom panels (c,d): Theoretical IR spectrum of maleic hydrazide isomer **13a** calculated at the DFT(B3LYP)/6-31++G(d,p) level and scaled by 0.950 (c) and 0.975 (d). Adapted from Ref. 34, Copyright 2012, with permission from Elsevier.

A type of systems for which matrix isolation infrared spectroscopy has been used very successfully to structural elucidation comprehends heterocyclic molecules bearing hydroxyl or methoxyl ring-substituents. These molecules most often have conformers whose structures differ only in the orientation of the substituent relatively to the molecular framework and that possess very similar energies. Also, frequently in these cases the vibrational spectra of the individual conformers are very much similar. The high spectral resolution achieved under matrix isolation conditions then becomes instrumental for structure characterization.

Methoxy-substituted indoles in position C5 or C6 have been studied by Lopes Jesus *et al.* [37,38]. Both molecules possess two conformers differing in the orientation of the methoxyl

substituent, whose energies have been estimated theoretically to be within 4 kJ mol<sup>-1</sup> (Figure 12.9).

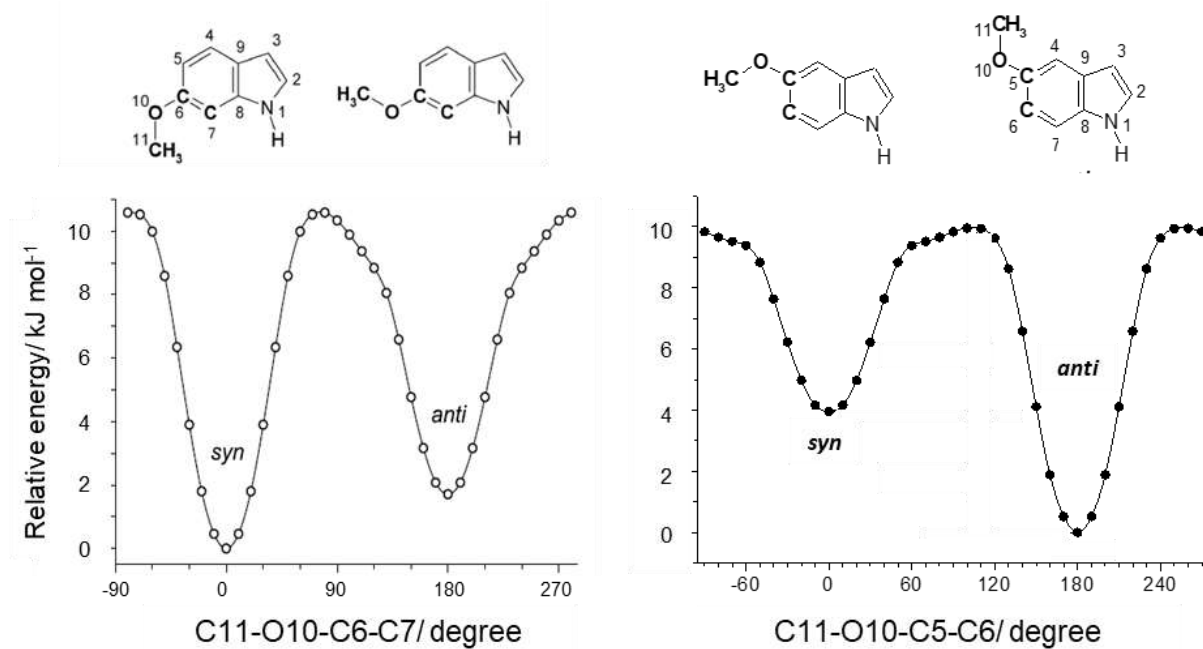


**Figure 12.9** DFT(B3LYP)/6-311++G(d,p) calculated potential energy profiles for internal rotation of the methoxyl substituent in 6-methoxyindole (*left*) and 5-methoxyindole (*right*). Adapted from ref. 37, with permission from AIP publishing. Adapted with permission from ref. 38. Copyright 2017 American Chemical Society.

The IR spectra of compounds isolated in noble gas matrices recorded immediately after isolation are represented in Figures 12.10 and 12.11. For 5-methoxyindole, a theoretical infrared spectrum of the gas-phase conformational mixture at 298.15 K, built based on the results of B3LYP/6-311++G(d,p) harmonic vibrational calculations carried out for the two conformers, with the infrared intensities calculated for each one of them scaled by the respective gas-phase Boltzmann population estimated at the same level of theory (80% *anti*; 20% *syn*), shows a very good agreement with the experimental spectrum (see Figure 12.10), indicating that both conformers are present in the matrix and also that their energy difference shall be very close to the predicted one. The experimental confirmation of the higher stability of the *anti* conformer was obtained by annealing the matrix up to 40 K, which resulted in conversion of the higher energy *syn* conformer into the most stable *anti* form, as shown in Figure 12.12.

For 6-methoxyindole, the infrared spectra of the as-deposited matrices (argon; xenon) also clearly reveal presence of both *anti* and *syn* conformers (see Figure 12.11). The performed annealing experiments confirmed that in this molecule the *syn* conformer corresponds to the most stable form, as predicted by the calculations. Indeed, during the annealing experiments

(xenon matrix), when the sample temperature reached 34 K, the intensity of the bands assigned to the *anti* conformer started to decrease, and concomitantly the bands ascribed to the *syn* form increased (Figure 12.13), which is an irrefutable evidence for occurrence of the *anti* → *syn* relaxation, thus confirming that *syn* is in fact the most stable conformer.

For both molecules, the relative stability of the conformers could be explained by determining the orbital stabilization interaction energies according to the Natural Bond Orbital Theory [39]. These results revealed that the most significant stabilizing effect comes from the  $Lp2(O10) \rightarrow \pi^*(C6C7)$ , in 5-methoxyindole, or  $Lp2(O10) \rightarrow \pi^*(C4C5)$ , in 6-methoxyindole, conjugative interactions.

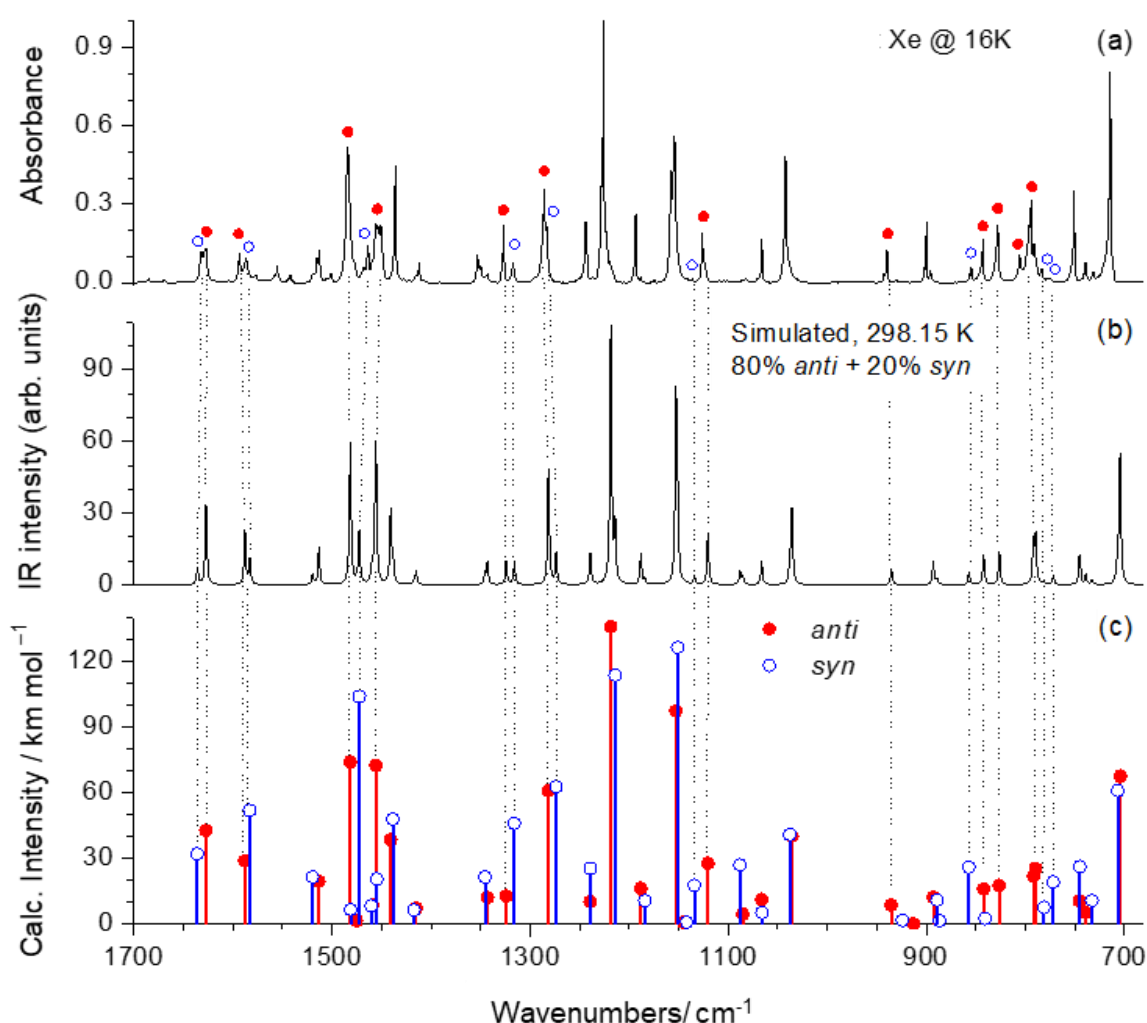


**Figure 12.10** *Top panel* (a): Experimental IR spectrum of 5-methoxyindole recorded immediately after isolating the compound in a low temperature xenon matrix at 16 K. *Middle panel* (b): Simulated IR spectrum of the gas-phase conformational mixture at 298.15 K, weighted by the calculated Boltzmann populations at 298.15 K for the conformers (80 % *anti* + 20 % *syn*). *Bottom panel* (c): Individual stick spectra calculated for the *anti* (closed red

circles) and *syn* (open blue circles) conformers at the B3LYP/6-311++G(d,p) level. Adapted with permission from ref. 38. Copyright 2017 American Chemical Society.

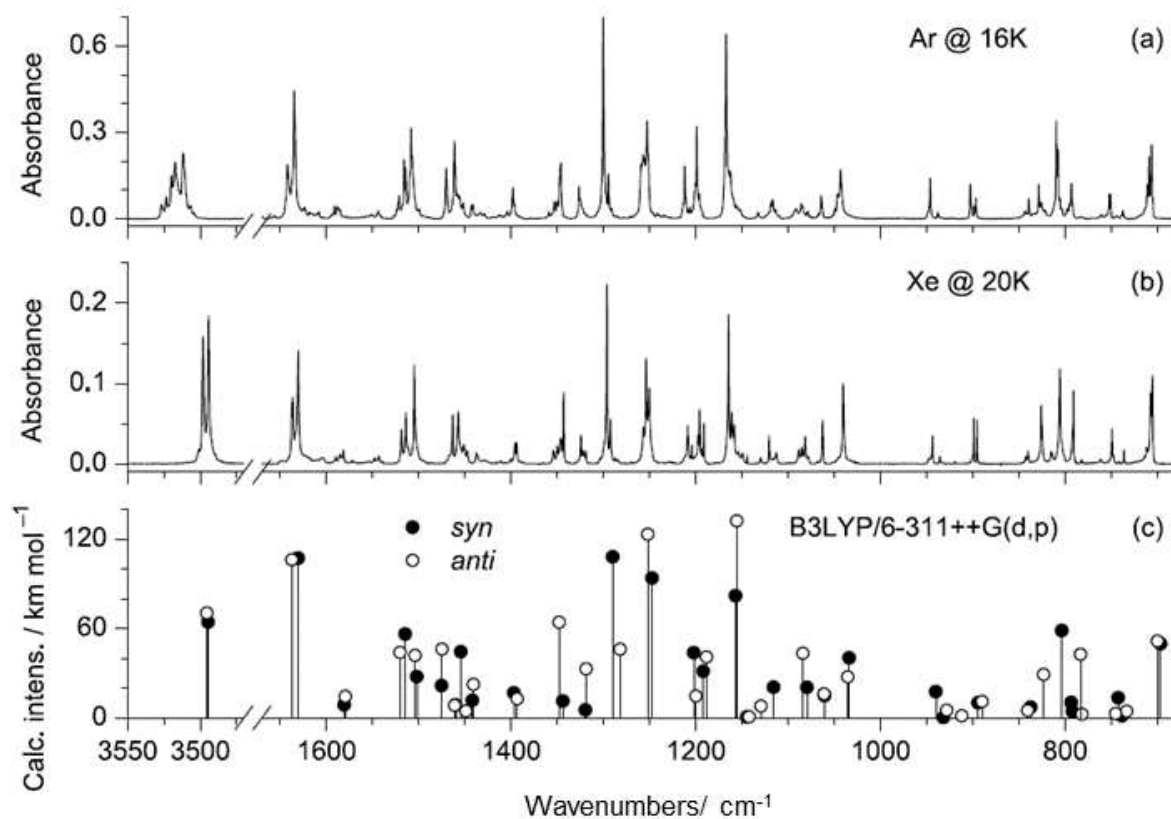


**Figure 12.11** Top and middle panels: Experimental IR spectrum of 6-methoxyindole isolated in an argon matrix at 16 K (a), or a xenon matrix at 20 K (b). Bottom panel (c): Theoretical spectra of the *syn* and *anti* conformers calculated at the B3LYP/6-311++G(d,p) level. Adapted from ref. 37, with permission from AIP publishing

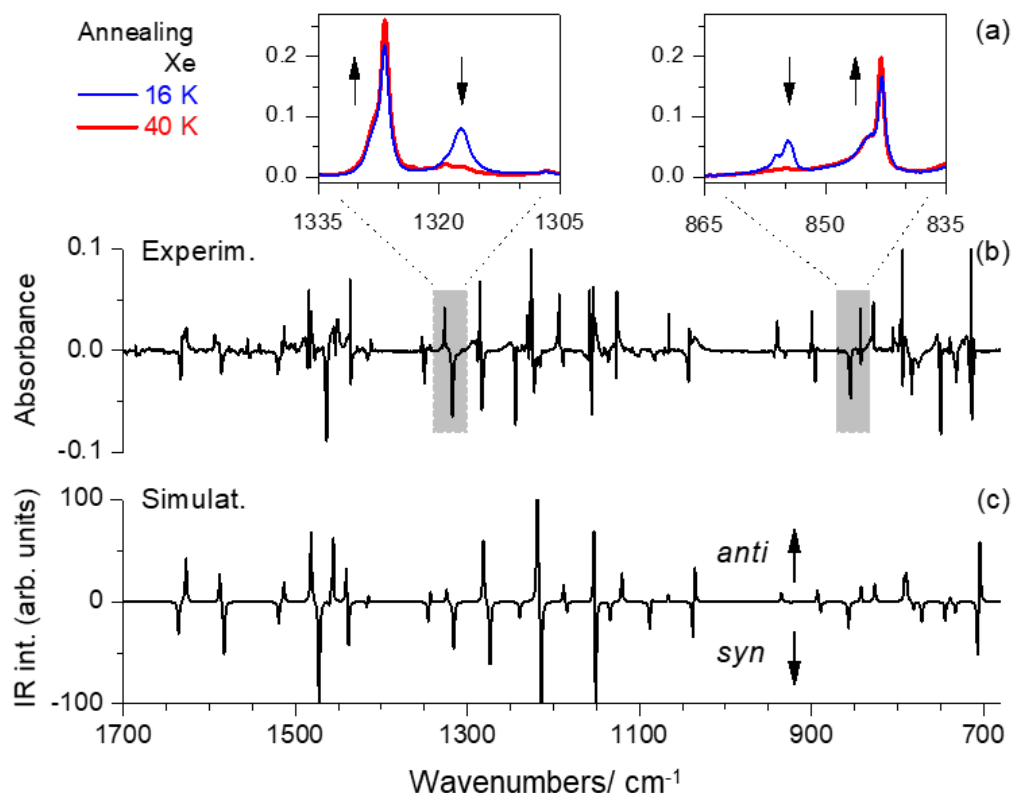


**Figure 12.12** Top panels (a): Fragments of the IR spectra of the as-deposited matrix of 5-methoxy-indole, at 16 K, and the same sample after annealing to 40 K. Middle panel (b): Experimental difference spectrum (40 K minus 16 K). Bottom panel (c): Simulated B3LYP/6-311++G(d,p) difference spectrum. Adapted with permission from ref. 38. Copyright 2017 American Chemical Society.

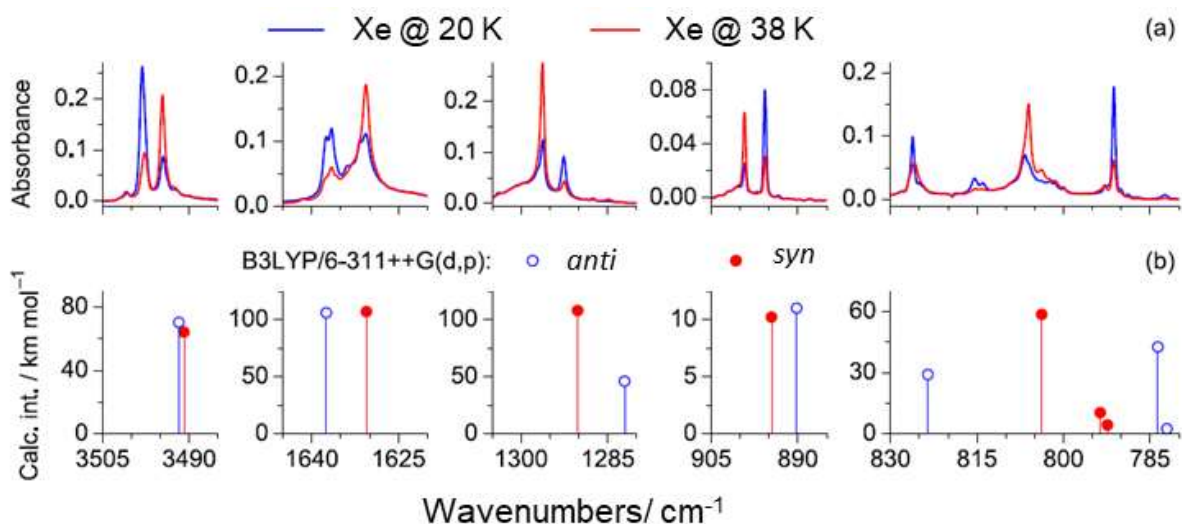


**Figure 12.13** Top panels (a): Selected spectral regions illustrating the changes taking place after annealing of 6-methoxyindole isolated in a Xe matrix from 20 K (red) to 38 K (blue). Middle panels (b): Theoretical spectra of



*syn* (open circles) and *anti* (closed circles) conformers of 6-methoxyindole calculated at the B3LYP/6-311++G(d,p) level of theory. Adapted from ref. 37, with permission from AIP publishing

### 12.3 UV-Induced Photochemical Reactivity

In the present section, illustrative examples on the UV-induced reactivity of heterocycles isolated in cryogenic matrices will be pinpointed. Special emphasis will be given on the capture of reactive intermediates, or elusive products, which allowed the establishment of mechanistic proposals or supported previous hypothesis.

The UV-induced photochemistry of heterocyclic compounds has been typically understood in terms of the chemistry of their  $\pi^* \leftarrow \pi$  or  $\pi^* \leftarrow n$  electronic excited states [40,41]. However, this paradigm was shifted in 2002, when Sobolewski *et al.* showed that dark  $\sigma^* \leftarrow \pi$  states featuring a dissociative character along a hydroxyl (OH) or azine (NH) group must also be taken into account [42]. Once populated, either by direct excitation from the ground electronic state or by interconversion from a  $\pi^* \leftarrow \pi$  state, these dark states can quickly relax back to their ground state, through a conical intersection, or follow its dissociative path and lose the labile hydrogen atom from the OH/NH groups. These predictions were later confirmed by photofragment translational spectroscopy studies on UV-induced indole molecules in supersonic jets, in which it was possible to detect fast and slow detached hydrogen atoms [43,44]. The co-fragment of the detached hydrogen atoms should be a radical species (the indolyl radical, for instance) and, to further support Sobolewski's hypothesis, such radicals species should be captured and experimentally characterized. The matrix isolation technique was originally conceived for this exact goal (capture of free radicals) [1,2,45], and thus appeared as a promising technique to address this question. This was indeed the motivation behind the study of the photochemistry of matrix-isolated indole reported recently by Reva *et al.* [46].

Deposition of indole with a large excess of either argon or neon at 15 K or 5 K, respectively, and monitorization by IR spectroscopy, reveal the sole presence in the matrices of the 1*H*-indole tautomeric form. This was particularly evident by the intense and characteristic  $\nu(\text{NH})$  stretching and  $\gamma(\text{NH})$  rocking bands found at 3523 and 395  $\text{cm}^{-1}$  in argon and at 3522 and 390  $\text{cm}^{-1}$  in neon matrices, respectively. Irradiations of the matrices with broadband light ( $\lambda > 270$  nm) led to the consumption of 1*H*-indole and formation of both the indolyl radical and the 3*H*-indole tautomer (Figure 12.14). The 1*H*-indole  $\rightarrow$  3*H*-indole tautomerization was interpreted as resulting from the recombination of the photodetached H-atom and indolyl radical formed initially. Studies on the gas-phase photochemistry of indole showed that the H-atom dissociation occurs to an extent that does not allow its back recombination with the indolyl radical [43]. However, as mentioned above, in matrix isolation conditions the two

photofragments are confined inside the same matrix site (cage effect) and, therefore, are most likely to recombine. Such a mechanism of phototautomeric reactions has recently been designated as photoinduced dissociation association (PIDA) and follows the Sobolewski's hypothesis [42,47].

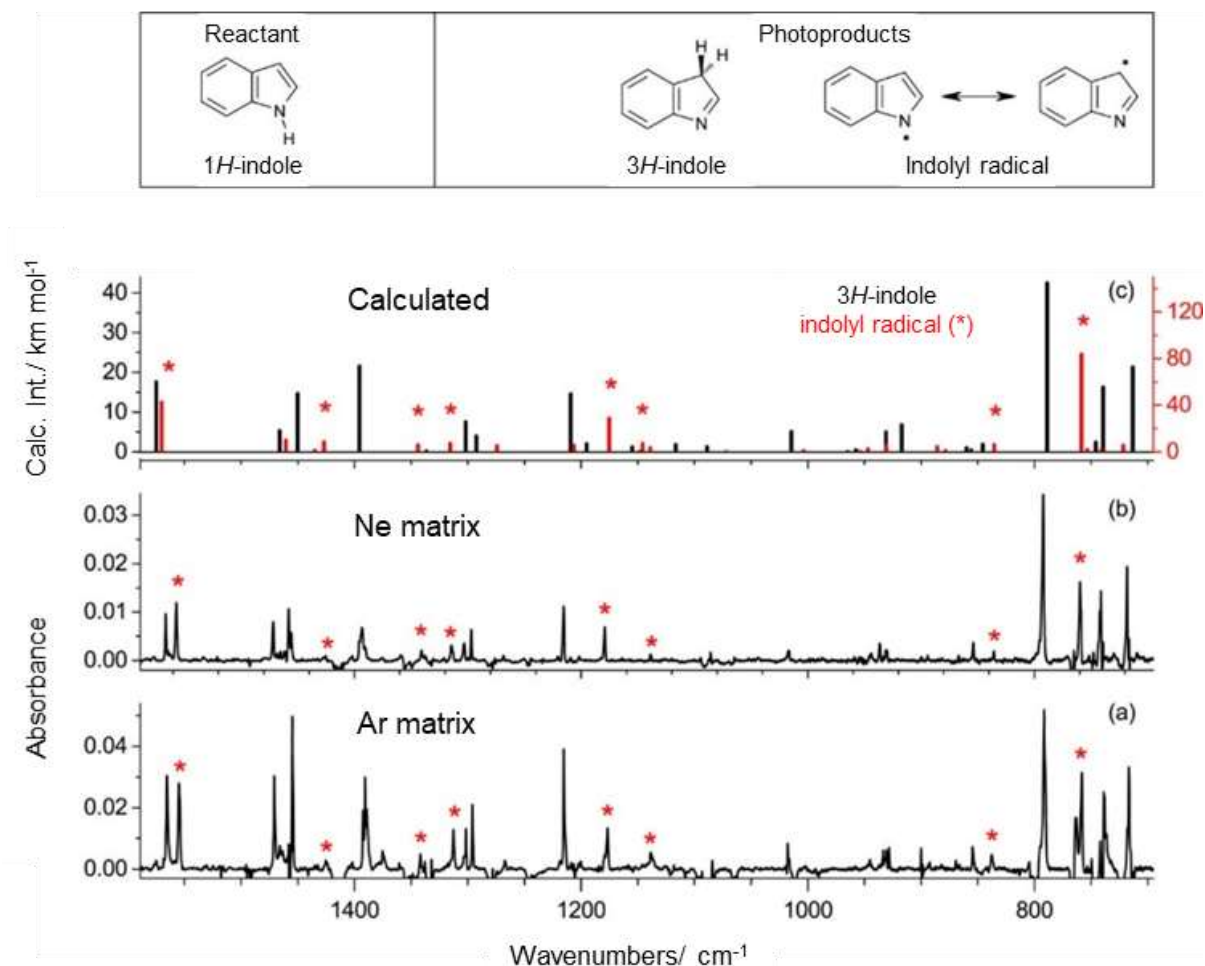


**Figure 12.14** *Bottom panels:* Infrared spectra of photoproducts generated upon UV ( $\lambda > 270$  nm) irradiation of indole monomers isolated in Ar (a) and Ne(b) matrices, compared with the calculated spectra of 3H-indole (black) and indolyl radical (red) (c). The *top panel* shows the structures of the different species. Adapted from ref. 46, with permission from AIP publishing.

A detailed theoretical analysis of the electronic structure of the indolyl radical was carried out by natural bond orbital (NBO) analysis. The indolyl radical is a doublet species with one unpaired electron. However, the unpaired electron is not located at the N1 position from where the H-atom has been detached (as one could intuitively expect), but otherwise it is delocalized along the entire structure. The natural spin density calculations provided a picture of where it

is most likely to find this electron, in this case, at the C3 center (+0.538; Figure 12.15), which shall justify the tendency for the recombination at this position and formation of 3*H*-indole.

The formation of the 3*H*-tautomer together with radical species is a common trend in the photochemistry of indole derivatives isolated in cryogenic matrices, and has been observed also, for instance, for 3-formylindole [46], 4-, 5- and 6-methoxyindoles [48,49], and even in the case of 7-azaindole [50]. It is worth mentioning that in the latter case, the 7*H*-azaindole tautomer has been identified as a photoproduct of 7-azaindole isolated in an argon matrix, but not for this compound isolated in a hydrogen (n-H<sub>2</sub>) matrix. In fact, it seems that phototautomeric reactions occurring by the PIDA mechanism are highly dependent on the matrix host, since some materials are more prone to restrict the radical and the H-atom inside the same cage than others [51]. Globally, the results that emerge from these studies support the earlier predictions by Sobolewski and coworkers and are consistent with the results obtained by photofragment translational spectroscopy.

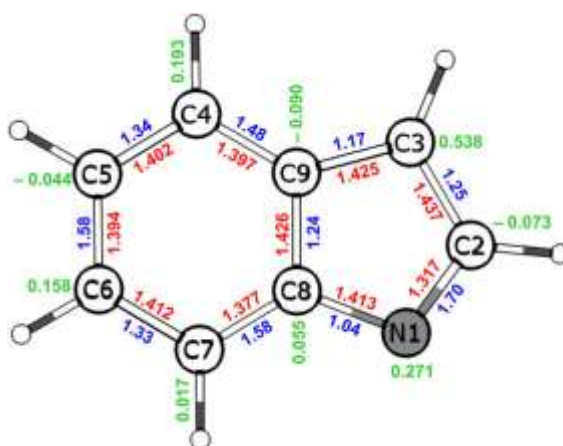


**Figure 12.15** Optimized C–C and N–C distances in Å (red), natural bond orders (blue), and natural spin densities (green) calculated for the indolyl radical at the B3LYP/6-311++G(d,p) level. Adapted from ref. 46, with permission from AIP publishing

Photoreactivity of cytosine has also been the subject of recent investigations using matrix isolation. Cytosine is a biologically relevant compound whose photochemistry is mainly governed by reactions involving hydrogen atoms. Spectroscopic studies on cytosine in the gas phase showed the existence of multiple cytosine tautomers. However, its exact number is still somewhat controversial [52]. While the identification of the amino-oxo isomer (**AO**) and the amino-hydroxy form (**AH**) is consistent through the use of several spectroscopic techniques [52-56], experimental evidence for the imino-oxo (**IO**) form has been very scarce and preliminary [52,55]. Recently, Lapinski *et al.* were able to successfully bring further support to the characterization of the elusive cytosine **IO** tautomer, in a photochemical study of the matrix-

isolated compound where tunable monochromatic radiation was used as excitation source. This approach not only provided the infrared spectra separation of the three major cytosine tautomers (**AO**, **AH** and **IO**), but also allowed to distinguish the vibrational signatures of the two possible isomeric forms of the tautomers **AH** (conformers **AH1** and **AH2**) and **IO** (*E* and *Z* isomers **IO1** and **IO2**) (Figure 12.16) [57].

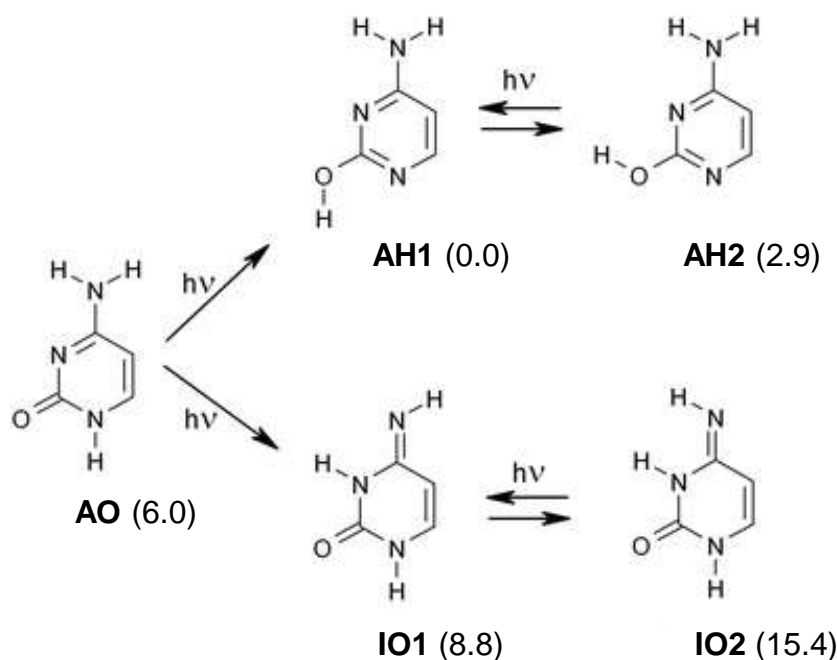


**Figure 12.16** UV-induced hydrogen-atom-transfer processes converting the amino-oxo tautomer of cytosine into the amino-hydroxy and imino-oxo forms. The numeric values shown in parentheses are the relative energies of the different forms expressed in kJ mol<sup>-1</sup>. Adapted from ref. 57 with permission from the PCCP Owner Societies.

According to quantum mechanical computations on the relative stability of cytosine isomers (see Figure 12.16) [57,58], one could expect **AH1** and **AH2** to dominate in the gas-phase, **AO** and **IO1** to have minor populations, and **IO2** to be present only in a trace amount. Deposition of cytosine vapors with a large excess of argon results in a matrix containing a mixture of cytosine isomers, whose exact nature could be identified through a series of photochemical experiments resulting in the separation of the infrared signatures of the different isomers.

Upon irradiations at  $\lambda = 314\text{--}312$  nm, the change in the intensity of a low- and of a very low-intensity set of bands in the infrared spectrum was observed, while the most intense set of bands remained unchanged. The reactive sets were assigned to **IO1** (consumed) and to **IO2** (produced), based on the comparison of the experimental data with the calculated IR spectra for the whole set of isomers shown in Figure 12.16. The observed reaction involves the *E*→*Z* isomerization of the imino group in the **IO** tautomer, which typically takes place due to a conical intersection between the *S*<sub>1</sub> and *S*<sub>0</sub> electronic states at the geometry where the hydrogen atom is nearly perpendicular to the C=N bond [59]. Interestingly, the depletion of **IO1** was never absolute,

indicating that a photostationary state between the two **IO** isomers was established, although dependent on the wavelength of irradiation.

Remarkably, the hypsochromic shift of the source of irradiation by 1 nm, to  $\lambda = 311$  nm, drastically changed the outcome of the photochemistry. At this wavelength, the IR bands ascribable to the **AO** form quickly lost their intensity and the bands due to all **IO1**, **IO2**, **AH1** and **AH2** forms increased (Figure 12.17).

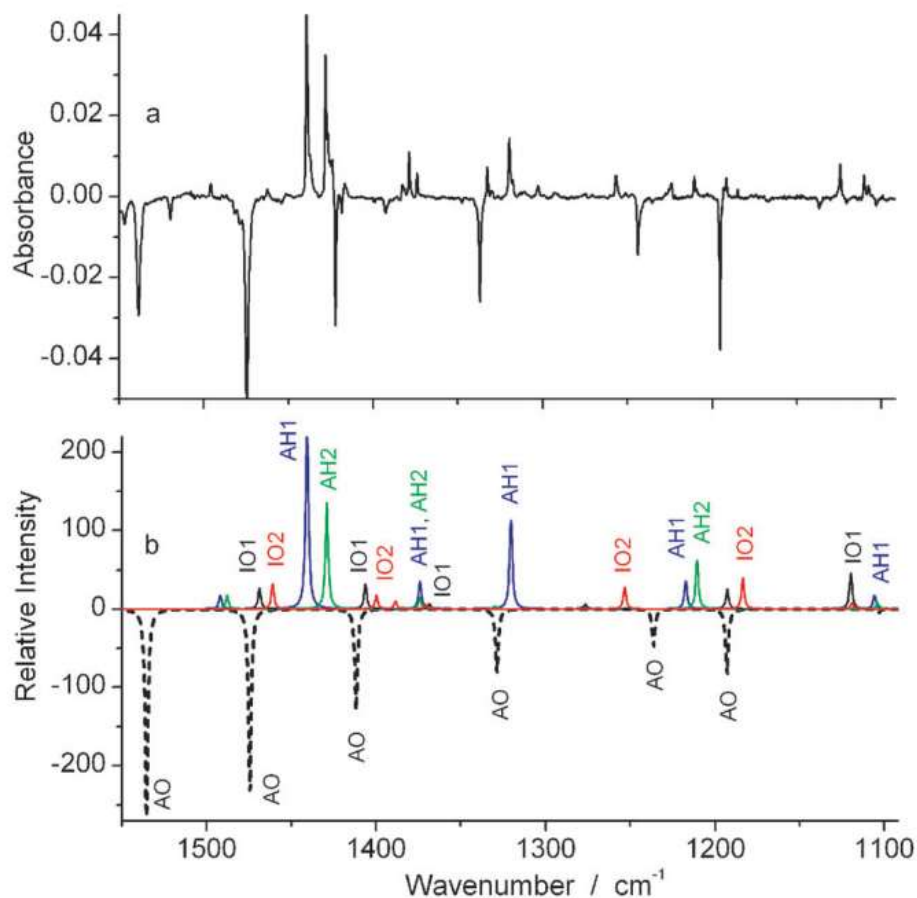


**Figure 12.17** Phototransformation of the **AO** tautomer of matrix-isolated cytosine into the **AH1**, **AH2**, **IO1** and **IO2** forms. (a) Subtraction result: experimental spectrum recorded after UV irradiation at 311 nm *minus* that recorded after the previous UV irradiation at 312 nm; (b) DFT(B3LYP)/6-31++G(d,p) simulated spectra for **AH1** (blue), **AH2** (green), **IO1** (black solid line), **IO2** (red) and **AO** (black dashed line) isomers of cytosine. Intensities in the theoretical spectra have the following weights: 2 for **AH1**, 1 for **AH2**, **IO1** and **IO2**, and  $-5$  for **AO**. Adapted from ref. 57 with permission from the PCCP Owner Societies.

It was suggested that not all photoproducts are necessarily the result of a primary reaction, but most likely are due to an initial oxo-hydroxy (**AO**→**AH1**) or amino-imino (**AO**→**IO1**) isomerization, followed by partial conversions to **AH2** and **IO2** by rotation around the C-O or C=N bonds, respectively. The initial consumption of the **AO** isomer might also take place along the repulsive  $\pi\sigma^*$  states, following the common trend of heterocyclic compounds containing azine (NH) [42] or amine (NH<sub>2</sub>) [60] groups. Analogous photoreactions were also found for cytosine derivatives isolated in cryogenic matrices, namely 1-methyl-, 5-methyl-, and 5-fluorocytosine [61,62].

In a final stage of irradiation (at  $\lambda = 300$  nm), the **AO** isomer was totally consumed, and the matrix was left with **AH** and **IO** isomers. At the **IO1/IO2** photostationary state resulting from those irradiations, **IO2** was left in a majority amount. However, subsequent irradiations at  $\lambda = 311$  nm disturbed the equilibrium and were found to lead to **IO1** at the cost of **IO2**, proving the photo reversibility of the **IO1**↔**IO2** reaction and providing a clear picture of the IR spectrum of each isomer (Figure 12.18).

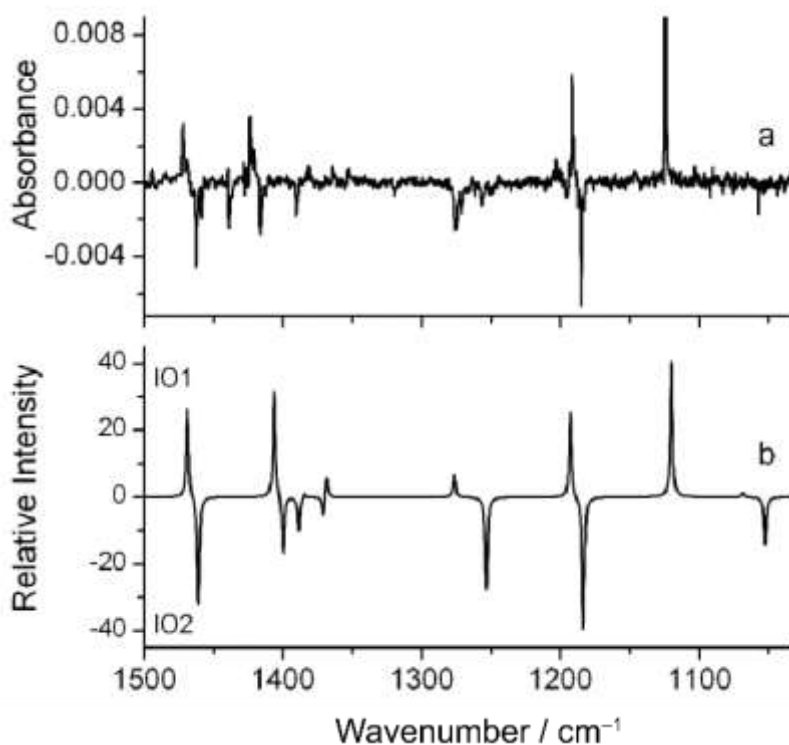


**Figure 12.18** Identification of **IO1** and **IO2** imino-oxo isomers of cytosine: (a) difference spectrum, obtained by subtraction of the spectrum recorded after UV ( $\lambda = 300$  nm) irradiation from the spectrum recorded after the subsequent UV ( $\lambda = 311$  nm) irradiation; (b) subtraction result: spectrum theoretically simulated for the **IO1** form *minus* the spectrum simulated for **IO2**. Adapted from ref. 57 with permission from the PCCP Owner Societies.

Concomitantly to the main reactions mentioned above, the consumption of **AO** also led to the appearance of a low-intensity and structured band in the 2300–2230  $\text{cm}^{-1}$  region, ascribable to the antisymmetric stretching of an isocyanate group. The amount of this isocyanate photoproduct in the matrix, which results from the cytosine ring opening, must be low, since the IR band corresponding to this type of vibration is characterized by their usual very high intensity (usually larger than 1000  $\text{km mol}^{-1}$ ) [63]. Controlled interconversion between **AH1** and **AH2** forms could also be successfully attained in the described study [57]. However, this was achieved by use of narrowband IR irradiations and will be discussed in detail in Section 12.5, which focuses on IR-induced processes.

Although it has been proven to be fundamental for a better understanding of the photochemistry of heterocycles, the model proposed by Sobolewski and coworkers is obviously not applicable for compounds that do not have any XH group ( $X = \text{O}, \text{N}, \text{NH}$ ). In that case, it is often seen that the photochemistry is centered on the cleavage of bonds formed by the ring heteroatoms. The photochemical behavior of the tetrazole moiety, a five-membered aromatic heterocyclic ring, is a good example.

Tetrazoles possess a very rich photochemistry, although strongly dependent on the ring substituents. Our group has been engaged in the study of the photochemistry of tetrazoles for many years. Here, our attention will be mainly focused in a recent case study, which will serve as an illustrative example [64]. For those interested in a more comprehensive analysis on the photochemistry of matrix-isolated tetrazoles, we encourage the reading of the reviews that can be found elsewhere [19,65].

Tetrazoles may exist in multiple tautomeric forms, depending on the ring substituents and the environment conditions. In the crystalline phase, the parent tetrazole **16** (see Figure 12.19) was found to exist exclusively in its *1H*-form, whereas in the gas-phase as the most stable *2H*-form [66]. Early studies on the photochemistry of matrix-isolated tetrazole **16** were conducted by Maier *et al.*, in 1996, and showed that *2H*-tetrazole was the tautomer trapped in argon at 12 K [67]. Thereafter, irradiation of the matrix at 193 nm induced  $\text{N}_2$  elimination and production of nitrile imine **17**, diazomethane **18**, carbodiimide **19** and cyanamide **20** (plus an  $\text{HCN}\cdots\text{NH}$  complex). The nitrile imine **17** was assigned as the primary photoproduct, since its bands were observed to grow up promptly in the first minutes of irradiation and, after 10 minutes, seen to start reducing of intensity. Subsequent irradiations of the matrix, with a low-pressure mercury lamp coupled to a vycor filter ( $\lambda = 254 \text{ nm}$ ), consumed the totality of **17** and produced the remaining photoproducts **18–20** (Figure 12.19).

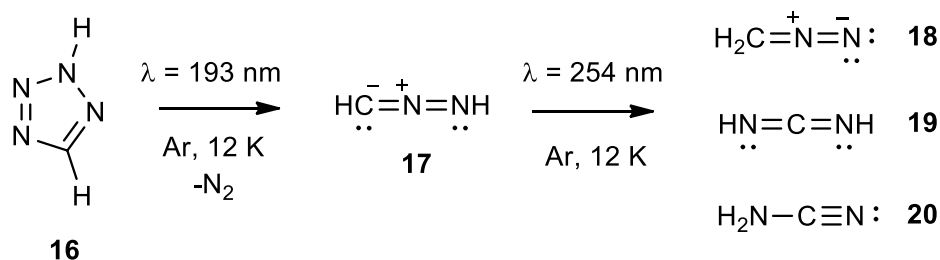


**Figure 12.19** Summary of the experimental observations for the photochemistry of tetrazole **16** isolated in a low-temperature argon matrix at 12 K [67].

These were very interesting results, not only because the detection of **17**, a species that for long remained elusive (despite the elusiveness of nitrile imine **17** until that point in time, Huisgen *et al.* had shown, in 1959, the formation of substituted nitrile imines as key intermediates in the thermolysis of 2,5-disubstituted tetrazoles [68]), was finally successful, but mostly because it opened doors for the detailed characterization of other nitrile imines, molecules that are of major practical application as reactants in 1,3-dipolar cycloaddition reactions [69,70]. The nitrile imines are in fact very intriguing species, because they may be described as a combination of multiple resonance structures (Figure 12.20), whose relative importance differs depending on its substituents. In 2012, Bégué and coworkers have characterized a series of nitrile imines, produced by either thermolysis or photolysis of tetrazoles [71]. They concluded that nitrile imines owning  $\nu_{\text{as}}(\text{CNN})$  modes with IR absorptions above  $2200 \text{ cm}^{-1}$  are described as essentially propargylic structures, (for example, diphenyl-nitrile imine PhCNNPh), whereas those with IR absorptions below  $2200 \text{ cm}^{-1}$  are predominantly of allenic character (*e.g.*, the parent nitrile imine **17**, HCNNH, or phenyl-nitrile imine PhCNNH). Moreover, it was also suggested that electronegative substituents with lone-pair donating groups, such as F,  $\text{NR}_2$  or OR (R= alkyl), should stabilize the carbenic structure of nitrile imines [72]. On the light of these predictions, we have investigated the photochemistry of matrix-isolated 5-aminotetrazole on a quest for experimental evidence of existence of carbenic nitrile imines [64].

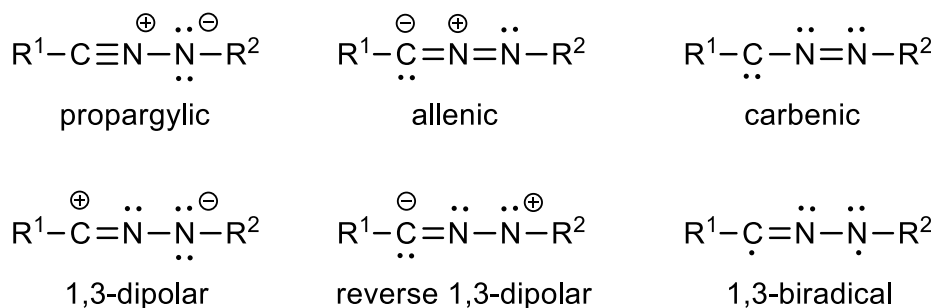


**Figure 12.20** Different resonance forms that can represent the structure of a nitrile imine. Adapted from ref. 64 with permission from John Wiley and Sons. Copyright 2020 WILEY-VCH Verlag GmbH & Co. KGaA, Weinheim.



Similarly to the studies on the simplest tetrazole **16**, only the 2*H*-form of 5-aminotetrazole **21** (Figure 12.21) was found in an argon matrix at 15 K. Irradiation of the matrix at  $\lambda = 220$  nm during 120 s consumed roughly 50 % of the tetrazole to yield C-amino nitrile imine **22** as primary photoproduct. After the initial 120 s, the IR bands assigned to **22** in the spectra of the irradiated matrix stopped growing, while many others continue to increase in intensity. These bands could be assigned to methylene imine **23**, 3-amino-1*H*-diazirine **24**, 1-aminocarbodiimide **25** and hydrogen isocyanide **26**, which were identify as secondary photoproducts. Subsequent irradiations performed at  $\lambda = 330$  nm, a wavelength at which **21** does not absorb, consumed the primary product **22** and populated photoproducts **23-25**, as monitored by IR spectroscopy (Figure 12.22).

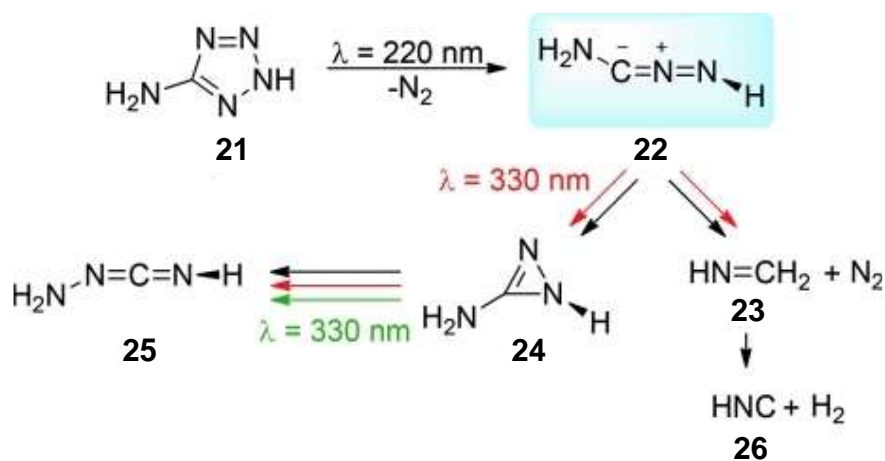


**Figure 12.21** Summary of experimental observations in the UV-induced photochemistry of 5-amino-2*H*-tetrazole **21** isolated in an argon matrix: Generation of C-amino nitrile imine **22** and its photochemical transformation into **25** via **24** and decomposition to **23**. The colors of the arrows are related to different wavelengths and irradiation stages:  $\lambda = 220$  nm (black),  $\lambda = 330$  nm first stage (red), and  $\lambda = 330$  nm second stage (green). Adapted from ref. 64 with permission from John Wiley and Sons. Copyright 2020 WILEY-VCH Verlag GmbH & Co. KGaA, Weinheim.

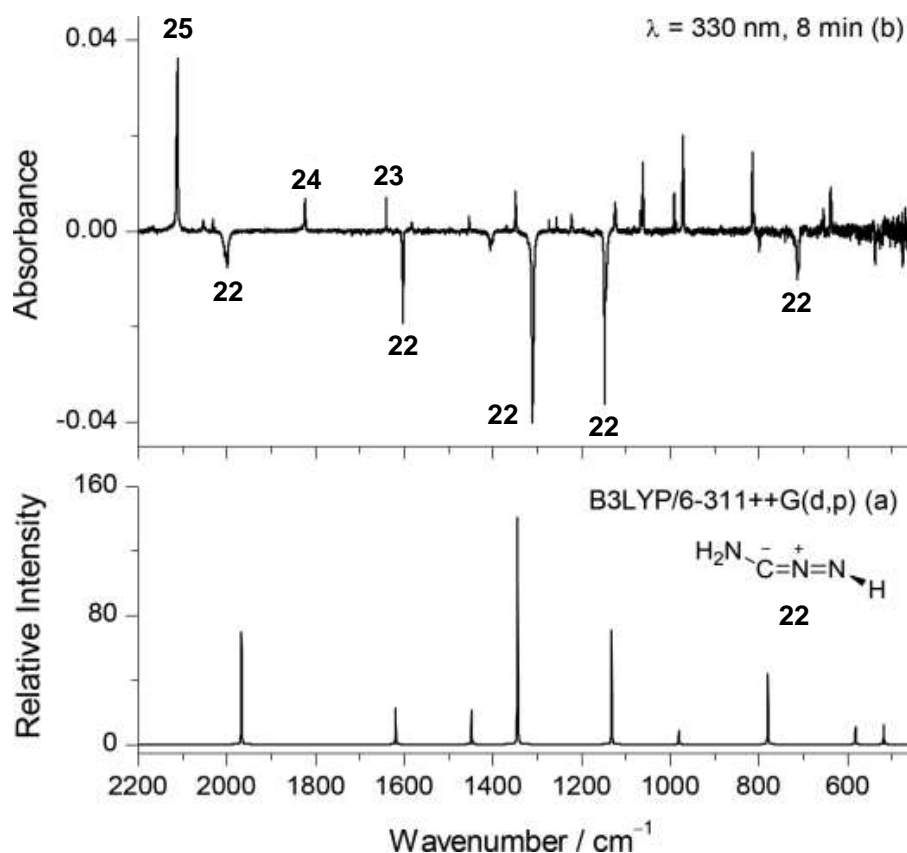


**Figure 12.22** (a) IR spectrum of *C*-amino nitrile imine **22** simulated at the B3LYP/6-311++G(d,p) level of theory. (b) Experimental difference IR spectrum showing changes after irradiation at  $\lambda = 330$  nm (8 min, 35 mW) in an argon matrix (subsequent to the initial irradiation of **21** at  $\lambda = 220$  nm; see Figure 12.21). The negative bands are due to the consumed photoproduct **22**. The positive bands are due to photoproducts **23–25**. Adapted from ref. 64 with permission from John Wiley and Sons. Copyright 2020 WILEY-VCH Verlag GmbH & Co. KGaA, Weinheim.

The reactivity of **22** must follow two distinct paths: i) cyclic rearrangement to the 3-membered ring **24** and ii) C-N bond cleavage to yield the decomposition photoproduct **23** and N<sub>2</sub>. 1-aminocarbodiimide **25** must not be a direct product of **22**, but rather produced at the cost of **24**. In fact, upon the total consumption of **22**, additional irradiations at 330 nm led to the selective conversion of **24** into **25**. Intermediacy of an 1*H*-diazirine in the conversion of a nitrile imine to the corresponding carbodiimide isomeric species was initially observed in the study of the photochemistry of matrix-isolated 5-methyltetrazole [73]. Furthermore, 1*H*-diazirines had also been previously identified as photoproducts of tetrazole derivatives by Gómez-Zavaglia *et al.* in their pioneering photochemistry studies of matrix-isolated 5-methoxy-1-phenyl-1*H*-tetrazole [74]. Additional studies on this topic, in particular dealing with the photochemistry of 1- and 2-methyl-5-aminotetrazoles, can be found elsewhere [75].

Unlike many other nitrile imines, the  $\nu_{\text{as}}(\text{CNN})$  mode of **22** was observed below 2000 cm<sup>-1</sup> (at *ca.* 1998 cm<sup>-1</sup>). This feature triggered a detailed theoretical characterization of this species,

carried out using natural resonance theory (NRT) calculations. It was found that for **22** the weight of the carbenic resonance structure amounts to 20 %, contrasting to the 0 % amount in the parent nitrile imine **17** and C-methyl nitrile imine [64].

Another type of molecules whose UV-induced photochemistry is initiated by the cleavage of a bond containing a heteroatom is the isoxazole family of compounds. The photochemical study of isoxazole derivatives has received significant attention from the scientific community for a long time. It has been demonstrated that the main reactive channel involves the isoxazole  $\rightarrow$  oxazole isomerization, mediated by a 2*H*-azirine intermediate [76-78]. However, only recently experimental results on the photochemistry of unsubstituted isoxazole **27** isolated in cryogenic matrices were reported [79].

Monomeric isoxazole **27** (Figure 12.23) isolated in an argon matrix at 15 K was found to react slowly by narrowband irradiation at  $\lambda = 238$  nm. The initial 70 minutes of irradiation consumed 10 % of **27** and led exclusively to its photodecomposition, yielding ketene **28** and hydrogen cyanide **29**. Irradiations of the matrix at shorter wavelength,  $\lambda = 221$  nm, not only led to enhance the reaction kinetics (10 % of **27** was consumed in only 1 minute), but also to an appearance of multiple new bands in the IR spectrum (Figure 12.24). The new photoproducts were assigned as 2-formyl-2*H*-azirine **30**, 3-formylketenimine **31**, 3-hydroxypropenenitrile **32**, imidoylketene **33**, and 3-oxopropanenitrile **34**. Photoproducts **30** and **31** were formed in a first stage as the primary photoproducts of isoxazole, since the bands assigned to this species reached their maxima intensity in the first minutes of irradiation (unlike the others). It was argued that vinylnitrene **I** must intermediate their formation. Indeed, the formation of 2-formyl-2*H*-azirine **30** must be intermediated by the singlet-state vinylnitrene **I**, which is the first species to be formed upon the cleavage of the isoxazole N-O bond. The singlet-state **I** has a 1,3-diradical character, and its isomerization to **30** only requires the closure of the N-C-C angle. On the other hand, 3-formylketenimine **31** should be formed by an [1,2]H-shift reaction in the ground electronic triplet-state **I**. The vinylnitrene **I** play a pivotal role in the theoretical models proposed to explain the reactivity of isoxazoles, as will be shown in Section 12.4 [80].

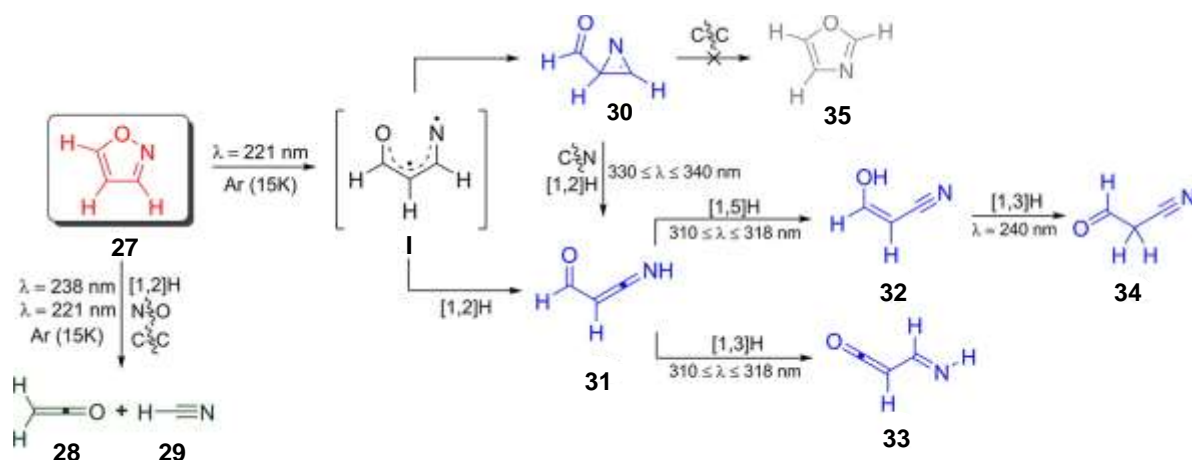


**Figure 12.23** Summary of experimental observations and the mechanistic proposal for the UV-induced photochemistry pathways of isoxazole **27** isolated in a low-temperature argon matrix. Structures given in blue possess different conformers (for simplicity not shown in the figure). Adapted with permission from ref. 79. Copyright 2017 American Chemical Society.

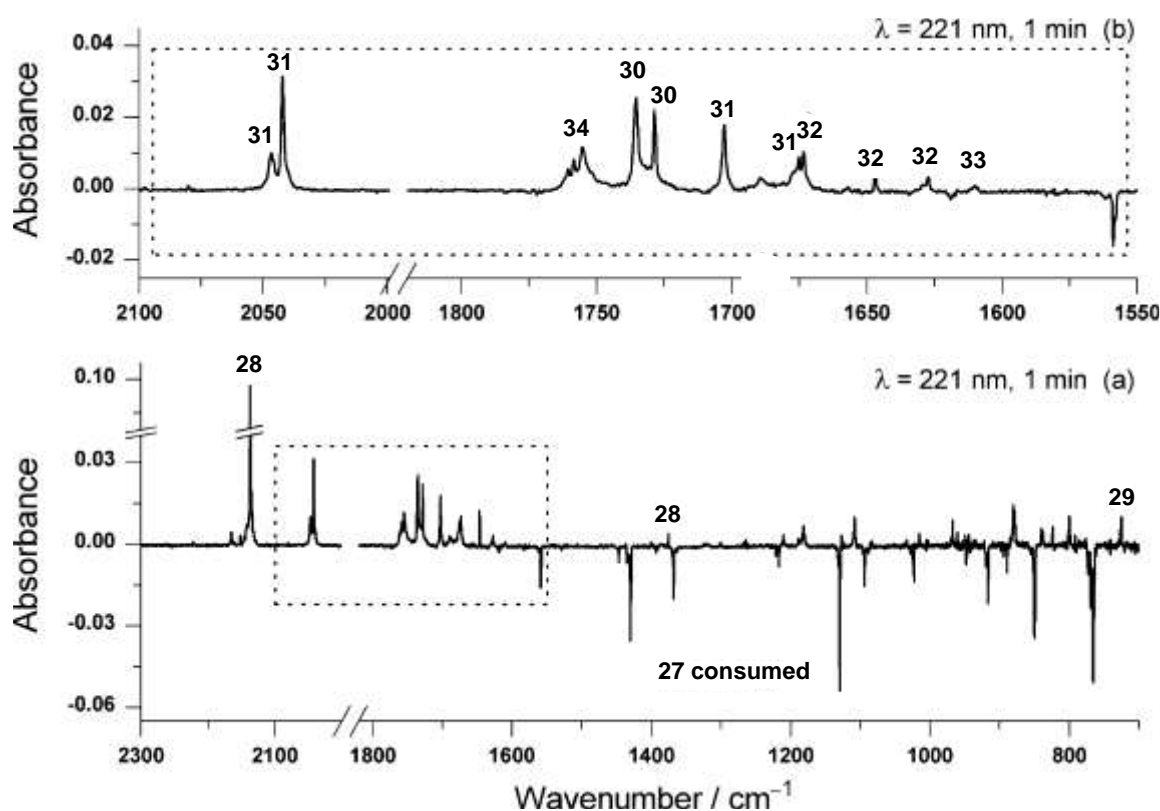


**Figure 12.24** (a) Experimental difference IR spectrum: spectrum obtained after UV-laser irradiation at  $\lambda = 221$  nm (1 min) of isoxazole **27** in argon matrix *minus* the spectrum of the sample before irradiation (as deposited matrix). Positive labeled bands are due to ketene **28** and hydrogen cyanide **29**. (b) Expanded view, corresponding

to the dashed rectangle in frame (a), showing only the 2100–2000  $\text{cm}^{-1}$  and 1800–1600  $\text{cm}^{-1}$  regions, where the most intense bands due to photoisomerization products (labels **30** to **34**) appear (see text). Adapted with permission from ref. 79. Copyright 2012 American Chemical Society.

In a second stage of irradiation, the photoproducts were consumed by irradiations above 240 nm, where isoxazole **27** does not absorb. Irradiations in the 340–330 nm wavelength range led to the conversion of the primary product **30** into **31**, through the cleavage of the C–N bond in **30**, followed by an [1,2] H-shift. Note that 2-formyl-2*H*-azirine **30** contains two distinct conformers, differing in the orientation of the aldehyde group relatively to the ring. In the *anti*-conformation, the aldehyde H-atom faces the N-atom of the ring, and facilitates the H migration from *anti*-**30** to *anti*-**31**. Subsequent irradiations in the 318–310 nm wavelength range induced a very interesting pair of conformer-selective reactions: the *anti*-**31** conformer reacted through a [1,3] H-shift and was converted to *anti*-(*E*)-**33**, whereas the *syn*-**31** conformer (less stable than its *anti* counterpart by 4–5  $\text{kJ mol}^{-1}$ ) reacted through a [1,5] H-shift to yield *syn*-(*Z*)-**32**. The spatial proximity between the H-donor (OH or CH) and the H-acceptor (C=O or C=N) in conformers *anti*-**31** and *syn*-**31**, respectively, is the reason for the preferential reaction path for each conformer. Finally, 3-hydroxypropenenitrile **32** was consumed by irradiation at  $\lambda = 240$  nm and isomerized by a [1,5] H-shift to 3-oxopropanenitrile **34**. Surprisingly, throughout the entire experiment, there were no signs of the formation of oxazole **35**.

In the view of the obtained results for isoxazole **27**, which deviated from the common trends reported for other isoxazoles (*i.e.*, formation of the corresponding oxazoles as final products), an interest arose to study 3,5-dimethylisoxazole **36** [81]. The motivation behind this study was that the unsaturation of positions 3 and 5 of the isoxazole ring could be expected to suppress most of the H-shift reactions observed for the primary photoproducts of the parent isoxazole **27**. Matrix-isolated **36** (argon, 15 K) was irradiated at  $\lambda = 222$  nm during 1 minute, which led to the consumption of ~2 % of the compound and production of 2-acetyl-3-methyl-2*H*-azirine **37** and 3-acetyl-*N*-methylketenimine **38** as primary photoproducts (Figure 12.25).

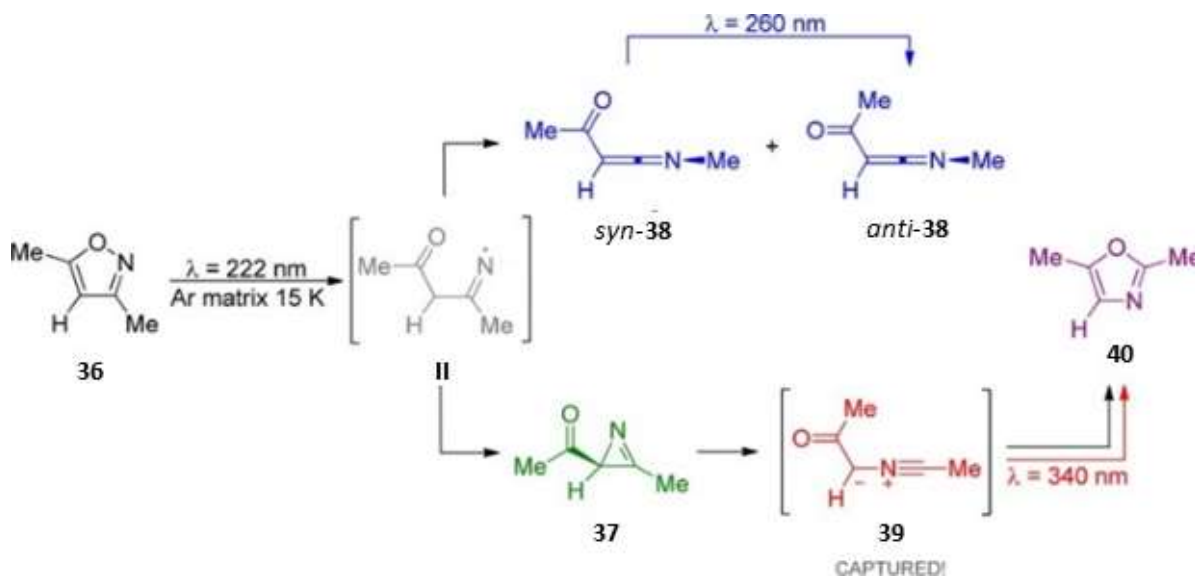


**Figure 12.25** Summary of the experimental observations and the mechanism for photochemistry of 3,5-dimethylisoxazole **36** isolated in a low-temperature argon matrix. Adapted with permission from ref. 81. Copyright 2013 American Chemical Society.

In this first stage of irradiation, the primary photoproducts are analogous to those formed in the study performed on the parent isoxazole **27** [79], and their formation must be intermediated by the vinylnitrene **II**. However, the second stage of reactivity of isoxazole **36** was found to be drastically different from that of isoxazole **27**. An extended irradiation of the matrix (80 minutes) consumed roughly 46 % of **36** and produced, in addition to the primary photoproducts **37** and **38**, the reactive intermediary 1-methyl-3-acetylnitrile ylide **39**, through a C–C bond cleavage of **37**. Additional irradiations at  $\lambda = 340$  nm resulted in the transformation of **39** into the final product 2,5-dimethyloxazole **40** (see Figure 12.25), which was also found to be present in the matrix after prolonged irradiation at only  $\lambda = 222$  nm.

The nitrile ylide **39** may exist in two conformational states (*syn* or *anti*), according to the relative orientation of the nitrile-ylide and carbonyl groups. Both conformers might have been produced by the UV-irradiation of **37**. However, only the *anti*-**39** conformer survived in the matrix and could be experimentally characterized. In the *syn*-**39** conformer, the nitrile-ylide and the carbonyl groups are properly aligned for an intramolecular 1,5-electrocyclization to **40**. Computations on the potential energy surface of this system revealed that *syn*-**39** connects with **40** through a  $10 \text{ kJ mol}^{-1}$  barrier. This barrier can be easily surmounted, especially since *syn*-**39** is produced by UV-irradiation and left in a vibrational excited state, which makes its capture virtually impossible. On the other hand, there is no direct path that connects *anti*-**39** to oxazole **40** and this reaction must go across the *syn*-**39** conformer. Therefore, the effective barrier for the *anti*-**39**  $\rightarrow$  **40** reaction corresponds to that of the conformational isomerization of **39** (*anti*-**39**  $\rightarrow$  *syn*-**39**) and amounts for  $54.5 \text{ kJ mol}^{-1}$  (Figure 12.26). Such a high energy barrier cannot be overcome under the matrix isolation conditions, and enabled the capture of *anti*-**39**. As a

consequence of these results, the theoretically formulated hypothesis [80] that a nitrile ylide should intermediate the isoxazole–oxazole photoisomerization received experimental confirmation.

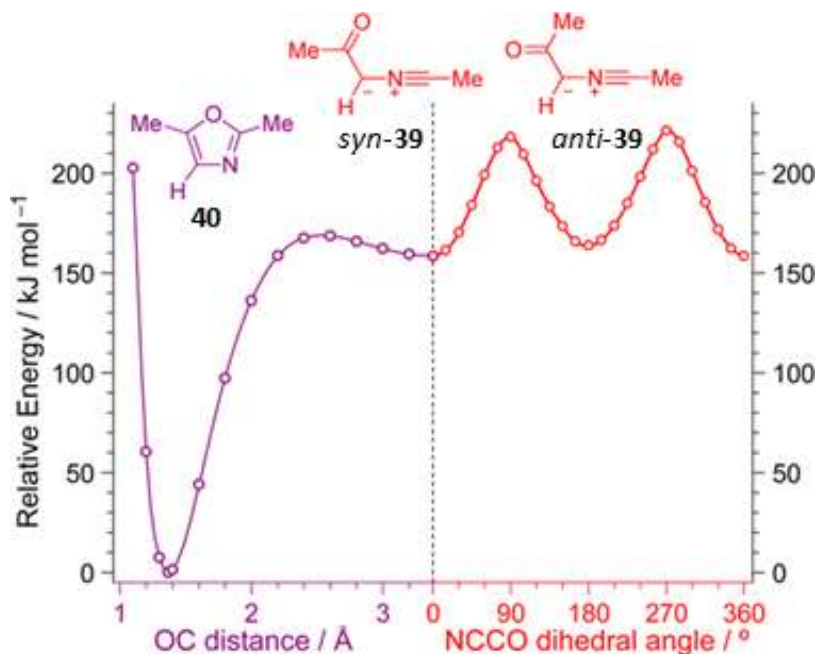


**Figure 12.26** Relaxed potential energy profiles for (right, red) the intramolecular rotation of the acetyl group in nitrile ylide **39** around the NCCO dihedral angle and (left, purple) the ring-contraction from nitrile ylide *syn*-**39** to 2,5-dimethyloxazole (**40**) as a function of the OC distance. The energy of **40** was chosen as the relative zero. Both scans were carried out at the B3LYP/6-311++G(d,p) level of theory. Adapted with permission from ref. 81. Copyright 2013 American Chemical Society.

## 12.4 Thermal Reactivity

In the present section, thermally activated reactions of heterocyclic compound studied by matrix isolation IR spectroscopy will be considered. The chosen examples are reactions involving isoxazoles, whose photoinduced reactions were also considered in the previous section.

As it has already been pointed out, the chemistry of isoxazoles is very rich, due to the simultaneous feature of aromaticity and the presence of a weak N–O bond. For long, studies have been reported that focused on the thermal reactivity of this family of heterocycles. As a common fact, it has been shown that 2*H*-azirines are formed in the initial stages of the thermolysis of isoxazoles. However, the final products depend on the substituents present at positions 3 ( $R^3$ ) and 5 ( $R^5$ ) of the ring. For instance, the flash vacuum pyrolysis (FVP) of

isoxazoles with  $R^3 = H$  preferably leads to the formation of nitrile species, which involve H-shift reactions [82,83], whereas the FVP of isoxazoles with  $R^3 \neq H$  produces the corresponding oxazoles [84,85]. Recently, we have revisited the pyrolysis of isoxazoles using the high-pressure pulsed-pyrolysis method coupled to matrix isolation [80]. In pulsed-pyrolysis, a pre-mixture of a noble-gas and the compound to investigate pass through a heated SiC tube and the activation occurs by collision of the molecules of the targeted compound with the noble gas molecules, thus avoiding possible side reactions that could be catalyzed by the walls of the pyrolysis tube. The proposed mechanistic interpretation for the thermolysis of isoxazole was supported by high-level quantum mechanical electronic structure calculations [80].

The pyrolysate of isoxazole **27** and Ar mixture (~1:1000) was deposited onto a cryogenic substrate at 15 K and probed by IR spectroscopy. Bands assigned to pyrolysis products began to appear at the temperature of 600 °C (Figure 12.27). At 800 °C, the most intense bands observed in the spectrum were already due to pyrolysis products. One immediate remark on the infrared spectrum of the pyrolysate is the absorption at 2138  $\text{cm}^{-1}$ , the characteristic vibrational mode of carbon monoxide (CO). Another characteristic band was found in the 2100-2000  $\text{cm}^{-1}$  range and assigned to the  $\nu_{\text{as}}(\text{NCC})$  mode of a ketenimine group. However, the lack of observation of any band in the  $\nu_{\text{as}}(\text{C=O})$  region excludes 3-formylketenimine **31** (see Figure 12.23), a found photoproduct of isoxazole [79], as the possible responsible for the band observed in the 2100-2000  $\text{cm}^{-1}$  region. In turn this band was assigned to the  $\nu_{\text{as}}(\text{NCC})$  mode of the parent ketenimine **41**, which must be formed alongside with CO (Figure 12.28). Additionally, a new primary product of isoxazole's thermolysis was identified, the 3-hydroxypropenenitrile **32** (which was also observed as secondary photoproduct in the photolysis of **27** [79]; see also Figure 12.23). 3-Hydroxypropenenitrile **32** may exist in four distinct conformations, but only the most stable *syn*-(*Z*)-**32** was found in the matrix, which suggest that this species is formed in a stereospecific fashion. At the end of the pyrolysis at 800 °C, the matrix was irradiated at  $\lambda = 240$  nm until a photostationary state was reached. At that point, the bands previously assigned to *syn*-(*Z*)-**32** decreased in intensity and new bands emerged in the spectrum, corresponding to the isomeric *syn*-(*E*)-**32** and *anti*-(*E*)-**32** species.



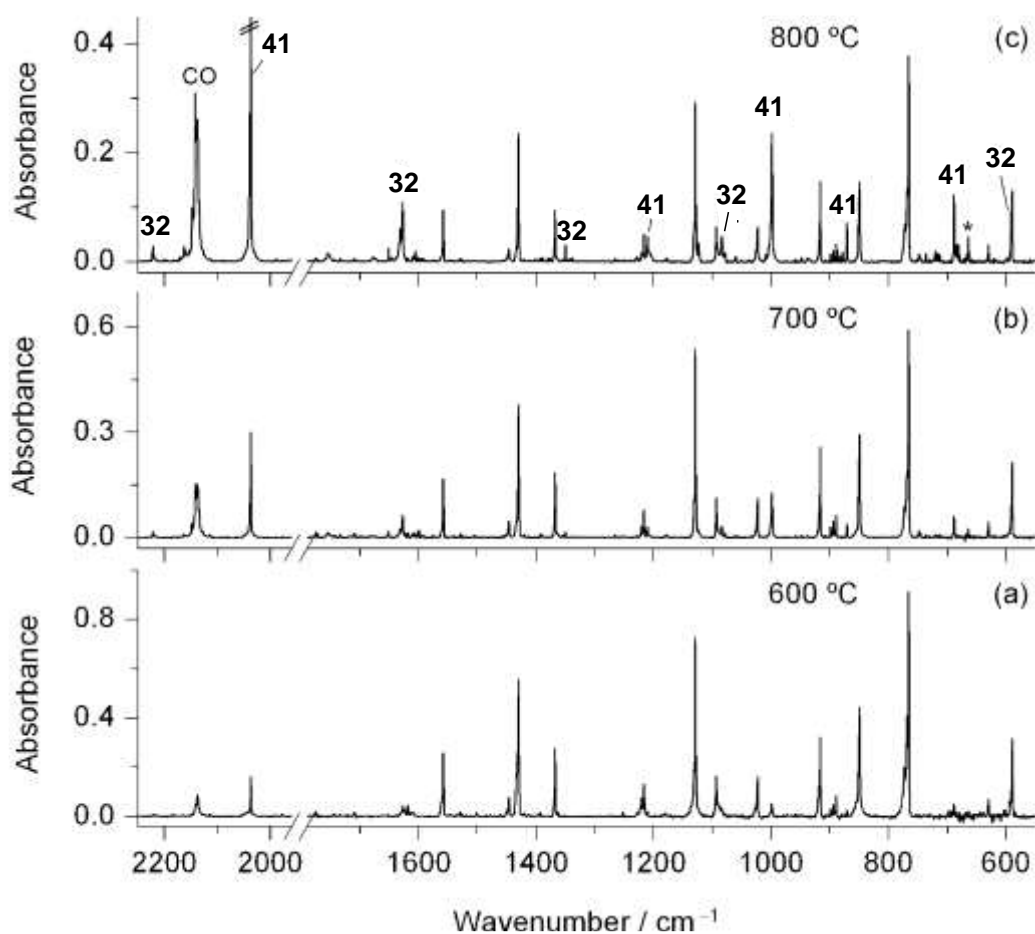


**Figure 12.27** Experimental IR spectra of products of pulsed pyrolysis of isoxazole **27** trapped in argon matrices at 15 K. The temperature of the SiC tube was at (a) 600, (b) 700, and (c) 800 °C. The new major bands in the spectrum (c) are assigned to **32** and **41**. The band marked with an asterisk is due to an impurity from the pyrolysis system. Reprinted with permission from ref. 80. Copyright 2011 American Chemical Society.

A similar study was undertaken on 5-methylisoxazole **42** [80], to evaluate the influence of  $R^5 \neq H$  on the pyrolysis of isoxazoles. The pyrolysis of **42** led to the formation of 3-hydroxybutanenitrile *syn*-(*Z*)-**43**, which, like the equivalent nitrile species resulting from the pyrolysis of the parent isoxazole **27** (*i.e.*, 3-hydroxypropenenitrile **32**), was found to photoisomerize to conformers *syn*-(*E*)-**43** and *anti*-(*E*)-**43** upon UV-irradiation. However, no signs of carbon monoxide and methyl-ketenimine could be found in the spectra of the pyrolysate of **42**. The path for decomposition seems indeed to be blocked by the presence of the methyl group in the position 5 of the ring, because in order to be possible this reaction would require a migration of the methyl group, which is a very improbable process in a cryogenic solid matrix. Instead, the infrared signature of 3-oxobutanenitrile **44** was found. It might be that also

3-oxopropanenitrile **34** is formed during pyrolysis of unsubstituted isoxazole **27**, but promptly decomposes to form CO and ketenimine, since in that case the H-shift is likely to occur.

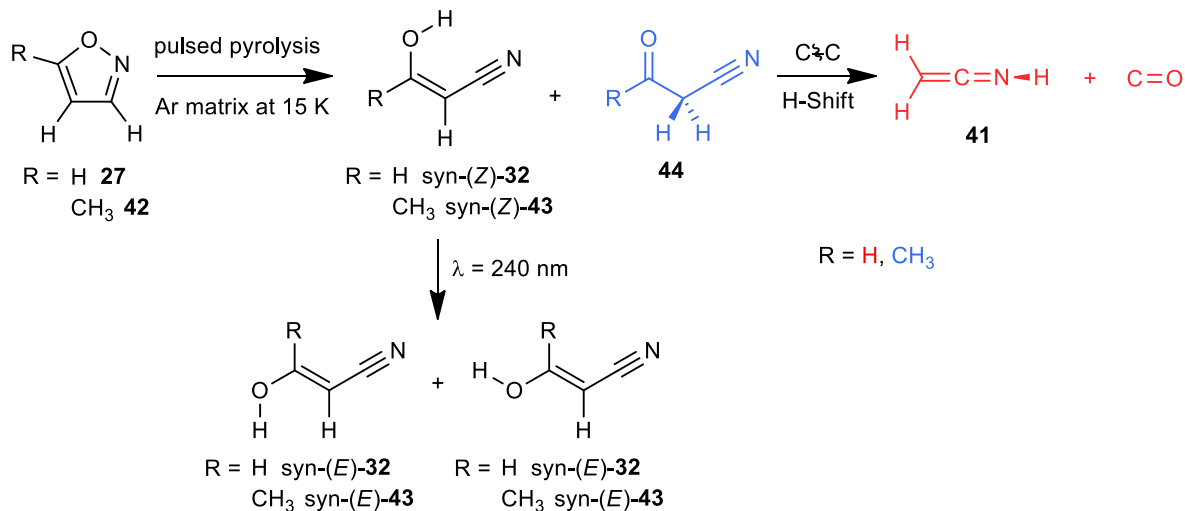


**Figure 12.28.** Summary of observations from the pulsed pyrolysis of isoxazole **27** (R = H) and 5-methylisoxazole **42** (R = CH<sub>3</sub>). Detection of an oxo-nitrile **44** (blue) was only found in the pyrolysis of **42**, whereas decomposition (red) to ketenimine **41** and carbon monoxide was only observed in the pyrolysis of **27** [80].

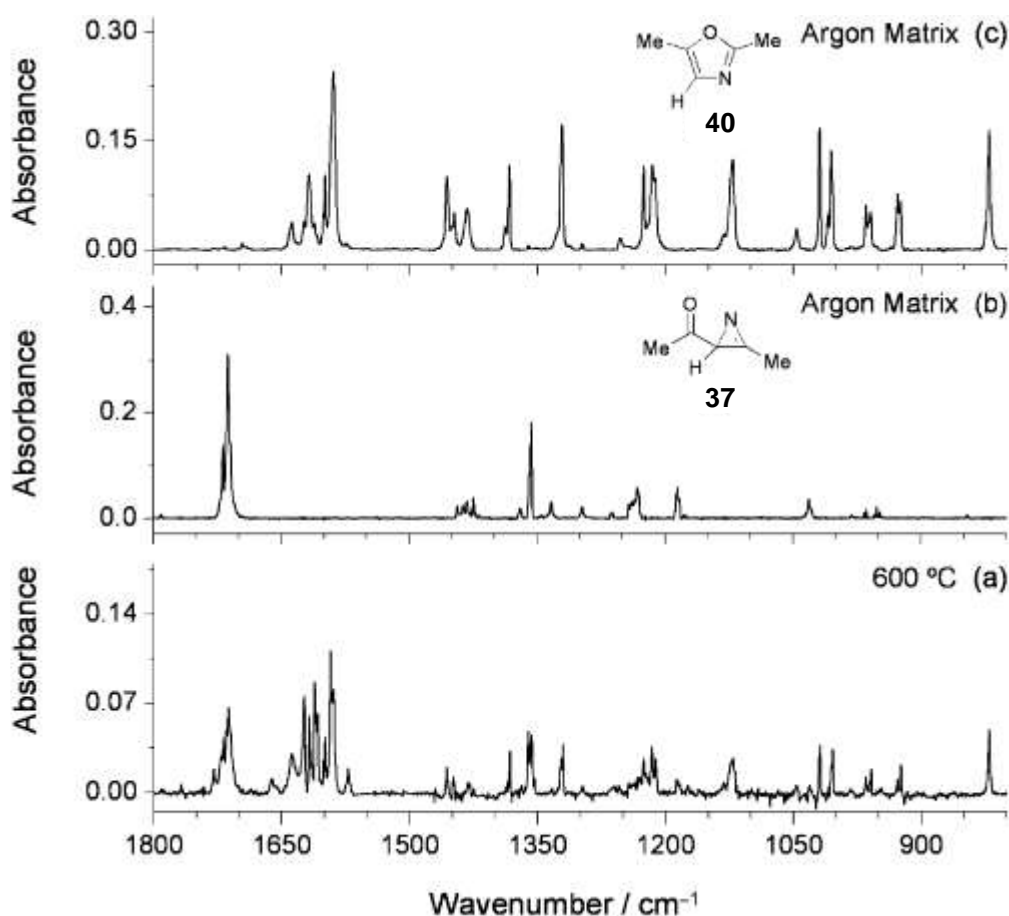


**Figure 12.29** (a) Experimental IR spectrum of products of pulsed pyrolysis of 3,5-dimethylisoxazole **36** (600 °C), trapped in an argon matrix at 15 K. The absorptions due to the reagent were eliminated. (b,c) Experimental IR spectra of 2-acetyl-3-methyl-2*H*-azirine **37** (b) and 2,5-dimethyloxazole **40** (c) isolated in argon matrices at 15 K in separate experiments. Adapted with permission from ref. 80. Copyright 2011 American Chemical Society.

Finally, the pyrolysis of 3,5-dimethylisoxazole **36** at 600 °C yielded 2-acetyl-3-methyl-2*H*-azirine **37** and 2,5-dimethyloxazole **40**. At higher temperatures, **40** continued to be produced at the cost of **37** (Figure 12.29). These results agree with the earlier studies on the thermolysis of **36** by Murature *et al.* [84]. In a similar picture to that found for the photochemistry of isoxazoles **27** and **36** (see previous section), the dimethyl derivative was found to yield oxazole as final product, whereas the unsubstituted isoxazole underwent H-shift reactions to open ring products.

In an attempt to shed light on the experimental results, a theoretical investigation was held by state-of-the-art quantum chemistry computations. The first step in isoxazoles thermolysis is unquestionably the cleavage of the N–O bond, which should in principle produce vinyl nitrene intermediates. However, the detection of these species has not yet been successful, and earlier

theoretical calculations on the thermolysis of isoxazoles failed to recognize its pivotal role [86]. The reason for such failure was the misperception that the lowest singlet state of vinyl nitrenes would be of closed-shell nature. In fact, their lowest singlet state has actually been shown to be of open-shell nature [87] and, therefore, any single-determinant method fails to correctly describe it. The reinvestigation on this topic by Nunes *et al.* [80] using multiconfigurational complete active space self-consistent field (CASSCF) methods showed that open-shell vinyl nitrenes are indeed minima, although almost barrierless regarding their decay to *2H*-azirines. Moreover, it was found that vinyl nitrene **I** could be produced at the cost of isoxazole **27** by surmounting a barrier of roughly 50 kcal mol<sup>-1</sup>. Then, the transition states for the candidate reactions departing either from vinyl nitrene **I** or 2-formyl-*2H*-azirine **30** were searched. Remarkably, the lowest energy barrier (49 kcal mol<sup>-1</sup>) reaction found resulted to be that leading to the formation of 3-hydroxypropenenitrile **32**, at the cost of vinyl nitrene **I**. This was indeed the first product to be seen during the pyrolysis of isoxazole **27**. Further computations were carried to rationalize the formation of secondary products, namely ketenimine **41** and CO in the case of isoxazole **27**, and 2,5-dimethyloxazole **40** in the case of 3,5-dimethylisoxazole **36**. In the end, a general picture of isoxazole thermolysis, with an open-shell vinyl nitrene as the pivotal intermediate for all subsequent transformations, was presented that fully supports the experimental observations and, in particular, explains the reasons for the observed selective transformations.

## 12.5 IR-Induced Processes

As already mentioned, the low temperature of the cryogenic matrices suppress thermal conversions, providing, in this way, ideal conditions to investigate conformational isomerization processes, which are in general characterized by relative low-energy barriers. Infrared vibrational excitation in conjugation with the matrix isolation technique has in fact been successfully used for more than two decades to manipulate in a very precise and selective way molecular conformations of different types of organic compounds [88-90]. The idea behind this approach is to use frequency-tunable narrowband IR light to deposit energy in a vibrational state of a molecular system. If subsequent energy dissipation by intramolecular vibrational energy redistribution (IVR) is partially channeled to a torsional reaction coordinate, conformational isomerization might be activated [90]. This methodology has been proved to be extremely selective, since vibrational energy can be specifically deposited in a chosen molecular species, in a particular conformation, and in a particular environment (which can result from different accommodations of the molecule in the cryogenic matrix; matrix sites) [88-90].

In this section, we will describe a few examples of IR-induced conformational isomerizations taking place in heterocyclic systems, focusing on recent advances achieved in our group. We will also mention recent pioneer results demonstrating that the above-mentioned

approach can also be developed as a promising way to induce and control bond-breaking/bond-forming reactions.

In order to deposit energy into a torsional reactive coordinate so that it takes the molecule to a state above the torsional barrier or close to its top, vibrational excitation is typically carried out at first XH (X = O or N) stretching overtones with significant enough absorption cross section [88,90]. This is nicely illustrated in the work carried out by Lapinskli *et al.* on cytosine [91].

As mentioned in Section 12.3, the two amino-hydroxy conformers of cytosine, **AH1** and **AH2**, differing by the rotation of the hydroxy group, are the most stable forms of the monomeric compound under matrix-isolation conditions (Figure 12.30). Their energy difference is 1-3 kJ mol<sup>-1</sup> in favor of **AH1**. The amino-oxo (**AO**) and imino-oxo (**IO**) tautomeric forms are less stable by 4–6 and ≥8 kJ mol<sup>-1</sup>, respectively [57,58,92,93].

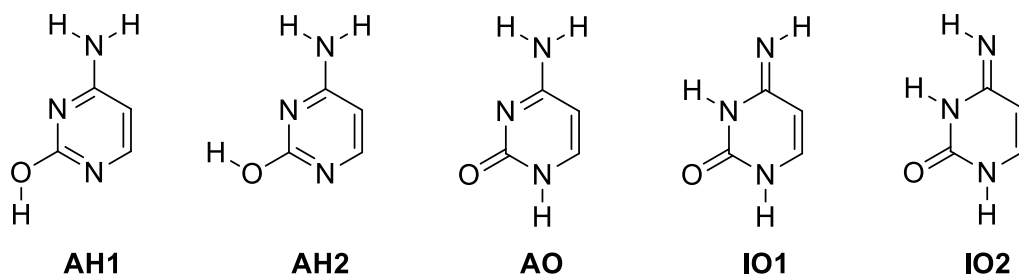


**Figure 12.30** Most relevant forms of cytosine monomers ordered from left to right by their thermodynamic stability.

As it could be expected, **AH1** and **AH2** forms of cytosine dominate in a freshly deposited low-temperature matrix. Selective and reversible interconversion between these two forms was successfully achieved upon narrowband (0.2 cm<sup>-1</sup>) IR irradiation [57,91]. Vibrational excitation of the first OH stretching overtone of **AH1** conformer at 7013 cm<sup>-1</sup> leads to its conversion into **AH2**, whereas vibrational excitation of the first OH stretching overtone of **AH2** conformer at 7034 cm<sup>-1</sup> leads to its conversion into **AH1** (Figure 12.31). The population of **AH1** and **AH2** conformers was experimentally transferred many times using irradiation cycles (7013 and 7034 cm<sup>-1</sup>) without any loss of the total amount and without affecting the population of **AO** and **IO** tautomeric forms present in the matrix in smaller amounts.

After shifting the population in favor of **AH2** or **AH1** by narrowband IR irradiation, it was found that broadband IR radiation from the global source of the FTIR spectrometer affects the population of these conformers [94]. In fact, independently of the initial **AH1**:**AH2** ratio, the exposure of the matrix sample to the IR spectrometer radiation induces changes towards a photostationary state where the **AH1**:**AH2** ratio is approximately 1:1. Experiments with IR

bandpass filters led to the interpretation that excitations at the fundamental OH and NH stretching vibrations also induce mutual conversion between **AH1** and **AH2** conformers. These excitations provide  $\sim 40 \text{ kJ mol}^{-1}$ , which is enough to induce the conformational isomerizations, since the higher barrier for the **AH1:AH2** interconversion was estimated as  $\sim 30 \text{ kJ mol}^{-1}$ . Therefore, having access to narrowband IR light in the mid-IR region, one should also be able to attain control of **AH1** and **AH2** relative populations by irradiations at the frequencies of their fundamental OH stretching modes.

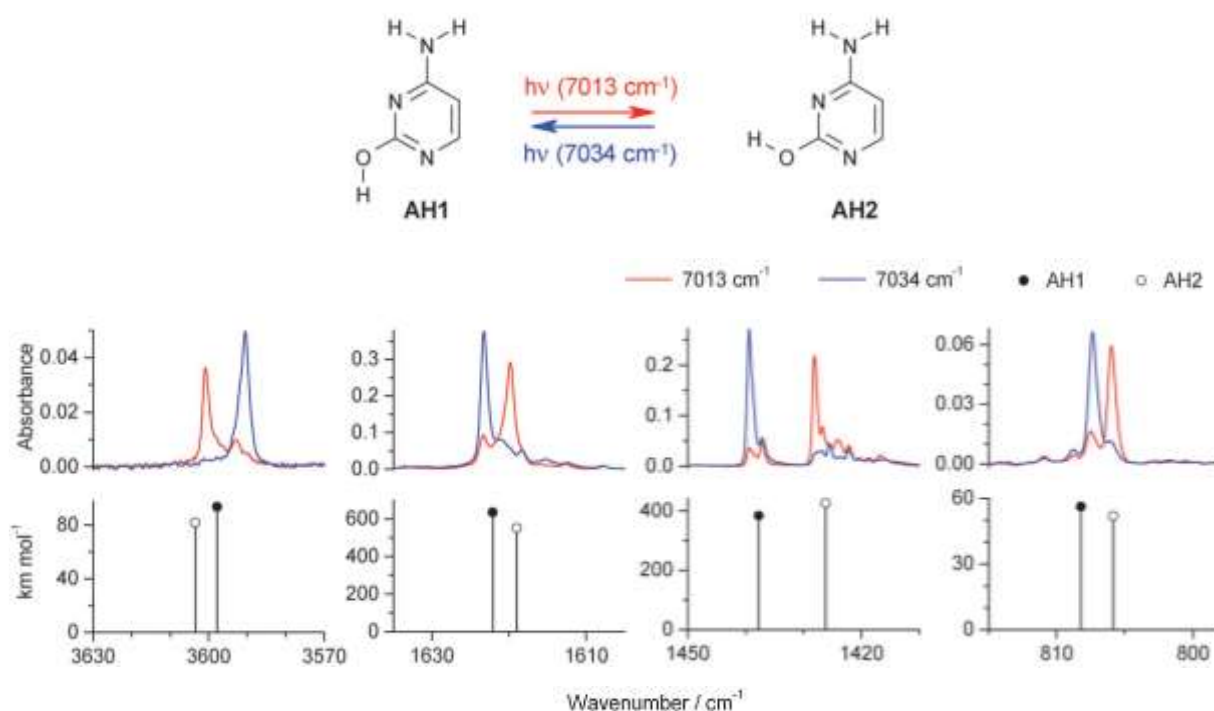


**Figure 12.31** The effects of narrowband IR irradiations. Fragments of the IR spectra of cytosine isolated in an argon matrix: (red) after irradiation at  $7013 \text{ cm}^{-1}$ ; (blue) after irradiation at  $7034 \text{ cm}^{-1}$ ; compared to the IR spectra computed for **AH1** and **AH2** at the B3LYP/6-31++G(d,p) level of theory. Adapted from ref. 91 with permission from the PCCP Owner Societies.

In experiments carried out on 5-methylcytosine and 5-fluorocytosine [62], it was analogously demonstrated that the corresponding amino-hydroxy conformers, **AH1** and **AH2**, can be selectively and reversibly interconverted upon narrowband IR irradiation at the frequencies of their first OH stretching overtones. Conformational manipulation by IR vibrational excitation was demonstrated as well as for other heterocyclic compounds having an OH fragment, such as 9-methylguanine [95], thiazole-2-carboxylic acid [96], and tetrazole-5-carboxylic acid [97].

An important breakthrough on this methodology was made by our group in 2015 by demonstrating that reversible interconversion between two conformational states can be

achieved by selective vibrational excitation of a bond remotely located in relation to the conformational isomerization coordinate (Figure 12.32) [98].

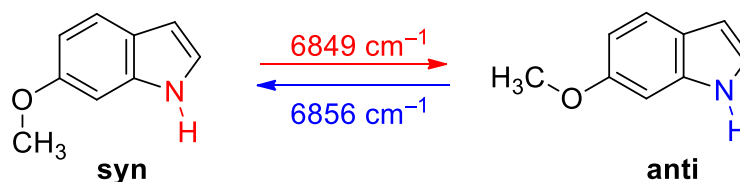


**Figure 12.32.** Conformational switching of 6-methoxyindole (**6MOI**) promoted by vibrational excitation of the remote NH bond at its first stretching overtone frequency.

6-Methoxyindole (**6MOI**) was used as molecular model. This molecule can adopt two conformations, *syn* and *anti*, where the methoxy fragment (OCH<sub>3</sub>) points to the same or to the opposite direction of the NH group, respectively. Their energy difference is 2–3 kJ mol<sup>-1</sup> in favor of the *syn* conformer, the energy barrier separating the two conformers being ~9 kJ mol<sup>-1</sup>. According to the relative energy of the conformers, in a freshly deposited cryogenic matrix a *syn:anti* population ratio ~65:35 was observed. Distinctive NH stretching vibrations were measured for these conformers: in a xenon matrix at 30 K, *syn*-**6MOI** shows the  $\nu(\text{NH})$  at 3494.5 cm<sup>-1</sup> and the  $2\nu(\text{NH})$  at 6849.3 cm<sup>-1</sup> whereas *anti*-**6MOI** shows the  $\nu(\text{NH})$  at 3498.0 and the  $2\nu(\text{NH})$  at 6855.6 cm<sup>-1</sup>. Narrowband IR irradiation tuned at 6849 cm<sup>-1</sup> for 30 min was then found to promote a large scale *syn* → *anti* isomerization, as evidenced by the difference IR spectrum shown in Figure 12.33a (spectrum obtained after irradiation *minus* spectrum of the as-deposited matrix). The comparison of this spectrum with the B3LYP/6-311++G(d,p) computed IR spectra of the two conformers (Figure 12.33b) undoubtedly allows assigning the bands that decrease of intensity to the *syn* conformer and those that concomitantly increase to the *anti* conformer. Subsequent irradiation tuned at 6856 cm<sup>-1</sup> was found to promote the inverse *anti* → *syn* isomerization, as evidenced by the corresponding difference IR spectrum (Figure 12.33c), which mirrors that previously described. Remarkably, these results prove the possibility of efficient intramolecular vibrational relaxation to carry the energy deposited in the NH stretching bond into a distant reactive C–O torsional mode to induce conformational switching of the methoxy group.

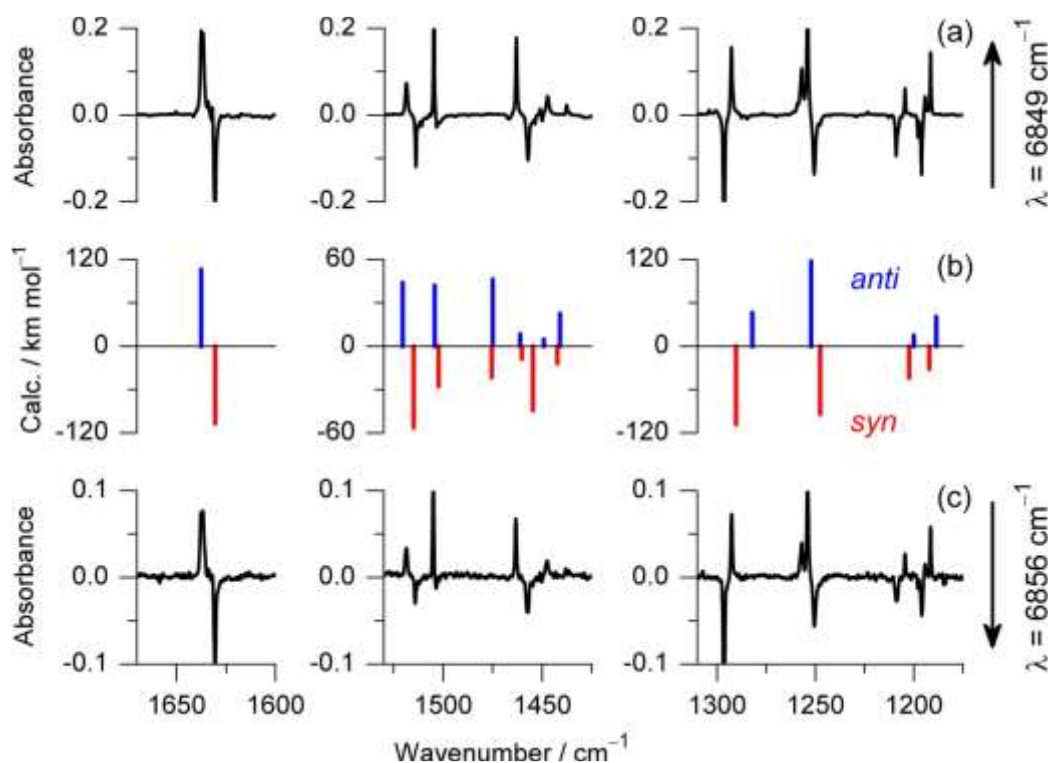


**Figure 12.33** Fragments of experimental (Xe, 30 K) and theoretical IR spectra of **6MOI** in the fingerprint region showing the effect of the IR irradiations: (a) experimental spectrum registered after irradiation at  $6849\text{ cm}^{-1}$  minus that obtained before any irradiation; (c) experimental spectrum registered before any irradiation at  $6856\text{ cm}^{-1}$  minus that obtained after irradiation at this frequency. Arrows indicate the direction of the bands growing upon irradiation; (b) IR spectra of the *anti* (upward bars, blue) and *syn* (downward bars, red) **6MOI** conformers computed at the B3LYP/6-311++G(d,p) level of theory. Reprinted with permission from ref. 98. Copyright 2015 American Chemical Society.

Conformational isomerizations induced by vibrational excitation of a remote bond relatively to the fragment that changes its orientation were also reported for matrix-isolated 2-thiocytosine [99] and 5-hydroxy-2-hydroxymethyl-4*H*-pyran-4-one (kojic acid) [100] (Figure 12.34).

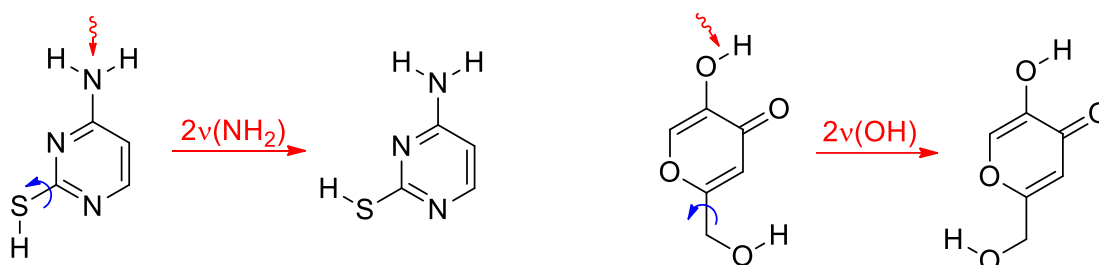


**Figure 12.34** Conformational isomerization by vibrational excitation of a remote bond reported for matrix-isolated 2-thiocytosine and kojic acid.



We have further extended the concept of remote vibrational antenna, by introducing the concept of interchangeable remote vibrational antennas. Specifically, it was demonstrated that the conformation of an aldehyde ( $-CHO$ ) fragment attached to a  $2H$ -azirine ring can be controlled by excitation of interchangeable  $NH_2$  or  $OH$  vibrational antennas attached to the opposite position of the ring (Figure 12.35) [101].

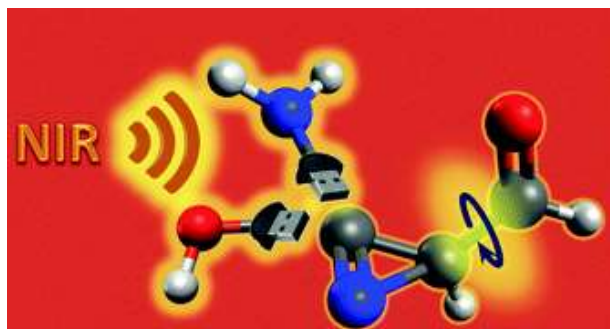


**Figure 12.35** Conformational control over an aldehyde fragment of a  $2H$ -azirine by selective vibrational excitation of interchangeable  $NH_2$  and  $OH$  remote antennas. Reproduced from ref. 101 with permission from the Royal Society of Chemistry.

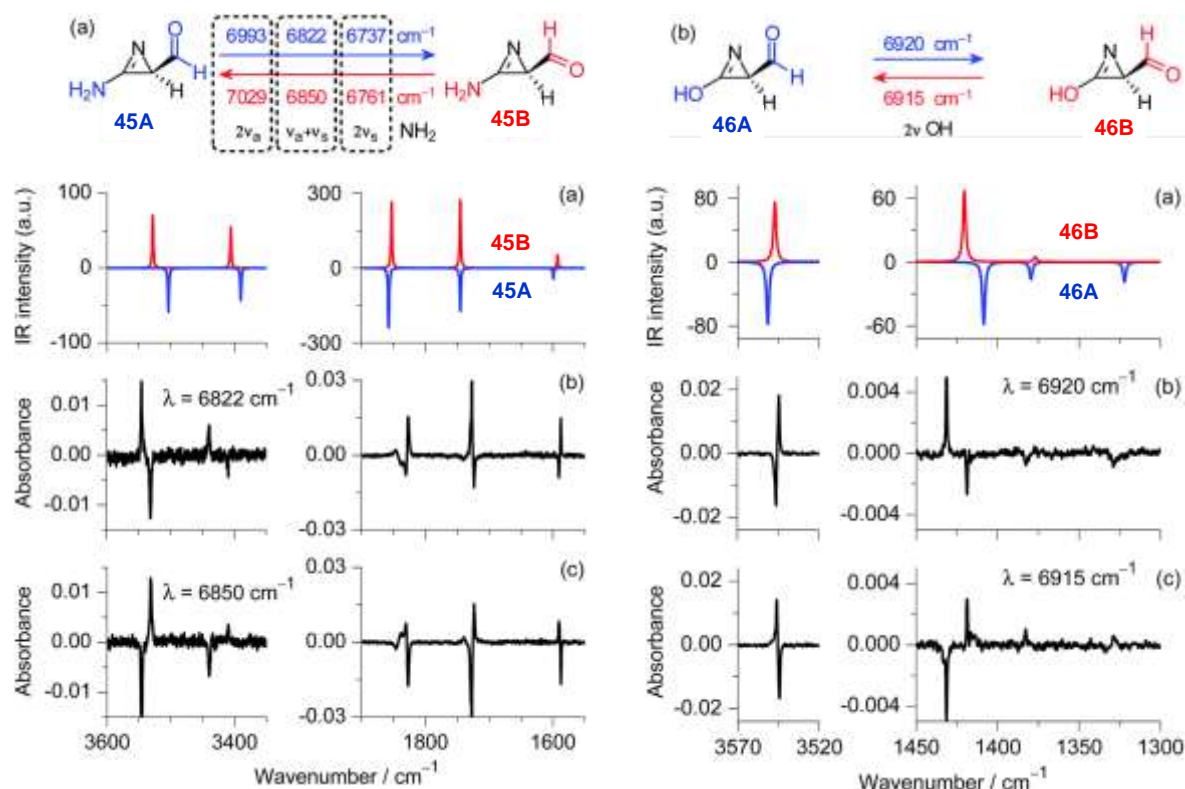


**Figure 12.36** Conformational interconversions of a remove aldehyde induced by selective narrowband IR irradiation of the NH<sub>2</sub> antenna of **45** (left panel) and OH antenna of **46** (right panel). Left panel: (a) Computed IR spectra for **45A** (blue, intensities multiplied by -1) and **45B** (red) at the B3LYP/6311++G(d,p) level of theory; IR spectral changes resulting from irradiation of **45** isolated in an Ar matrix at 15 K, (b) at 6822 cm<sup>-1</sup> and (c) at 6850 cm<sup>-1</sup>. Right panel: Computed IR spectra for **46A** (blue, intensities multiplied by -1) and **46B** (red) at the B3LYP/6-311++G(d,p) level of theory; IR spectral changes resulting from irradiation of **46** isolated in an Ar matrix at 15 K, (b) at 6920 cm<sup>-1</sup> and (c) at 6915 cm<sup>-1</sup>. In both panels, the positive bands grow upon IR irradiations. Adapted from ref. 101 with permission from the Royal Society of Chemistry.

Computations for 3-amino-2-formyl-2*H*-azirine **45** and 3-hydroxy-2-formyl-2*H*-azirine **46** show that both molecules possess two conformers concerning the orientation of the aldehyde group, *i.e.* whether the C=O is *syn*-periplanar (**45A** and **46A**) or *anti*-periplanar (**45B** and **46B**) relative to the three-membered ring. For both molecules their energy difference is 6–7 kJ mol<sup>-1</sup> in favor of the conformer **B**, which is separated from the conformer **A** by an energy barrier of ~17 kJ mol<sup>-1</sup>. Upon generation of 2*H*-azirines **45** and **46**, by UV irradiation of the corresponding isoxazole precursors isolated in argon matrixes at 15 K, both conformers **A** and **B** were identified by IR spectroscopy. Particularly relevant was the identification of six bands of **45** (three for each, **45A** and **45B**) in the near-IR 7100–6700 cm<sup>-1</sup> range, ascribed to the first overtones of the antisymmetric [2*v*(NH<sub>2</sub>)<sub>a</sub>] and symmetric [2*v*(NH<sub>2</sub>)<sub>s</sub>] stretching vibrations and to the combination band [*v*(NH<sub>2</sub>)<sub>a</sub> + *v*(NH<sub>2</sub>)<sub>s</sub>]. In the case of **46**, a doublet band was identified covering the 6927–6910 cm<sup>-1</sup> range, which was ascribed to the first overtone of the OH stretching vibrations [2*v*(OH)] of **46A** and **46B**. The two aldehyde conformers of **45** and **46** (**A**

and **B**) were then manipulated bi-directionally and reversibly by narrowband IR irradiation tuned at the identified frequencies of the NH<sub>2</sub> and OH vibrational antennas (Figure 12.36).

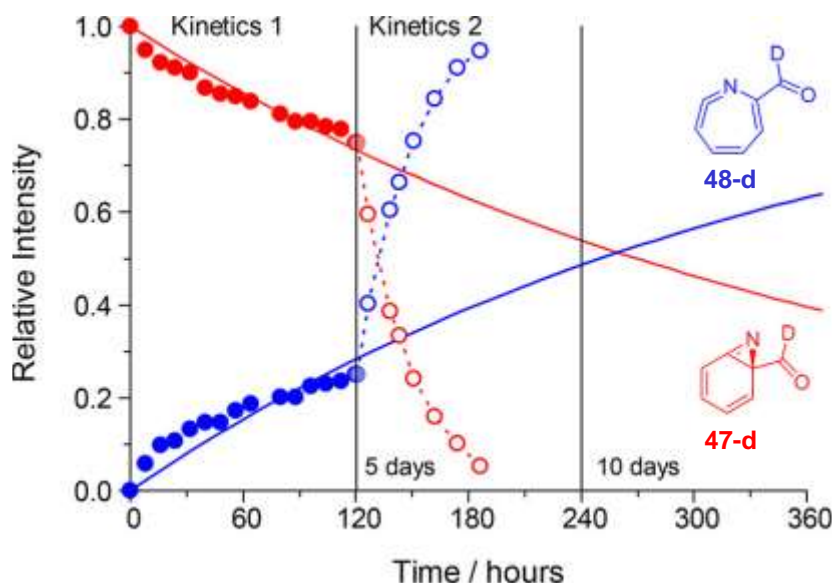


**Figure 12.37** Kinetics of rearrangement of benzazirine **47-d** to cyclic ketenimine **48-d** in an argon matrix at 10 K. Kinetics 1 (initial 5 days, left): rearrangement of **47-d** [solid red circles (●), consumption] into **48-d** [solid blue circles (●), production] with the sample kept in the dark, except when the spectra were recorded, the sample was then protected by an infrared long-pass cut-off-filter transmitting only below 2200 cm<sup>-1</sup>. Kinetics 2 (after 5 days in the dark, right): rearrangement of **47-d** [empty red circles (○), consumption] into **48-d** [empty blue circles (○), production] with the sample permanently exposed to the IR light source of the FTIR spectrometer. Adapted with permission from ref. 102. Copyright 2017 American Chemical Society.

Finally, two examples reported by us demonstrate that vibrational excitation can also be used induce and control bond-breaking/bond-forming reactions.

The first example was the discovery that broadband IR radiation induces electrocyclic ring-expansion of benzazirine **47** to a cyclic ketenimine **48** (Figure 12.37) [102]. As it will be addressed in more detail in Section 12.6, we observed that upon generation of **47** in an argon matrix at 10 K, it undergoes spontaneous ring-expansion tunneling to cyclic ketenimine **48**. The process was measured to take place with a half-life time of  $t_{1/2} \sim 260$  h both under dark conditions or when the sample was kept permanently exposed to the IR light source of the spectrometer with a cutoff filter transmitting only below 2200 cm<sup>-1</sup>. However, when the sample was kept permanently exposed to the IR light source of the spectrometer without any filter, the ring-expansion was found to take place with a  $t_{1/2} \sim 13$  h, which clearly provides evidence of an IR-induced process. In a recent study not yet published, we were also able to demonstrate that by introducing appropriate substituents on the benzazirine **47**, the spontaneously tunneling can be suppressed and exploitation of the use of a remote OH vibrational antenna to selectively trigger ring-expansion to ketenimine **48** can be achieved.

The second example was the demonstration that bidirectional tautomerization of thiotropolone **49** can be achieved by vibrational excitation (Figure 12.38) [8]. Narrowband IR irradiations of the hydroxy-tautomer of thiotropolone (**OH-TT**) isolated in an argon matrix at the frequency of its first CH stretching overtone or combination modes lead to its conversion into the thiol-tautomer (**SH-TT**). The irradiations of the thiol-tautomer at the frequency of its first CH stretching overtone or combination modes lead to the reverse tautomerization.

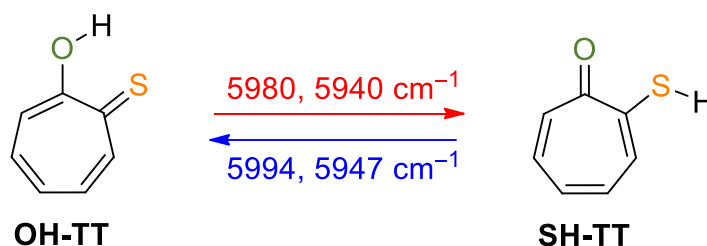


**Figure 12.38** Bidirectional tautomerization in thiotropolone induced by vibrational excitation.

These two unprecedented examples open prospects for new advances on infrared vibrational excitation as a promising approach for gaining exceptional control of chemical reactions, in ways that cannot be attained *via* thermal or electronic excitations.

## 12.6 Tunneling in Heterocyclic Chemistry

Quantum mechanical tunneling (QMT) is a fascinating phenomenon that allows particles to penetrate through potential energy barriers regardless of insufficient thermal energy to surmount them [103]. In this way, QMT breaks the classic transition state theory (TST), commonly used by the organic chemistry community to rationalize molecular transformations [104,105]. An interesting consequence is that a QMT reaction can lead to a product whose reaction path faces a higher barrier (compared to other *a priori* possible processes) and whose formation is then not expected on the basis of classic TST [106]. Such discovery led to the emerging of tunneling control as the third paradigm in chemical reactivity, next to the kinetic and thermodynamic control [11,107].

For a chemical reaction under ordinary laboratory conditions, the existence of QMT contribution can be assessed indirectly by the observation of non-linear Arrhenius plots or abnormal kinetic isotopic effects, and typically results in an increase of the reaction rate compared to the expectations based on the classical TST [108]. On the other hand, under cryogenic conditions (*e.g.*, 3–10 K), thermal activated rates are negligible for systems having barrier as low as 1 kcal mol<sup>-1</sup> (~4 kJ mol<sup>-1</sup>), and the occurrence of a chemical reaction can only be due to QMT from the vibrational ground state [7]. The rates of the reactions governed by QMT are usually temperature independent and, if occurring on the timescale of seconds to days, they can be directly observed using steady-state spectroscopic techniques [7].

In a simplified manner, the tunneling probability ( $P$ ) depends linearly on the width of the barrier ( $w$ ) and on the square root of both the moving mass ( $m$ ) and the height of the barrier ( $\Delta E^\ddagger$ ) (Eq. 1) [109]. Therefore, QMT is expected to be particularly relevant for reactions involving the motion of light particles, like an electron, a hydrogen atom or a proton [109]. Although heavy-atoms, such as carbon, have been assumed to behave classically for long, recent discoveries suggest that heavy-atom QMT can actually occur through very narrow and moderated to small energy barriers [7,110,111].

$$P \sim e^{-xw\sqrt{\Delta E^\ddagger m/\hbar}} \quad (1)$$

In this section, we will highlight examples described by our group regarding QMT reactions directly observed by matrix isolation spectroscopy. Those comprise tunneling-driven chemical processes ranging from conformational isomerizations to H-atom and heavy-atom bond-breaking/bond-forming reactions, in which a heterocyclic compound is either a precursor, a reactant, or a product.

The story of our investigations on the photochemistry of 1,2-benzisoxazoles began with the goal of generating vinyl nitrenes [112-114], and end up being the starting point for a series of discoveries on QMT-driven reactions.

UV irradiation of parent 1,2-benzisoxazole **50** was found to lead to 2-cyanophenol **53** via *spiro-2H*-azirine **51** and ketenimine **52** intermediates (Figure 12.39) [112]. Although in polar solvents the irradiation of **50** affords mainly 1,3-benzoxazole **54** [115], no trace of this species was observed in argon and nitrogen matrices [112]. UV-irradiation of **54** was found to lead to 2-isocyanophenol **55**, which was characterized as a kinetically unstable species that rearranges back to **54** upon thermal annealing or by UV irradiation (Figure 12.39) [116]. Intriguing, at that time, **53** and **55** in nitrogen matrices were generated in the *anti*-OH (**53a** and **55a**) and *syn*-OH (**53s** and **55s**) conformations, whereas in argon matrices only in the *syn*-OH (**53s** and **55s**) conformation [112,116,117].

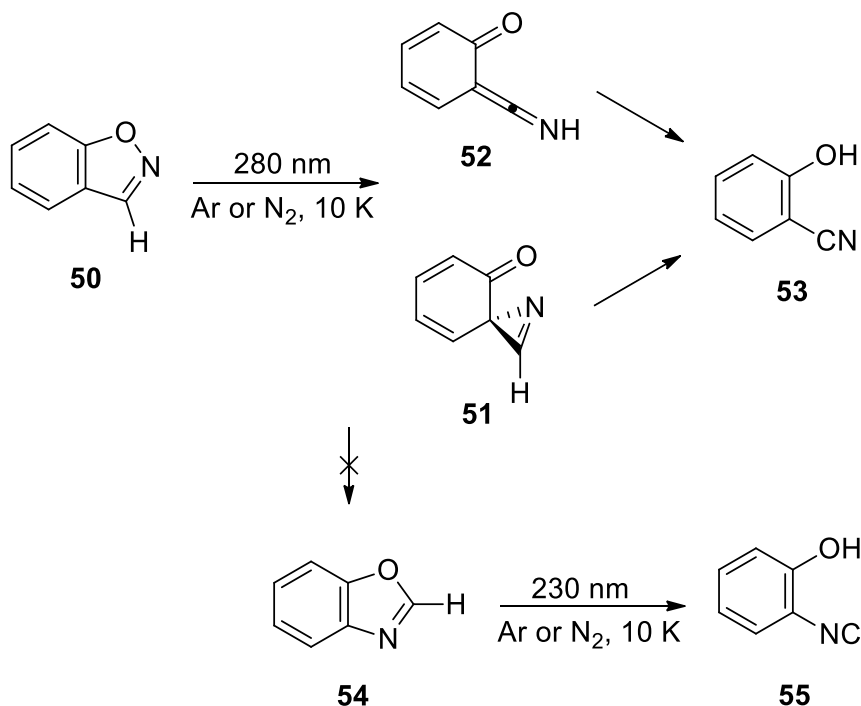


**Figure 12.39** Photochemistry of 1,2-benzisoxazole **50** and 1,3-benzoxazole **54** in cryogenic matrices leads to 2-cyanophenol **53** and 2-isocyanophenol **55**, respectively [112,116].

In further investigations, it was discovered that keeping 2-cyanophenol **53** or 2-isocyanophenol **55** in a nitrogen matrix at 10 K, in the dark, resulted in a decrease of the population of the less stable **53a** or **55a** conformer and a concomitant increase of the population of the most stable **53s** or **55s** form [116,117]. Fitting the kinetic data to a single-exponential equation, rate constants of  $\sim 2.8 \times 10^{-4}$  and  $\sim 3.2 \times 10^{-4} \text{ s}^{-1}$  [corresponding to half-life times ( $t_{1/2}$ ) of  $\sim 40$  and  $\sim 36$  min] were estimated for the spontaneous **53a**  $\rightarrow$  **53s** and **55a**  $\rightarrow$  **55s** conformational isomerizations, respectively. These transformations cannot take place over the barrier [ $\sim 12$  and  $\sim 11 \text{ kJ mol}^{-1}$ , respectively, at the B3LYP/6-311++G(d,p) level] due to the absence of enough thermal energy at such low temperatures and, therefore, should be governed by tunneling (Figure 12.40) [116,117]. That was unequivocally confirmed upon increasing the temperature by a factor of 2 (from 10 to 20 K) and observing a negligible effect on the conformational isomerization rate constants.

The lack of detection of the **53a** and **55a** conformers in argon matrices was attributed to the occurrence of a much faster conformational isomerization by tunneling [116,117]. This behavior has been reported for simple carboxylic acids having conformers differing by the OH rotation. For example, the OH isomerization tunneling of the higher energy conformers of formic and acetic acids was found to be approximately 55 and 600 times faster in argon matrices than in nitrogen matrices [118]. Apparently, this effect is due to the increased stability of the higher energy conformers in a nitrogen matrix as a result of the formation of specific  $\text{OH}\cdots\text{N}_2$

interactions, which is associated with the fact that  $N_2$  molecules have a permanent quadrupole moment and noble gas atoms do not [118].

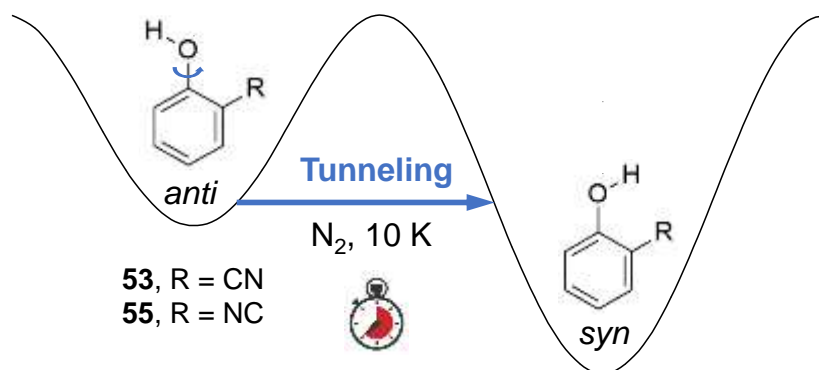


**Figure 12.40** Conformational isomerization tunneling (*anti*-OH→*syn*-OH) of 2-cyanophenol **53** and 2-isocyanophenol **55** isolated in nitrogen matrices at 10 K [116,117].

Isomerization tunneling of higher energy conformers differing by an OH rotation were also observed for heterocyclic compounds such as 2-furoic acid [119], tetrazole-5-acetic acid [97], 2-hydroxy-3-nitropyridine [120], cytosine [94] and cytosine derivatives [62]. Indeed, isomerization tunneling seems to be a ubiquitous phenomenon on the conformational dynamic of monomeric molecules having an OH fragment.

The photochemistry of 2,1-benzisoxazole **56** was also investigated as a possible gateway to nitrenes. Irradiation of **56** in an argon matrix was shown to lead to the concomitant formation of several products, making their identification problematic. However, we discovered that one of the products, formed in trace amount, disappeared spontaneously when the sample was kept in the dark. This allowed us to record its spectral signature and identify it as the triplet 2-formylphenyl nitrene *anti*-<sup>3</sup>**58**. Nitrene *anti*-<sup>3</sup>**58** was also generated *via* photolysis of 2-formylphenylazide **57** isolated in Ar, Kr and Xe matrices and characterized by IR, UV-Vis and electron paramagnetic resonance (EPR) spectroscopies (Figure 12.41) [121].

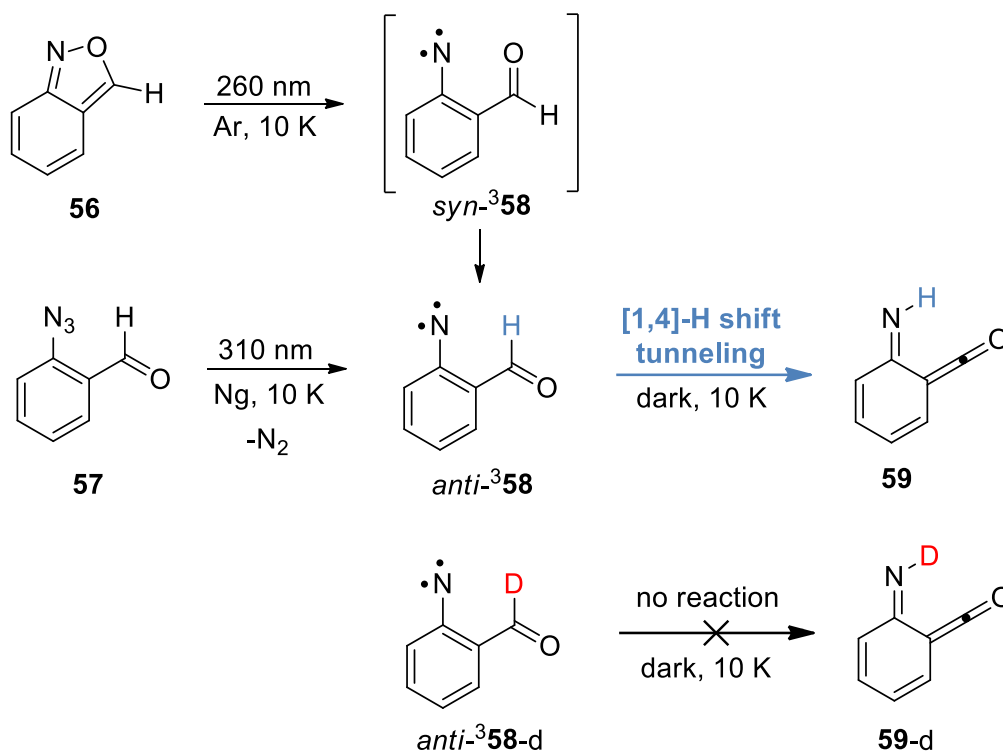


**Figure 12.41** Summary of experimental observation regarding [1,4]-H shift tunneling from triplet nitrene *anti*-<sup>3</sup>58 to imino-ketene **59** in cryogenic matrices at 10 K.

Upon its generation in matrices at 10 K, *anti*-<sup>3</sup>58 spontaneously rearranges in the dark to imino-ketene **59** (Figure 12.42). The kinetics of this transformation was monitored in an argon matrix and a rate constant of  $\sim 3 \times 10^{-5} \text{ s}^{-1}$  ( $t_{1/2} \sim 5.8 \text{ h}$ ) was measured, which implies a barrier of only  $\sim 0.8 \text{ kJ mol}^{-1}$ , if determined using the classical TST. The existence of such low barrier is inconceivable, which suggests that the reaction proceeds *via* tunneling. Unequivocal evidences for [1,4]-H shift tunneling from *anti*-<sup>3</sup>58 to **59** was provided by experiments with the deuterated derivative *anti*-<sup>3</sup>58-d, which shows no conversion to **59-d** (see Figure 12.41) [121].

It is plausible that *anti*-<sup>3</sup>58 undergoes [1,4]-H shift tunneling on the triplet surface to <sup>3</sup>59, followed by intersystem crossing (ISC) to singlet ground state **59**. Computations at different levels of theory on this triplet surface estimate a reaction barrier around *ca.*  $82 \text{ kcal mol}^{-1}$ , which precludes any contribution from a classical thermal over-the-barrier process. B3LYP/6-311++G(d,p) computations provide a barrier with a height of  $72.8 \text{ kJ mol}^{-1}$  and a width of  $1.3\text{--}1.4 \text{ \AA}$ . The tunneling probabilities of the H and D atoms penetration through such barrier were assessed based on the Wentzel–Kramers–Brillouin (WKB) approximation, which provided half-lives times on the order of tens-of-minutes/hours and  $10^5$  years, respectively, in agreement with the experimental observations [121]. This example constituted the first direct experiment evidence of a tunneling reaction involving a nitrene species.



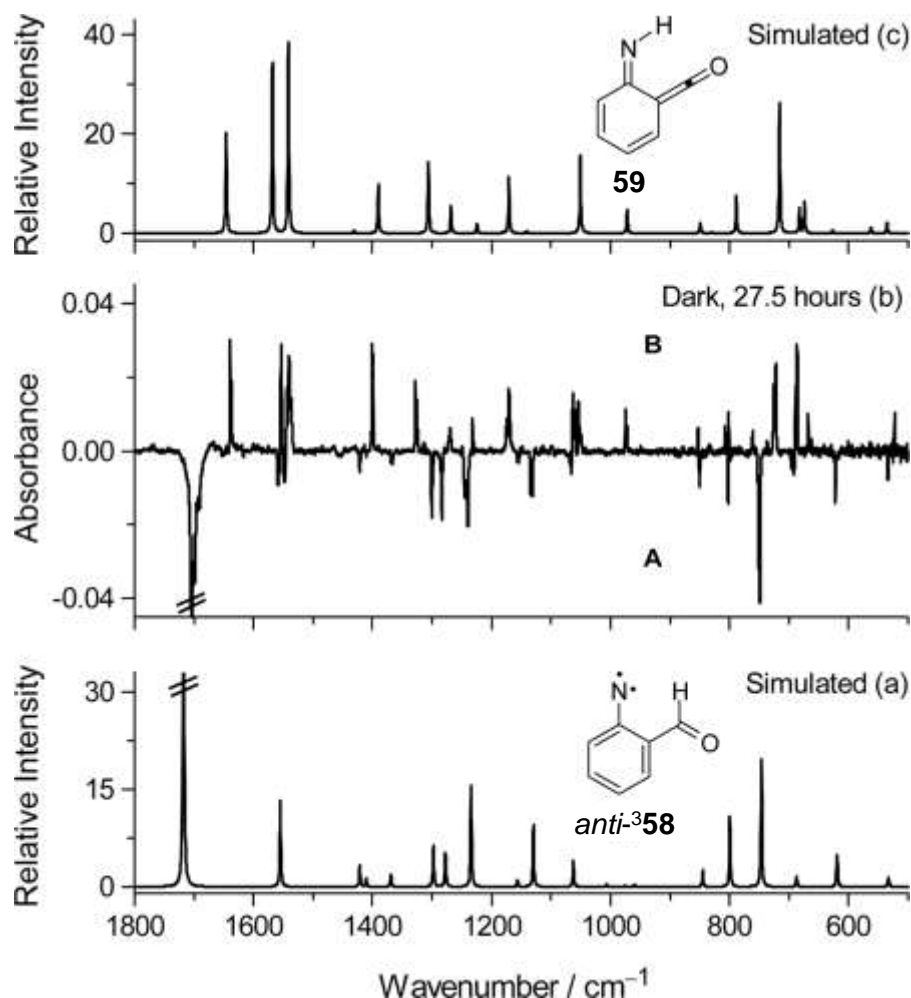


**Figure 12.42** (a) B3LYP/6-311++G(d,p) computed IR spectrum of imino-ketene **59**. (b) Spontaneous changes in the IR spectrum upon keeping the sample for 27.5 h in the dark, after UV-irradiation (308 nm) of 2-formylphenylazide **57** isolated in Ar matrix at 10 K. (c) B3LYP/6-311++G(d,p) computed IR spectrum of triplet nitrene *anti*-**358**. Adapted with permission from ref. 121. Copyright 2016 American Chemical Society.

In subsequent investigations, it was found that irradiation of protium or deuterated triplet 2-formylphenylnitrene **358** with visible light (530 nm) generates benzazirine **60**. Interestingly, in this way, we then discovered the heavy-atom tunneling reaction involving the spontaneous ring-expansion of **60** into its isomeric cyclic ketenimine **61** (Figure 12.43) [102]. In an argon matrix at 10 K, the reaction takes place with a rate constant of  $\sim 7.4 \times 10^{-7} \text{ s}^{-1}$  ( $t_{1/2} \sim 260 \text{ h}$ ), despite a reaction barrier of  $31.4 \text{ kJ mol}^{-1}$  estimated at the CCSD(T)//M06-2X level of theory. Solid evidence for the occurrence of the heavy-atom tunneling process was provided by the observation of the almost invariance of the reaction rate ( $\sim 8.9 \times 10^{-7} \text{ s}^{-1}$  at 20 K) upon increasing the temperature by a factor of 2. Computed rate constants without ( $1.8 \times 10^{-177} \text{ s}^{-1}$ )

and with tunneling ( $3.5 \times 10^{-5} \text{ s}^{-1}$ ) consideration (using canonical variational transition state theory [CVT] and small curvature tunneling [SCT]) confirmed that the observed spontaneous process can only occur by heavy-atom tunneling [102].

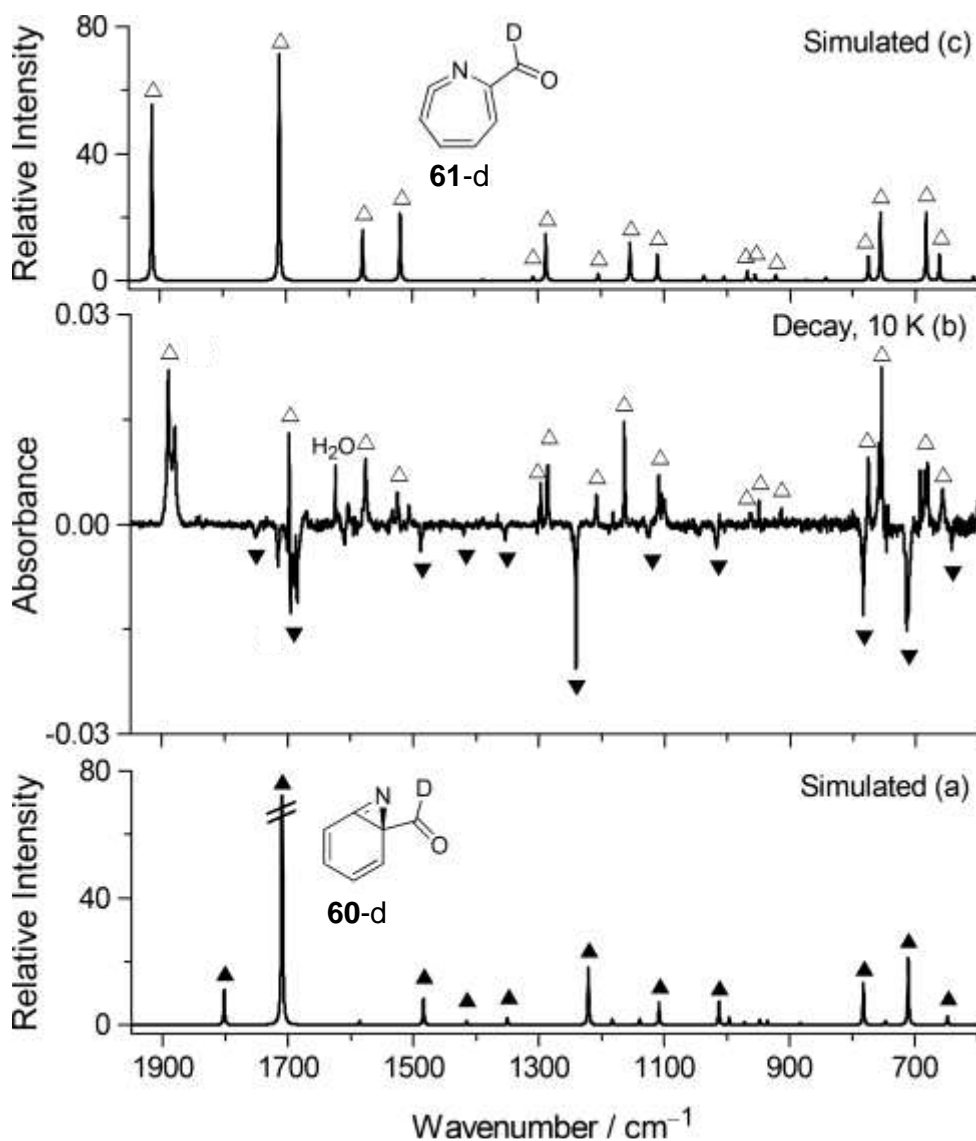


**Figure 12.43** (a) B3LYP/6-311++G(d,p) computed IR spectrum of benzazirine **60-d**. (b) Spontaneous changes in the IR spectrum upon keeping the sample in an argon matrix at 10 K for 3 days, after irradiation (530 nm) of 2-formylphenylnitrene **58-d**. (c) B3LYP/6-311++G(d,p) computed IR spectrum of cyclic ketenimine **61-d**. Adapted with permission from ref. 102. Copyright 2017 American Chemical Society.

McMahon, Sander and co-workers reported heavy-atom tunneling in other benzazirine derivatives by matrix isolation spectroscopy (Figure 12.44) [122,123]. They found that the type, position, and conformation of a substituent can enormously influence the tunneling probability of benzazirines ring-expansion to cyclic ketenimines. While some substituents provide the right tunneling rates for observations by steady-state spectroscopy, others make tunneling rates too

slow or too fast for detection. In the cases where the tunneling rate is too fast, the molecular system is characterized as having quantum tunneling instability and, therefore, although having a structure corresponding to a local minimum on the PES, it is not a stable observable molecule even at cryogenic temperatures [124].

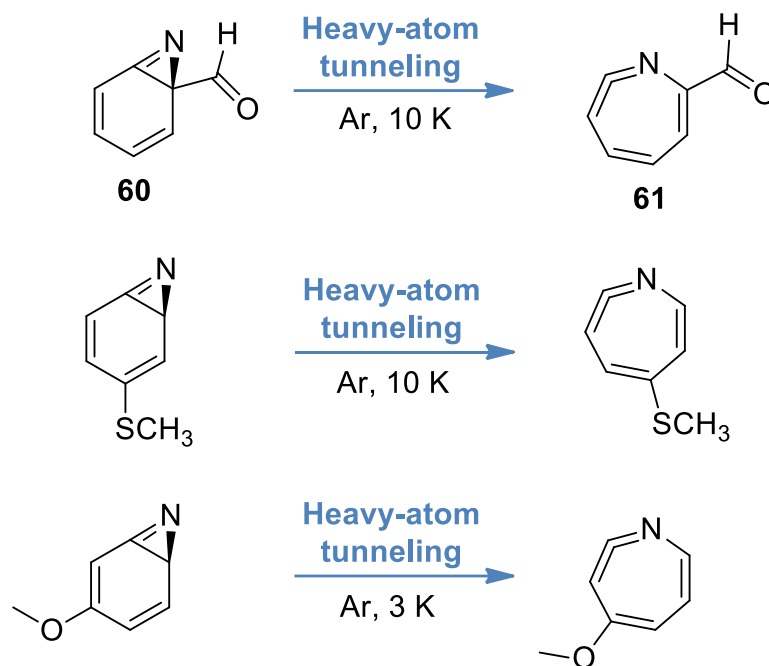


**Figure 12.44** Heavy-atom tunneling ring-expansion of benzazirine derivatives to cyclic ketenimines, directly observed by matrix isolation steady-state spectroscopy [102,122,123].

Remarkably, we have recently discovered that tunneling reactions can even be competitive and, thereby, determine the selectivity outcome of a reaction that cannot be predicted based on the classic TST model. Upon the generation of 4-amino-2*H*-benzazirine **63** in an argon matrix at 3 K, it was found that this compound spontaneously decays in the dark to concomitantly yield two different products, the triplet nitrene  $^3\mathbf{62}$  and the cyclic ketenimine **64** (Figures 12.45) [9]. Following the process by IR spectroscopy (Figure 12.46), the detailed identification of **63** was established with the support of its B3LYP/6-311+G(2d,p) computed IR spectrum, whereas the identification of  $^3\mathbf{62}$  and **64** was performed based on the IR signature of these two species, which were obtained upon selective conversion of **64** to  $^3\mathbf{62}$  by irradiation at 350 nm. A rate constant of  $\sim 5.5 \times 10^{-5} \text{ s}^{-1}$  ( $t_{1/2} \sim 210 \text{ min}$ ) and a product ratio  $^3\mathbf{62}:\mathbf{64}$  of 15:85 was measured. Increasing the absolute temperature by a factor up to five (up to 18 K) barely produced any change in both the rate constant and the product ratio, confirming that the decay of **63** and the formation of  $^3\mathbf{62}$  and **64** was not due to thermal over-the-barrier processes but to two independent and competitive heavy-atom tunneling reactions [9].

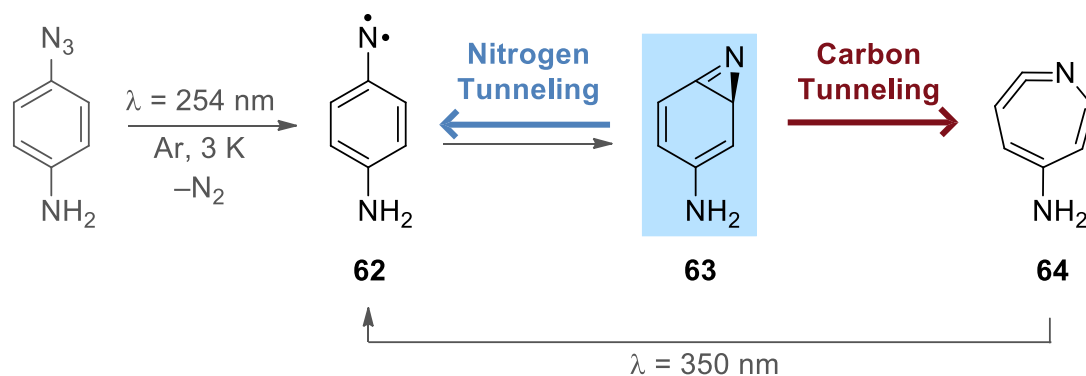


**Figure 12.45** Summary of the UV-induced reactions and the observed competitive tunneling ring-open *versus* ring-expansion of benzazirine **63** to triplet nitrene **62** and cyclic ketenimine **64**, respectively.

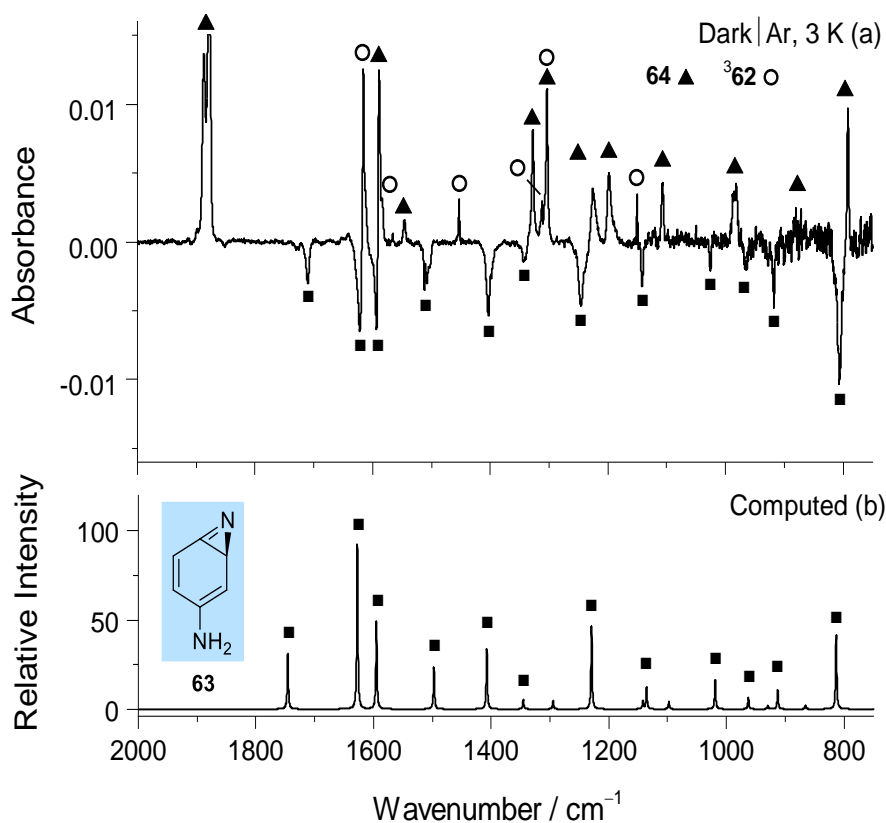


**Figure 12.46** (a) Experimental difference IR spectrum showing changes after keeping the sample at 3 K (argon matrix) in the dark for 24 h, subsequent to depletion of nitrene **62** at 435 nm. The downward bands are due to the consumption of **63**. The upward bands arise from the formation of both **62** and **64**. (b) B3LYP/6-311+G(2d,p) computed IR spectrum of benzazirine **63**. Adapted with permission from ref. 9. Copyright 2019 American Chemical Society.

The ring-opening of **63** should lead to an open-shell singlet (OSS)  $^1\mathbf{62}$ , which then relax fast by ISC to triplet ground state  $^3\mathbf{62}$ . For that process, computations at NEVPT2(8,8)//CASSCF(8,8) multiconfigurational level predict an energy barrier of  $\sim 10$  kJ mol $^{-1}$  [9]. For the ring-expansion of **63** to **64**, computations at CCSD(T)//B3LYP level predict an energy barrier of  $\sim 30$  kJ mol $^{-1}$ . These barriers are clearly prohibitive for a thermal activated process to take place at the experimental cryogenic temperatures. Moreover, the major product **64** faces a higher energy barrier than the minor product  $^3\mathbf{62}$ , which cannot be explained based on the classical TST. The computed tunneling probabilities through these barriers, applying the WKB formalism, predict the existence of two competitive tunneling reactions in accordance with the experimental observations. The ring-opening **63**  $\rightarrow$   $^1\mathbf{62}$  is predominantly a case of nitrogen-atom tunneling, since the nitrogen atom in the three-membered ring is the heavy atom having by far the largest displacement. On the other hand, the ring-expansion **63**  $\rightarrow$  **64** is predominantly a case of carbon-atom tunneling, since the two carbon atoms in the three-membered ring are clearly the heavy atoms with the largest displacements [9].

Our most recent (2020) example of heavy-atom tunneling was discovered in continuation of our studies with 2-formylphenyl nitrenes. The precursor 2-formyl-3-fluorophenylazide **65** was designed to achieve stabilization of the *syn*-aldehyde conformation; the fluorine atom acts as a hydrogen bond acceptor for aldehyde hydrogen [10]. That conformational tuning provided access to triplet *syn*-2-formylphenyl nitrene  $^3\mathbf{66}$  via UV irradiation of **65** isolated in argon matrix (Figure 12.47). Triplet nitrene  $^3\mathbf{66}$  was then observed to spontaneously cyclize in the dark to 2,1-benzisoxazole **67**. The kinetics of the process was followed by IR spectroscopy, and a rate constant of  $\sim 1.4 \times 10^{-3}$  s $^{-1}$  ( $t_{1/2} \sim 8$  min) was measured at 10, 15 and 20 K. The fast and temperature-independent cyclization of  $^3\mathbf{66}$  to **67** at extremely low temperatures provided strong arguments for the occurrence of a heavy-atom tunneling process. Computations indicated that  $^3\mathbf{67}$  is much more energetic than  $^3\mathbf{66}$ , precluding the possibility of a tunneling event on the triplet surface (which followed by ISC would give singlet ground state **67**). A minimum energy crossing point was located at  $\sim 50$  kJ mol $^{-1}$  (MRMP(10,10)//CASSCF(10,10) level) connecting the triplet surface of  $^3\mathbf{66}$  and the singlet surface of **67** (Figure 12.48). Calculations based on non-adiabatic models [10] estimated rate constants in fair agreement with experimental values, providing evidence for a mechanism of heavy-atom tunneling from  $^3\mathbf{66}$  to **67** through crossing triplet and singlet potential energy surfaces. Another feature that makes this heavy-atom tunneling reaction distinctive is the considerable displacement of the oxygen atom along the process, which puts a new limit for the heavier atom that can significantly participate in a tunneling reaction under low temperature matrix isolation conditions.

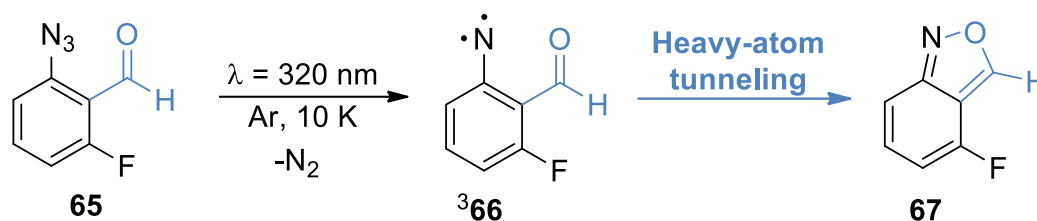


**Figure 12.47** Summary of experimental observation regarding heavy-atom tunneling cyclization of triplet nitrene  $^3\mathbf{66}$  to 2,1-benzisoxazole  $\mathbf{67}$  in argon matrix at 10 K.

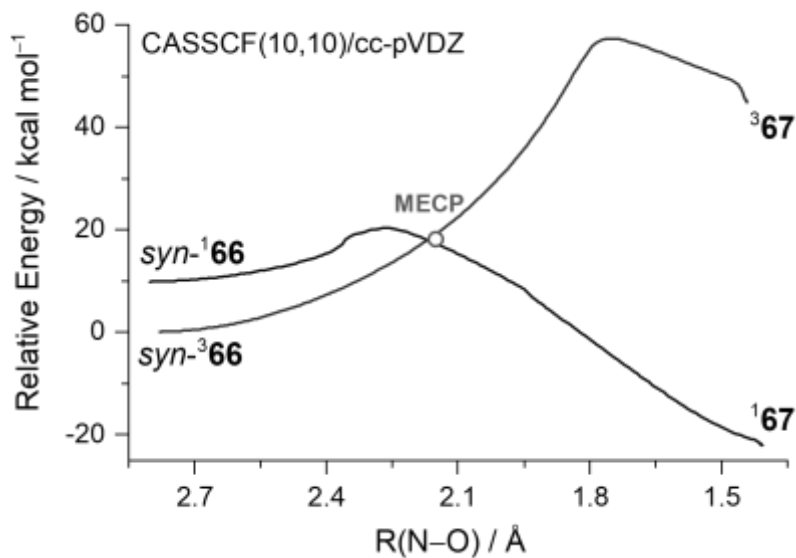


**Figure 12.48** Intrinsic reaction coordinate (IRC) path for the cyclization of  $^3\mathbf{66}$  to  $\mathbf{67}$  on the singlet (grey) and triplet (black) surfaces computed the CASSCF/cc-pVDZ level of theory as a function of the N $\cdots$ O distance (Å). The minimum energy crossing point (MECP) is shown in an open circle. To included dynamic correlations, single point energies were subsequently computed at MRMR level of theory. Adapted from ref. 10 with permission from John Wiley and Sons. Copyright 2020 WILEY-VCH Verlag GmbH & Co. KGaA, Weinheim.

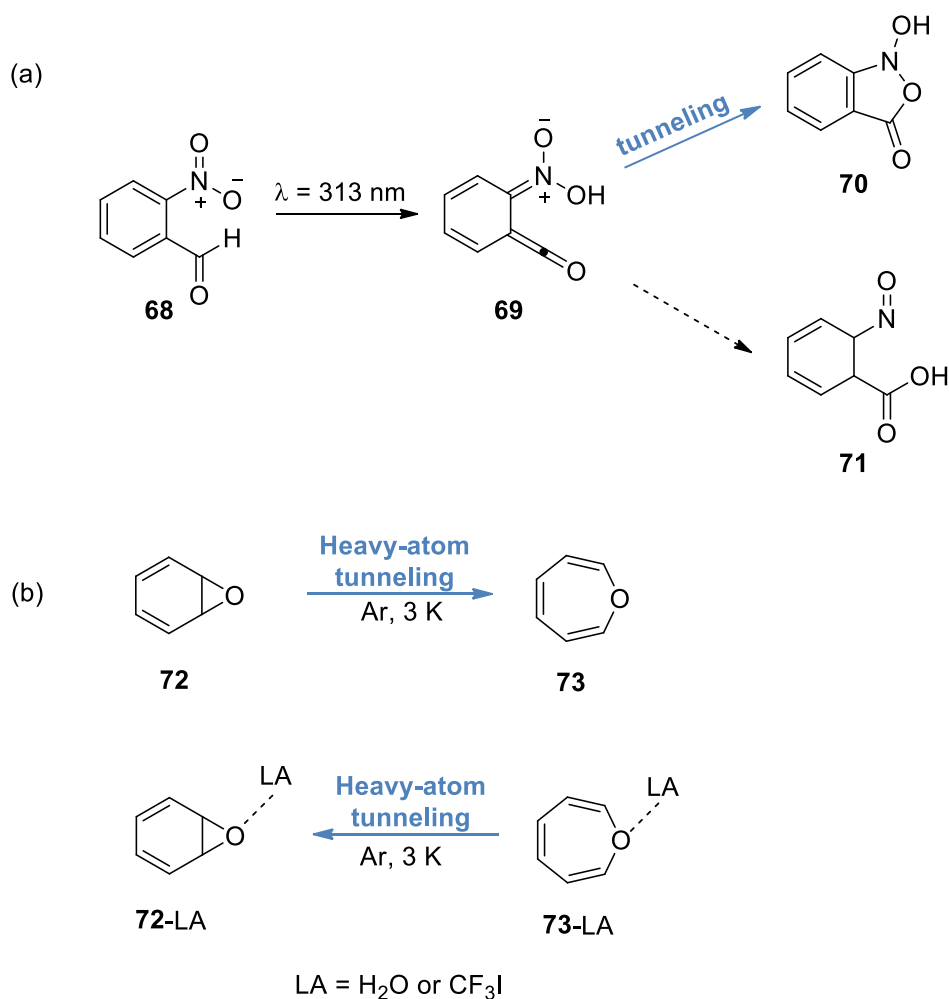


**Figure 12.49** Additional examples of tunneling directly observed by matrix isolation spectroscopy: (a) the rearrangement of ketene **69** to isoxazolone **70**; (b) the transformation between benzene oxide **72** and oxepin **73**.

Finally, we are aware of only two additional examples of tunneling directly observed by matrix isolation spectroscopy in the context of heterocyclic chemistry. One of such examples was reported by Gerbig and Schreiner demonstrating that ketene **69**, prepared by irradiation of *o*-nitrobenzaldehyde **68**, rearranges spontaneously to isoxazolone **70** *via* tunneling, at temperatures as low as 3 K (Figure 12.49a) [106]. Interestingly, based on computations performed at the CCSD(T)//MP2 level, **70** is neither thermodynamically nor kinetically favored, because the pathway to the energetically more stable product **71** has a lower energy barrier. Therefore, **70** constitutes an intriguing tunneling product. The other example was reported by Schleif *et al.* [125], who showed that the equilibrium between benzene oxide **72** and oxepin **73** is governed by heavy-atom tunneling (Figure 12.49b). In argon matrices at 3 K, **72** rearranges to **73** by tunneling, which conciliates well with results from CCSD(T) computations that

estimate **73** to be more stable by  $3.8 \text{ kJ mol}^{-1}$ . When the matrix is doped with  $\text{H}_2\text{O}$  or  $\text{CF}_3\text{I}$  (LA) the **73**·LA complexes formed upon annealing rearrange by tunneling to **72**·LA, which conciliates also well with computations that estimate the non-covalent complexes **72**·LA to be more stable than the **73**·LA species by  $2.5\text{--}3.8 \text{ kJ mol}^{-1}$  [125].

## 12.5 Conclusion and Perspectives

As shown in this chapter, matrix isolation has been given major contributions to the field of heterocyclic chemistry since its debut in the 50ies of the twenty century. Noteworthy, as mentioned in the Introduction section, it was its application to a heterocyclic reaction (the photochemistry of  $\alpha$ -pyrone [3-5]) that made it popular among the organic chemists community.

Recent developments in the technique, as well as in the auxiliary instrumentation (particularly in lasers, but also the appearance of more sensitive detectors for infrared spectrometers), have allowed matrix isolation to be used, nowadays, to extract detailed mechanistic insights on reactions involving heterocyclic compounds in an unprecedented way. In particular, when narrowband-light is used, excitation of a given reactant or intermediate can be performed in a very selective way. This gives access, frequently, to the possibility to follow individual steps of the reaction, once at a time, in an exclusive way. Besides, the cage effect most of the times simplifies extraordinarily the chemical processes, precluding undesired reactions involving recombination of fragments initially produced from different molecules, so that unimolecular chemistry is easily accessible.

The examples we provided in this Chapter illustrate clearly the potential of the technique when combined with infrared spectroscopy to address both photochemical reactions (either resulting from UV-Vis or IR excitation) and thermal processes. We also showed that tunneling-driven reactions can also be followed *directly* under matrix isolation conditions, and this possibility has opened a new field of research in this area. In this domain, recent studies like those described in this chapter have demonstrated that quantum mechanical tunneling is in fact more relevant in organic chemistry than it has been considered hitherto. Moreover, other detection techniques can also be used together with matrix isolation, and these may considerably expand the range of application of the method in the field of heterocyclic chemistry (and in organic chemistry in general), like EPR, for the detection of radicals and other species with unshared electrons, or Raman spectroscopy, including resonance Raman, which may open an entirely new field of studies on systems where more complex species play a major role.



## Acknowledgements

The authors thank the Portuguese Science Foundation (*Fundação para a Ciência e a Tecnologia* (FCT)), Lisbon (Portugal), for the financial support through Projects POCI-01-0145-FEDER-028973, UIDB/QUI/0313/2020 and UIDP/QUI/0313/2020, also co-funded by FEDER (via Portugal 2020-POCI) or by COMPETE-UE. C. M. Nunes and J. P. L. Roque also acknowledge FCT for an Auxiliary Researcher grant and a PhD (2020.04467.BD) grant, respectively. We also thank all members of the Laboratory of Molecular Criospectroscopy and Biospectroscopy (LMCB) of the Coimbra Chemistry Centre (present and past) as well as our co-authors from other research laboratories who participated in the studies mentioned in this Chapter.

## 12.8 References

1. Whittle E, Dows DA, Pimentel GC. *J. Chem. Phys.* 1954; 22: 1943-1944. doi:10.1063/1.1739957.
2. Norman I, Porter G. *Nature.* 1954; 174: 508-509. doi:10.1038/174508a0.
3. Lin CY, Krantz A. *J. Chem. Soc. Chem. Commun.* 1972: 1111-1112. doi:10.1039/C39720001111.
4. Chapman OL, McIntosh CL, Pacansky J. *J. Am. Chem. Soc.* 1973; 95(1): 244-246. doi:10.1021/ja00782a047.
5. Pong, RGS, Shirk JS. *J. Am. Chem. Soc.* 1973; 95(1): 248-249. doi:10.1021/ja00782a049
6. Breda S, Reva I, Lapinski L, Fausto R. *Phys. Chem. Chem. Phys.* 2004; 6(5): 929-937. doi:10.1039/B309660B.
7. Nunes CM, Reva I, Fausto R. Direct Observation of Tunneling Reactions by Matrix Isolation Spectroscopy. In: Kästner J, Kozuck S, editors. *Tunnelling in Molecules: Nuclear Quantum Effects from Bio to Physical Chemistry*. London, UK: Royal Society of Chemistry, *Theoret. Comput. Chem. Series*, Nº 18, Chapter 1, pp. 1-60; 2021.
8. Nunes CM, Pereira NAM, Reva I, Amado PSM, Cristiano MLS, Fausto R. *J. Phys. Chem. Lett.* 2020; 11(19): 8034-8039. doi:10.1021/acs.jpcclett.0c02272.
9. Nunes CM., Eckhardt AK., Reva I, Fausto R, Schreiner PR. *J. Am. Chem. Soc.* 2019; 141(36): 14340-14348. doi:10.1021/jacs.9b06869
10. Nunes, CM., Viegas LP, Wood SA, Roque JPL, McMahon RJ, Fausto R. *Angew. Chem. Int. Ed.* 2020; 59(40): 17622-17627. doi:10.1002/anie.202006640
11. Schreiner PR. *J. Am. Chem. Soc.* 2017; 139(43): 15276-15283. doi:10.1021/jacs.7b06035
12. Fausto R, Reva ID, Gómez-Zavaglia A. Matrix Isolation Spectroscopy in Heterocyclic Chemistry. In: Pinho e Melo TMVD, Rocha Gonsalves, AMd'A, editors. *Recent Research Developments in Heterocyclic Chemistry*. Kerala, India: Research Signpost, 37/661 (2), Fort P.O., Trivandrum-695 023, Chapter 7; 2007.
13. Meyer B. *Low Temperature Spectroscopy*. New York, USA: American Elsevier Publishers Company; 1971.

14. Andrews L, Moskovits M. *Chemistry and Physics of Matrix Isolated Species*. Amsterdam, Holland: Elsevier; 1989
15. Barnes A, Orville-Thomas WJ, Gauffrès, R, Müller A. *Matrix Isolation Spectroscopy*. London, UK: Springer; 1981
16. Dunkin IR. *Matrix Isolation Techniques: A Practical Approach*. Oxford, UK: Oxford University Press; 1998
17. Fausto R. *Low Temperature Molecular Spectroscopy*. Amsterdam, Holland: NATO-ASI Series C483, Kluwer; 1996
18. Khriachtchev L. *Physics and Chemistry at Low Temperatures*. New York, USA: Jenny Stanford Publishing; 2011.
19. Frija LMT, Cristiano MLS, Gómez-Zavaglia A, Reva I, Fausto R. *J. Photochem. Photobiol. C: Photochem. Rev.* 2014; 18: 71-90. doi:10.1016/j.jphotochemrev.2013.09.001.
20. Nunes CM, Gudmundsdottir AD, Fausto R. Special Issue: Structure, Spectroscopy and Chemistry of Reactive Species. *J. Mol. Struct.* Vol. 1172; 2018.
21. Breda S, Reva ID, Lapinski L, Nowak MJ, Fausto R. *J. Mol. Struct.* 2006; 786(2-3): 193-206. doi:10.1016/j.molstruc.2005.09.010.
22. Lobastov, VA, Srinivasan R, Goodson, BM, Ruan Ch-Y, Feenstra, JS, Zewail AH. *J. Phys. Chem. A*, 2001; 105(50): 11159-11164. doi:10.1021/jp013705b.
23. Kanamaru N. *Bull. Chem. Soc. Jap.* 1998; 71(10): 2299-2308. doi:10.1246/bcsj.71.2299.
24. Domcke W, Sobolewski AL, Woywod C. *Chem. Phys. Lett.* 1993; 203(2-3): 220-226. doi:10.1016/0009-2614(93)86391-Z.
25. Sobolewski AL, Woywod C, Domcke W. *J. Chem. Phys.* 1993; 98(7): 5627-5641. doi:10/1063/1.464907.
26. Lopes S, Nunes CM, Fausto R, Pinho e Melo TMVD. *J. Mol. Struct.* 2009; 919(1-3): 47-53. doi:10.1016/j.molstruc.2008.08.014.
27. Pinho e Melo TMVD, Lopes CSJ, Rocha Gonsalves AMd'A, Storr RC. *Synthesis*. 2002; 5: 605-608. doi:10.1055/s-2002-23542.
28. Palacios F, Retana AMO, Marigorta EM, Santos JM. *Eur. J. Org. Chem.* 2001; 2001(13): 2401-2414. doi:10.1002/1099-0690(200107)2001:13<2401::AID-EJOC2401>3.0.CO;2-U.
29. Gómez-Zavaglia A, Kaczor A, Cardoso AL, Pinho e Melo TMVD, Fausto R. *J. Phys. Chem. A*. 2006; 110(26): 8081-8092. doi:10.1021/jp062094q.
30. Kaczor A, Gómez-Zavaglia A, Cardoso AL, Pinho e Melo TMVD, Fausto R. *J. Phys. Chem. A*. 2006; 110(37): 10742-10749. doi:10.1021/jp064049o.
31. Gómez-Zavaglia A, Kaczor A, Cardoso AL, Pinho e Melo TMVD, Fausto R. *J. Mol. Struct.* 2007; 834-836: 262-269. doi:10.1016/j.molstruc.2006.12.027.
32. Inui H, Murata S. *Chem. Phys. Lett.* 2002; 359(3-4): 267-272. doi:10.1016/S0009-2614(02)00708-X.
33. Inui H, Murata S. *J. Am. Chem. Soc.* 2005; 127(8): 2628-2636. doi:10.1021/ja040109x.
34. Reva I, Almeida BJAN, Lapinski L, Fausto R. *J. Mol. Struct.* 2012; 1025: 74-83. doi:10.1016/j.molstruc.2011.11.051.
35. Piacenza M, Grimme S. *J. Comput. Chem.* 2004; 25(1): 83-89. doi:10.1002/jcc.10365.
36. Taft RW, Anvia F, Taagepera M, Catalan J, Elguero J. *J. Am. Chem. Soc.* 1986; 108(12): 3237-3239. doi:10.1021/ja00272a013.

37. Lopes Jesus, AJ, Reva I, Araujo-Andrade C, Fausto R. *J. Chem. Phys.* 2006; 144(12): 124306. doi:10.1063/1.4944528.
38. Lopes Jesus AJ, Fausto R, Reva I. *J. Phys. Chem. A.* 2017; 121(18): 3372-3382. doi:10.1021/acs.jpca.7b01713.
39. Weinhold F, Landis CR. *Valency and Bonding: A Natural Bond Orbital Donor–Acceptor Perspective.* New York, USA: Cambridge University Press; 2005.
40. Reid ST. *Adv. Heterocycl. Chem.* 1970; 11; 1-121. doi:10.1016/S0065-2725(08)60774-6.
41. Klán P, Wirz J. *Photochemistry of Organic Compounds: From concepts to Practice.* Chichester, UK: Wiley; 2009.
42. Sobolewski AL, Domcke W, Dedonder-Lardeux C, Jouvet C. *Phys. Chem. Chem. Phys.* 2002; 4(7): 1093-1100. doi:10.1039/B110941N.
43. Lin, MF, Tseng CM, Lee YT, Ni CK. *J. Chem. Phys.* 2005; 123(12): 124303. doi:10.1063/1.2009736.
44. Nix MGD, Devine AL, Cronin B, Ashfold MNR. *Phys. Chem. Chem. Phys.* 2006; 8(22): 2610-2618. doi:10.1039/B603499C.
45. Orville-Thomas WJ. *The history of matrix isolation Spectroscopy.* In: Barnes AJ, Orville-Thomas WJ, Müller A, Gaufrès R, editors. *Matrix Isolation Spectroscopy.* London, UK: Springer, pp. 1–11; 1981
46. Reva I, Lapinski L, Lopes Jesus AJ, Nowak MJ. *J. Chem. Phys.* 2017; 147(19): 194304. doi:10.1063/1.5003326.
47. Chmura B, Rode MF, Sobolewski AL, Lapinski L, Nowak MJ. *J. Phys. Chem. A.* 2008; 112(51): 13655-13661. doi:10.1021/jp8070986.
48. Lopes Jesus AJ, Reva I, Fausto R. *J. Photochem. Photobiol. A Chem.* 2017; 336: 123-130. doi:10.1016/j.jphotochem.2016.12.024.
49. Lopes Jesus AJ, Rosado MTS, Fausto R, Reva I. *Phys. Chem. Chem. Phys.* 2020; 22(40): 22943-22955. doi:10.1039/D0CP04354K.
50. Nowak MJ, Reva I, Rostkowska H, Lapinski L. *Phys. Chem. Chem. Phys.* 2017; 19(18): 11447-11454. doi:10.1039/C7CP01363A.
51. Lapinski L, Nowak MJ, Rostkowska H. *J. Chem. Phys.* 2017; 146(9): 094306. doi:10.1063/1.4977604.
52. Feyer V, Plekan O, Richter R, Coreno M, Vall-Ilosera G, Prince KC, Trofimov AB, Zaytseva IL, Moskovskaya TE, Gromov EV, Schirmer J. *J. Phys. Chem. A.* 2009; 113(19): 5736-5742. doi:10.1021/jp900998a.
53. Szczesniak M, Kwiatkowski JS, Szczepaniak K, KuBulat K, Person WB. *J. Am. Chem. Soc.* 1988; 110(25): 8319-8330. doi:10.1021/ja00233a006.
54. Nowak MJ, Lapinski L, Fulara J. *Spectrochim. Acta, Part A.* 1989; 45(2): 229-242. doi:10.1016/0584-8539(89)80129-1.
55. Brown, RD, Godfrey PD, McNaughton D, Pierlot AP. *J. Am. Chem. Soc.* 1989; 111(6): 2308-2310. doi:10.1021/ja00188a058.
56. Nir E, Müller M, Grace LI, De Vries MS. *Chem. Phys. Lett.* 2002; 355(1-2): 59-64. doi:10.1016/S0009-2614(02)00180-X.

57. Lapinski L, Reva I, Nowak MJ, Fausto R. *Phys. Chem. Chem. Phys.* 2011; 13(20): 9676-9684. doi:10.1039/C0CP02812F
58. Trygubenko SA, Bogdan TV, Rueda M, Orozco M, Luque FJ, Šponer J, Slavíček P, Hobza P. *Phys. Chem. Chem. Phys.* 2002; 4(17): 4192-4203. doi:10.1039/B202156K.
59. Ruiz DS, Cembran A, Garavelli M, Olivucci M, Fuß W. *Photochem. Photobiol.* 2002; 76(6): 622-633. doi:10.1562/0031-8655(2002)076<0622:SOTCID>2.0.CO;2
60. King GA, Oliver TAA, Ashfold MNR. *J. Chem. Phys.* 2010; 132(21): 214307. doi:10.1063/1.3427544
61. Reva I, Nowak MJ, Lapinski L, Fausto R. *J. Phys. Chem. B.* 2012; 116(19): 5703-5710. doi:10.1021/jp302375u.
62. Lapinski L, Reva I, Rostkowska H, Fausto R, Nowak MJ. *J. Phys. Chem. B.* 2014; 118(11): 2831-2841. doi:10.1021/jp411423c.
63. Lapinski L, Rostkowska H, Khvorostov A, Fausto R, Nowak M. J. *J. Phys. Chem. A.* 2003; 107(31): 5913-5919. doi:10.1021/jp035155i.
64. Nunes CM, Reva I, Rosado MTS, Fausto R. *Eur. J. Org. Chem.* 2015; 2015(34): 7484-7493. doi:10.1002/ejoc.201401153.
65. Gómez-Zavaglia A, Reva ID, Frija LMT, Cristiano MLS, Fausto R. Photochemistry of Tetrazole Derivatives in Cryogenic Rare Gas Matrices. In: Sánchez A, Gutierrez SJ, editors. Photochemistry Research Progress. New York, USA: Nova Science Publishers, pp. 295-324; 2008.
66. Bugalho SCS, Maçôas EMS, Cristiano MLS, Fausto R. *Phys. Chem. Chem. Phys.* 2001; 3(17): 3541-3547. doi:10.1039/B103344C.
67. Maier G, Eckwert J, Bothur A, Reisenauer HP, Schmidt C. *Liebigs Ann.* 1996; 1996(7): 1041-1053. doi:10.1002/jlac.199619960704.
68. Huisgen R, Seidel M, Sauer J, McFarland J, Wallbillich G. *J. Org. Chem.* 1959; 24(6): 892-893. Doi10.1021/jo01088a034.
69. Tasdelen MA, Yagci Y. *Angew. Chem. Int. Ed.*, 2013; 52(23): 5930-5938. doi:10.1002/anie.201208741
70. Lim RKV, Lin Q. *Acc. Chem. Res.* 2011; 44(9): 828-839. doi:10.1021/ar200021p.
71. Bégué D, Qiao GG, Wentrup C. *J. Am. Chem. Soc.* 2012; 134(11): 5339-5350. doi:10.1021/ja2118442
72. Bégué D, Wentrup C. *J. Org. Chem.* 2014; 79(3): 1418-1426. doi:10.1021/jo402875c.
73. Nunes CM, Araujo-Andrade C, Fausto R, Reva I. *J. Org. Chem.* 2014; 79(8): 3641-3646. doi:10.1021/jo402744f.
74. Gómez-Zavaglia A, Reva ID, Frija L, Cristiano MLS, Fausto R. *J. Photochem. Photobiol. A Chem.* 2006; 180(1-2): 175-183. doi:10.1016/j.jphotochem.2005.10.012.
75. Ismael A, Fausto R, Cristiano MLS. *J. Org. Chem.* 2016; 81(23): 11656-11663. doi:10.1021/acs.joc.6b02023
76. Ullman EF, Singh B. *J. Am. Chem. Soc.* 1966; 88(8): 1844-1845. doi:10.1021/ja00960a066.
77. Sauers RR, Van Arnum SD. *Tetrahedron Lett.* 1987; 28(47): 5797-5800. doi:10.1016/S0040-4039(01)81056-X.
78. Pavlik JW, Martin HST, Lambert KA, Lowell JA, Tsefrikas VM, Eddins CK, Kebede N. *J. Heterocycl. Chem.* 2005; 42(2): 273-281. doi:10.1002/jhet.5570420215.

79. Nunes CM, Reva I, Pinho e Melo TMVD, Fausto R. *J. Org. Chem.* 2012; 77(19): 8723-8732. doi:10.1021/jo301699z.
80. Nunes CM, Reva I, Pinho e Melo TMVD, Fausto R, Šolomek T, Bally T. *J. Am. Chem. Soc.* 2011; 133(46): 18911-18923. doi:10.1021/ja207717k.
81. Nunes CM, Reva I, Fausto R. *J. Org. Chem.* 2013; 78(21): 10657-10665. doi:10.1021/jo4015672.
82. Pérez JD, Yranzo GI, Wunderlin DA. *J. Org. Chem.* 1982; 47(6): 982-984. doi:10.1021/jo00345a017.
83. Pérez JD, Wunderlin DA. *Int. J. Chem. Kinet.* 1986; 18(12): 1333-1340. doi:10.1002/kin.550181205.
84. Murature DA, Pérez JD, De Bertorello MM, Bertorello HE. *Anal. Asoc. Quim. Argentina.* 1976; 64, 337.
85. Pérez JD, de Diaz RG, Yranzo GI. *J. Org. Chem.* 1981; 46(17): 3505-3508. doi:10.1021/jo00330a025.
86. Tanaka H, Osamura Y, Matsushita T, Nishimoto K. *Bull. Chem. Soc. Jpn.* 1981; 54(5), 1293-1298. doi:10.1246/bcsj.54.1293.
87. Parasuk V, Cramer CJ. *Chem. Phys. Lett.* 1996; 260(1-2): 7-14. doi:10.1016/0009-2614(96)0865-2.
88. Nunes CM, Reva I, Fausto R. *Phys. Chem. Chem. Phys.* 2019; 21(45): 24993-25001. doi:10.1039/C9CP05070A.
89. Góbi S, Reva I, Csonka IP, Nunes CM, Tarczay G, Fausto R. *Phys. Chem. Chem. Phys.* 2019; 21(45): 24935-24949. doi:10.1039/C9CP05370K.
90. Fausto R, Khriachtchev L, Hamm P. Conformational Changes in Cryogenic Matrices. In: Khriachtchev L, editor. *Physics and Chemistry at Low Temperatures.* New York, USA: Jenny Stanford Publishing, pp. 51-84; 2010.
91. Lapinski L, Nowak MJ, Reva I, Rostkowska H, Fausto R. *Phys. Chem. Chem. Phys.* 2010; 12(33): 9615-9618. doi:10.1039/C0CP00177E.
92. Fogarasi G. *J. Phys. Chem. A.* 2002; 106(7): 1381-1390. doi:10.1021/jp013067.
93. Wolken JK, Yao C, Tureček F, Polce MJ, Wesdemiotis C. *Int. J. Mass Spectrom.* 2007; 267(1-3): 30-42. doi:10.1016/j.ijms.2007.02.016.
94. Reva I, Nowak MJ, Lapinski L, Fausto R. *J. Chem. Phys.* 2012; 136(6): 064511. doi:10.1063/1.3683217.
95. Nowak MJ, Reva I, Lopes Jesus AJ, Lapinski L, Fausto R. *Phys. Chem. Chem. Phys.* 2019; 21(41): 22857-22868. doi:10.1039/C9CP04487F.
96. Halasa A, Reva I, Lapinski L, Nowak MJ, Fausto R. *J. Phys. Chem. A.* 2016; 120(13): 2078-2088. doi: 10.1021/acs.jpca.5b11615.
97. Araujo-Andrade C, Reva I, Fausto R. *J. Chem. Phys.* 2014; 140(6): 064306. doi: 10.1063/1.4864119.
98. Lopes Jesus AJ, Reva I, Araujo-Andrade C, Fausto R. *J. Am. Chem. Soc.* 2015; 137(45): 14240-14243. doi:10.1021/jacs.5b08588.
99. Halasa A, Lapinski L, Rostkowska H, Nowak MJ. *J. Phys. Chem. A.* 2015; 119(35): 9262-9271. doi:10.1021/acs.jpca.5b06221.

100. Halasa A, Reva I, Lapinski L, Rostkowska H, Fausto R, Nowak MJ. *J. Phys. Chem. A.* 2016; 120(17): 2647-2656. doi:10.1021/acs.jpca.6b01275.
101. Lopes Jesus AJ, Nunes C, Fausto R, Reva I. *Chem. Commun.* 2018; 54(38): 4778-4781. doi:10.1039/C8CC01052H.
102. Nunes CM, Reva I, Kozuch S, McMahon RJ, Fausto R. *J. Am. Chem. Soc.* 2017; 139(48): 17649-17659. doi:10.1021/jacs.7b10495.
103. Kästner J, Kozuch S, editors. *Tunnelling in Molecules*. London, UK: The Royal Society of Chemistry, Theoret. Comput. Chem. Series, N° 18; 2021
104. Carey FA, Sundberg RJ. *Advance Organic Chemistry Part A: Structure and Mechanisms*. New York, USA: Kluwer Academics / Plenum Publishers; 2000.
105. Schreiner PR. *Trends Chem.* 2020; 2(11): 984-989. doi:10.1016/j.trechm.2020.08.006
106. Gerbig D, Schreiner PR. *Angew. Chem. Int. Ed.* 2017; 56(32): 9445-9448. doi:10.1002/anie.201705140
107. Schreiner PR, Reisenauer HP, Ley D, Gerbig D, Wu C-H, Allen WD. *Science.* 2011; 332(6035): 1300-1303. doi:10.1126/science.1203761.
108. Greer EM, Kwon K, Greer A, Doubleday C. *Tetrahedron*, 2016; 72(47): 7357-7373. doi:10.1016/j.tet.2016.09.029.
109. Bell RP. *The Tunnel Effect in Chemistry*. Boston, USA: Springer; 1980.
110. Borden WT. *WIREs Comput. Mol. Sci.* 2016; 6(1): 20-46. doi:10.1002/wcms.1235.
111. Castro C, Karney WL. *Angew. Chem. Int. Ed.* 2020; 59(22): 8355-8366. doi:10.1002/anie.201914943
112. Nunes CM, Pinto SMV, Reva I, Fausto R. *Eur. J. Org. Chem.* 2016; 2016(24): 4152-4158. doi:10.1002/ejoc.201600668.
113. Nunes CM, Pinto SMV, Reva I, Fausto R. *Tetrahedron Lett.* 2016; 57(46): 5038-5041. doi:10.1016/j.tetlet.2016.09.098.
114. Nunes CM, Pinto SMV, Reva I, Rosado MTS, Fausto R. *J. Mol. Struct.* 2018; 1172: 33-41. doi:10.1016/j.molstruc.2017.11.009.
115. Ferris JP, Antonucci FR. *J. Am. Chem. Soc.* 1974; 96(7): 2010-2014. doi:10.1021/ja00814a005
116. Lopes Jesus AJ, Reva I, Nunes CM, Roque JPL, Pinto SMV, Fausto R. *Chem. Phys. Lett.* 2020; 747: 137069. doi:10.1016/j.cplett.2019.137069.
117. Lopes Jesus AJ, Nunes CM, Reva I, Pinto SMV, Fausto R. *J. Phys. Chem. A.* 2019; 123(20): 4396-4405. doi:10.1021/acs.jpca.9b01382.
118. Lopes S, Domanskaya AV, Fausto R, Räsänen M, Khriachtchev L. *J. Chem. Phys.* 2010; 133(14): 144507. doi:10.1063/1.3484943.
119. Halasa A, Lapinski L, Reva I, Rostkowska H, Fausto R, Nowak MJ. *J. Phys. Chem. A.* 2015; 119(6): 1037-1047. doi:10.1021/jp512302s
120. Nagaya M, Nakata M. *J. Phys. Chem. A.* 2007; 111(28): 6256-6262. doi:10.1021/jp0726687.
121. Nunes CM, Knezz SN, Reva I, Fausto R, McMahon RJ. *J. Am. Chem. Soc.* 2016; 138(47): 15287-15290. doi:10.1021/jacs.6b07368.
122. Inui H, Sawada K, Oishi S, Ushida K, McMahon RJ. *J. Am. Chem. Soc.* 2013; 135(28): 10246-10249. doi:10.1021/ja404172s
123. Schleif T, Mieres-Perez J, Henkel S, Mendez-Vega E, Inui H, McMahon RJ, Sander W. *J. Org. Chem.* 2019; 84(24): 16013-16018. doi:10.1021/joc.9b02482.

124. Amlani H, Frenklah A, Kozuch S. Tunnelling Instability in Molecular Systems. An Exercise in Computational Chemistry Prediction Power. In: Kästner J, Kozuck S, editors. Tunnelling in Molecules: Nuclear Quantum Effects from Bio to Physical Chemistry. London, UK: Royal Society of Chemistry, *Theoret. Comput. Chem. Series*, N° 18, Chapter 2, pp. 61-87; 2021.
125. Schleif T, Merini MP, Sander W. *Angew. Chem. Int. Ed.* 2020; 59(46): 20318-20322. doi:10.1002/anie.202010452.